



Terms and Conditions of Use of Digitised Theses from Trinity College Library Dublin

Copyright statement

All material supplied by Trinity College Library is protected by copyright (under the Copyright and Related Rights Act, 2000 as amended) and other relevant Intellectual Property Rights. By accessing and using a Digitised Thesis from Trinity College Library you acknowledge that all Intellectual Property Rights in any Works supplied are the sole and exclusive property of the copyright and/or other IPR holder. Specific copyright holders may not be explicitly identified. Use of materials from other sources within a thesis should not be construed as a claim over them.

A non-exclusive, non-transferable licence is hereby granted to those using or reproducing, in whole or in part, the material for valid purposes, providing the copyright owners are acknowledged using the normal conventions. Where specific permission to use material is required, this is identified and such permission must be sought from the copyright holder or agency cited.

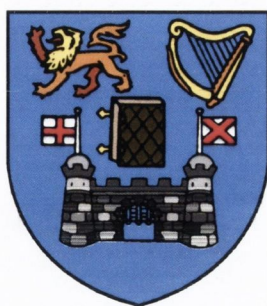
Liability statement

By using a Digitised Thesis, I accept that Trinity College Dublin bears no legal responsibility for the accuracy, legality or comprehensiveness of materials contained within the thesis, and that Trinity College Dublin accepts no liability for indirect, consequential, or incidental, damages or losses arising from use of the thesis for whatever reason. Information located in a thesis may be subject to specific use constraints, details of which may not be explicitly described. It is the responsibility of potential and actual users to be aware of such constraints and to abide by them. By making use of material from a digitised thesis, you accept these copyright and disclaimer provisions. Where it is brought to the attention of Trinity College Library that there may be a breach of copyright or other restraint, it is the policy to withdraw or take down access to a thesis while the issue is being resolved.

Access Agreement

By using a Digitised Thesis from Trinity College Library you are bound by the following Terms & Conditions. Please read them carefully.

I have read and I understand the following statement: All material supplied via a Digitised Thesis from Trinity College Library is protected by copyright and other intellectual property rights, and duplication or sale of all or part of any of a thesis is not permitted, except that material may be duplicated by you for your research use or for educational purposes in electronic or print form providing the copyright owners are acknowledged using the normal conventions. You must obtain permission for any other use. Electronic or print copies may not be offered, whether for sale or otherwise to anyone. This copy has been supplied on the understanding that it is copyright material and that no quotation from the thesis may be published without proper acknowledgement.



Preparation and Characterisation of Carbon Nanotube Films and Composites

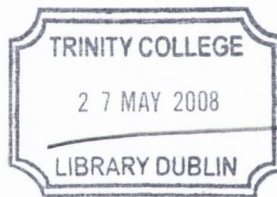
by

Fiona M. Blighe

A thesis submitted for the degree of
Doctor of Philosophy
in the University of Dublin

School of Physics
Trinity College Dublin

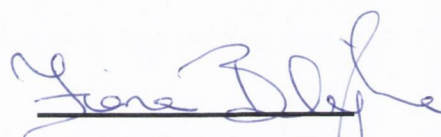
2008



TH681S
847

Declaration

I declare that the work in this thesis has not been previously submitted as an exercise for a degree to this or any other university. The work described herein is entirely my own, except for the assistance mentioned in the acknowledgements and the collaborative work mentioned in the list of publications. I agree that Trinity College Library may lend or copy this thesis on request.

A handwritten signature in blue ink, which appears to read "Fiona Blighe". The signature is written in a cursive style and is positioned above a solid horizontal line.

Fiona M. Blighe

October 2007

For my parents Michael and Elizabeth

Anyone who lives within their means suffers from a lack of imagination.
Oscar Wilde

When I'm working on a problem, I never think about beauty. I think only how to solve the problem. But when I have finished, if the solution is not beautiful, I know it is wrong.
R. Buckminster Fuller

Acknowledgements

Thinking about who I should thank for their help over the last few years I feel extremely lucky to have so many people to include.

Firstly I would like to thank Prof. Werner Blau for the giving me the opportunity to work in his group and for the chance to attend various conferences, trips and summer schools. I've really enjoyed it all. A special thanks to Prof. Jonathan Coleman whose group I am also a part of for all his supervision, assistance and time. Thanks so much, I really appreciate all the help you have given me.

It has been brilliant to come to work everyday with such a happy dynamic group of people. Your interest and love of science has been contagious. Thanks go in no particular order to.....Anna Drury for so much help over the years with chemistry related matters and for the many parties. To David Blond for plenty of help and advise and for teaching me the subtleties of the French aperitif. To Yenny Hernandez for help with electrical measurements and for having such cool taste in gym gear. To Philip Lyons for the masses of work he did on nanotube films. To Karen Young for her help with electrical measurements.

Thanks also to the other group members who have made this a great place to work; Martin, David Rickard, Ian, Ronan, Chris, Umar, Paula, Denise, Mustafa, Valeria, Take, Javier, Zhenyu, Sukanta, Eveyln and Darren & Niall (who keep everything going). The old team Sharon, Eimhin, Eleni, Schweta, Rory, Evan, Emer, Rob, Grace "get off my desk" Jordan, Kev, Nacho, Sandy, Adam, Margaret & Patrick, Cathal, Stephen (Slipper) ,Colin, James, Rebekah, Les and Denis.

Thanks to the guys in MI for all the assistance over the years. Especially Manual Ruther who trained me on so much equipment also Gordon, Keith, Ramesh, Jeannette, Marie, Chris and Trevor woods who has been so generous with his time and knowledge.

Thanks to the technical and administrative staff of the School of Physics for being so nice and helpful even when you were being pestered. I have to mention John Kelly for being such fun and brightening up the whole department.

The proof readers (a true test of friendship); Yenny, Shane, Helen, Emer, Denis and Siobain-thanks so much.

Out of all those I've worked with over the years I have to highlight Helen Cathcart and Shane Bergin who started with me (although they like to remind me they joined the group a week before me), thanks so much guys for all the help, interesting conversation and fun times- your friendship has meant a lot to me.

I would like to thank also my friends outside of college who have provided me with plenty of support and distraction! Especially Carmel, who had the pleasure of living with me through a lot of this. I owe you lady. And don't worry I don't expect you to read it. Also my fantastic flat mate Clodagh, fair is fair, I won't make you read it either.

Huge thanks to my family, especially my parents Michael and Elizabeth. Without your love, support and endless encouragement I couldn't have done it, thank you so much. Also my brother Shane who for some strange reason shows such an interest in what I do (and will actually want to read this), thanks bro. Lastly thanks to Colm who has made the last few months far nicer than I had imagined they would be.

Table of Contents

Abstract

ix

Chapter 1 Introduction	1
1.1 Background and Motivation	1
1.2 Thesis Outline	2
1.3 References	5
Chapter 2 Theory and Background	6
2.1 Introduction	6
2.2 Carbon Nanotubes	6
2.2.1 Structure of Carbon Nanotubes	7
2.2.2 Mechanical Properties of Carbon Nanotubes	9
2.2.3 Electronic Properties of Carbon Nanotubes	11
2.2.4 Production and Synthesis	13
2.2.5 Applications	16
2.3 Polymers	18
2.3.1 Mechanical Properties of Polymers	19
2.3.2 Electronic Properties of Polymers	21
2.4 Carbon Nanotube Polymer Composites	22
2.4.1 Theory of Polymer Matrix Reinforcement	22
2.4.2 Mechanical Reinforcement in Carbon Nanotube Polymer Composites	24
2.4.3 Theory of Electrical Conduction in Nanotube Polymer Composites	27
2.3.3.1 Percolation Theory	27
2.4.4 Conductivity in Carbon Nanotube Polymer Composites	30

2.5	Carbon Nanotube Macrostructures	30
2.5.1	Carbon Nanotube Fibres	31
2.5.2	Carbon Nanotube Bucky Papers	32
2.6	Conclusion	32
2.7	Reference	33
 Chapter 3 Materials and Methods		38
3.1	Introduction	38
3.2	Polymers	38
3.2.1	Polystyrene	38
3.2.2	Polyurethane	39
3.3	Carbon Nanotubes	40
3.4	Solvents Choice	41
3.4.1	N-methyl-2-pyrrolidone (NMP)	42
3.4.2	Chloroform	42
3.5	Sonication	42
3.6	Buchner Filtration	43
3.7	Thermogravimetric Analysis	43
3.8	UV-Vis Absorbance Spectroscopy	44
3.9	Raman Spectroscopy	44
3.10	Scanning Electron Microscopy	46
3.11	Tensile Testing	47
3.12	References	49
 Chapter 4 Carbon Nanotube Polystyrene Composites		50
4.1	Introduction and Relevant background Literature	50
4.2	Film Fabrication	53
4.3	Porosity Measurements	54
4.4	Thermogravimetric Analysis of Composite Films	54
4.5	Scanning Electron Microscopy of Composite Films	57

4.6	Mechanical Analysis of Composite Films	59
4.7	Electrical Measurements of Composites Films	62
4.8	Discussion and Conclusion	69
4.9	References	71

Chapter 5	The factors controlling the Mechanical and Electrical Properties of nanotube films	74
5.1	Introduction and Relevant background Literature	74
5.2	Film Fabrication	76
5.3	Film Analysis	76
5.3.1	Scanning Electron Microscopy of Carbon Nanotube Films	77
5.3.2	Raman Spectroscopy of Nanotube films	78
5.3.3	Mechanical Analysis of Carbon Nanotube Films	80
5.3.4	Electrical Characterisation of Carbon Nanotube Films	86
5.4	Further Analysis and Discussion with consideration of Inter-Nanotube Junction Density	88
5.4.1	Analyses of Mechanical Results	88
5.4.2	Analyses of Electrical Results	92
5.5	Conclusion	95
5.6	References	97

Chapter 6	Functionalised Single-walled Carbon Nanotube Polyurethane Composites	100
6.1	Introduction and Relevant background Literature	100

6.2	Film Fabrication	103
6.3	Film Analysis	104
6.3.1	Scanning Electron Microscopy of Elastomer Films	105
6.3.2	Mechanical Analysis of Carbon Nanotube Elastomer Films	109
6.3.3	Electrical Characterisation of Carbon Nanotube Films	114
6.4	Discussion and Conclusion	116
6.5	Conclusion	119
6.5	References	120
Chapter 7	Conclusions and Future Work	123
7.1	Conclusions	123
7.2	Future Work	125
Appendix	Publication List	127

Abstract

A simple method of carbon nanotube (NT) composite preparation has been demonstrated that produces wide ranging and extremely high carbon nanotube mass fraction, m_f , composites with minimal reaggregation of the nanotubes (up to 81 wt% NTs). High mass fraction polystyrene-nanotube composite films were fabricated using this method from very low concentration dispersions of *N*-Methyl-2-pyrrolidone by vacuum filtration. These films displayed conductivities between 100S/m and 10^4 S/m with densities in the region of 400kg/m^3 . Taking into account their porous nature, the conductivity, σ , was plotted as a function of the true nanotube volume fraction, p . The conductivity scaled according to a percolation scaling law: $\sigma \propto p^t$ right up to the nanotube only sample. This unexpected result shows that, in these systems at least, percolation scaling persists even at very high volume fractions. This indicates that the conductivity is limited only by the properties of the nanotube junctions of which the network is comprised, not by polymer tunnelling barriers. Mechanical analyses were also preformed on these films and prompted investigation into the factors that control the mechanical properties of nanotube films.

The mechanical and morphological properties of carbon nanotube films produced from a range of commercial nanotube suppliers were studied. Significant correlation was found between the mechanical parameters (modulus, strength, toughness and ductility) and the morphological parameters (porosity and bundle diameter) of the films. Little correlation was found between the nanotube graphitization of the nanotubes themselves (investigated using Raman spectroscopy) and the mechanical properties of the films. The majority of the mechanical properties showed decreased values at higher film porosity and nanotube bundle size. The number of inter-bundle junctions per unit volume, N_j , was calculated and related to the film porosity and nanotube bundle size. Both the strength and toughness scale linearly with this figure. These films were also characterised for DC conductivity. It was found that the film conductivity tends to improve with increasing nanotube graphitization. However, as the film porosity and mean bundle diameter increase, the conductivity falls. The conductivity scaled only approximately with N_j . However, it was observed to scale more clearly with the product of Raman G/D band ratio and the junction density indicating the importance of both nanotube and network properties for DC conductivity.

With the aim of increased stress transfer between the nanotubes and the polymer matrix, composites were prepared from polyurethane and functionalised (polyethylene glycol- PEG) nanotubes in a similar way. Layered composites were also prepared. Unfunctionalised nanotubes were dispersed in water using a surfactant and films prepared for comparison. Composites prepared with functionalised NTs dispersed in water show superior mechanical properties to those prepared using unfunctionalised tubes and a surfactant. The Youngs' Modulus of these composites increased by three orders of magnitude from 3.7MPa for the elastomer only sample to 3.29GPa for the highest NT load composite (75 wt% NTs). The toughness scaled linearly with nanotube m_f up to a nanotube load of 40 wt% after which the properties were dominated by those of the nanotube only network. These PEG-SWNT polyurethane composites exhibit tuneable toughness, without sacrificing strength.

Chapter 1

Introduction

1.1 Background and Motivation

Since primitive times mankind has constantly sought ways to improve his situation, quality of life and ease of existence. Designing and building increasingly elaborate shelters to live in, sophisticated tools to work with and modes of transportation. All his endeavours required knowledge and development of the materials around him. Composite materials have played a huge role in mans journey from hunter-gatherer to space-traveller.

Composites consist of two or more components, which complement each other to produce a material with specifically required properties. Cement and steel are composite materials and both have contributed in a significant way to the evolution of modern day life.

At the beginning of the 20th century a new chapter of material science began with the production of the first synthetic polymer, Bakelite[1]. Bakelite was used initially for radio and telephone casings replacing wood which was is more difficult to process. Nowadays thousands of natural and synthetic polymers (commonly referred to as plastics) are available to an ever growing consumer population.

The majority of organic polymers are insulating in nature. However work done by Alan Heeger, Alan MacDiarmid and Hideki Shirakawa in 1977 on doped polyacetylene was awarded the Nobel Prize in 2000 "*For the discovery and development of conductive polymers*". This advancement opened up new applications for polymers as light emitting diodes [2, 3]. However the intrinsic conductivity of these conducting polymers is still low and insufficient for many applications.

Overall polymers are light weight, chemically stable and are more easily processed than most natural materials. More importantly they are relatively cheap, a vital quality in our “use once, throw away” society. What they often do not possess however is high mechanical strength or electrical conductivity. Polymers in general have strengths of around 50MPa whereas high strength steel wires have shown strengths of 2390MPa[4]. Although specific polymers have higher values, such as Kevlar which has a strength of around 3600MPa[4] most do not. This can limit polymer use to low tech packaging type applications.

With this in mind polymers as the matrix for strong conducting composite materials hold much potential. Polymer reinforcement with fibres has been common for many years[5]. An ideal filler material for polymers should possess good mechanical properties, be electrically conductive and have a high aspect ratio. With the discovery of carbon nanotubes in 1991[6], a new extremely strong and conductive (both thermally and electrically) material became available. Carbon nanotubes since their discovery have been extensively studied in the field of polymer reinforcement[7].

Several difficulties have arisen to hamper this research. Firstly carbon nanotubes bundle together and are difficult to separate [8]. These bundles do not possess the same properties as individual tubes and therefore do not provide the desired levels of reinforcement. As nanotubes are chemically inert they do not interact well with polymer matrices and therefore contribute less than expected to reinforcement[9]. This thesis looks to overcome these problems and to investigate carbon nanotubes in a macroscopic form and as the filler in two polymer matrices, examining them for both their electronic and mechanical properties.

1.2 Thesis Outline

In this thesis, the electrical and mechanical properties of carbon nanotube films and composites based on these films are studied.

In Chapter 2, the structural, mechanical and electrical properties of carbon nanotubes are introduced. The most common methods of carbon nanotube production are explained and compared. The potential applications of carbon nanotubes and the difficulties facing researchers are also mentioned. Following this polymers are introduced with particular reference to their mechanical properties. The rest of the chapter focuses on carbon nanotube polymer composites. The theory of polymer matrix reinforcement is explained and a review of current carbon nanotube reinforced composite literature is included. Lastly the theory of electrical conduction in polymer composites is explained through percolation theory with reference to relevant literature.

In Chapter 3, all the polymers, nanotubes and solvents used throughout this work are described. The various experimental techniques for sample preparation and characterisation are outlined.

Chapter 4 discusses the measured electrical and mechanical properties of SWNT polystyrene composites with emphasis on the electrical results. It begins with a brief review of conducting nanotube-polymer composite literature. A novel method of carbon nanotube composite preparation is then introduced and described in detail. This method produces composites of extremely high nanotube mass fraction, m_f , something which has been previously very difficult to achieve. These high m_f films were characterised by measuring their porosity and carrying out thermogravimetric analysis and scanning electron microscopy. Tensile measurements were made to investigate the mechanical properties of the films. The focus of the chapter is on the electrical measurements where film conductivity versus true nanotube volume fraction is plotted and discussed in detail.

Chapter 5 investigates the mechanical and electrical properties of carbon nanotube films prepared from a variety of commercially available nanotubes. The films were prepared by vacuum filtration of nanotube dispersions. Some of the nanotube types have functional groups attached to their surfaces that allow them to disperse in water, others require an organic solvent to disperse. The films were characterised by measuring their porosity and through scanning electron microscopy and Raman spectroscopy.

Tensile measurements were made and plotted as a function of the Raman G:D band intensity, the nanotube bundle size and film porosity. The same was done for the measured conductivity values. In further analyses the chapter goes on to introduce a combined parameter, the nanotube inter bundle junction density which relates to both the porosity and the bundle diameter size of the nanotube film. This parameter scales well with the mechanical properties of the films, while the Raman G:D band intensity seems to have little influence. The Raman G:D band intensity ratio was however found to influence the electrical properties of the films. It is thus combined with the junction number density parameter and plotted against the conductivity.

In Chapter 6, composites were prepared using the method described in chapter four with functionalised nanotubes and the elastomer polyurethane. These films are compared to a set of composites prepared using pristine nanotubes which were dispersed using a surfactant in water. Composites were also prepared using a layer by layer method. The nanotube and polymer dispersions were prepared separately and alternate controlled volumes of each vacuum filtered as before. The films were characterised by thermogravimetric analysis and scanning electron microscopy. The electronic and mechanical properties of the films were investigated, the focus of discussion being on the mechanical results.

Chapter 7 summarises the research presented in this thesis, discussing its most significant findings. Applications of nanotube polymer composites are discussed, as well as possible further work.

1.3 References

1. Baekeland, L.H., *Method of making insoluble products of phenol and formaldehyde*. 1907: US.
2. Burroughes, J.H., et al., *Light-emitting diodes based on conjugated polymers*. Nature, 1990. **347**(6293): p. 539-541.
3. Brown, A.R., et al., *Poly(p-phenylenevinylene) light-emitting diodes: Enhanced electroluminescent efficiency through charge carrier confinement*. Applied Physics Letters, 1992. **61**(23): p. 2793-2795.
4. Callister, W.D., *Materials science and engineering: An introduction (2nd edition)*. Materials & Design, 1991. **12**(1): p. 59.
5. DiBenedetto, A.T., *Tailoring of interfaces in glass fiber reinforced polymer composites: a review*. Materials Science and Engineering A, 2001. **302**(1): p. 74-82.
6. Iijima, S., *Helical microtubules of graphitic carbon*. Nature, 1991. **354**(6348): p. 56-58.
7. Coleman, J.N., et al., *Small but strong: A review of the mechanical properties of carbon nanotube-polymer composites*. Carbon, 2006. **44**(9): p. 1624-1652.
8. Thess, A., et al., *Crystalline Ropes of Metallic Carbon Nanotubes*. Science, 1996. **273**(5274): p. 483-487.
9. Tan, H., et al., *The effect of van der Waals-based interface cohesive law on carbon nanotube-reinforced composite materials*. Composites Science and Technology, 2007. **67**(14): p. 2941-2946.

Chapter 2

Theory and Background

2.1 Introduction

This chapter introduces carbon nanotubes (CNTs), their properties, synthesis and applications. Polymers and their properties are also introduced. It follows on to discuss nanotube polymer composites with reference to literature and explains the theory of polymer matrix reinforcement and the electrical theory of polymer composites. Carbon nanotube films, also known as Bucky papers, are introduced as a macroscopic form of carbon nanotubes. These films and composites prepared by a similar method are the subject of study throughout this thesis.

2.2 Carbon Nanotubes

In 1991, while studying high resolution transmission electron microscopy images of the soot created in an electrical discharge between two carbon electrodes, Iijima[1], observed structures that consisted of several concentric tubes of carbon nested inside each other like Russian dolls ,figure 2.1.

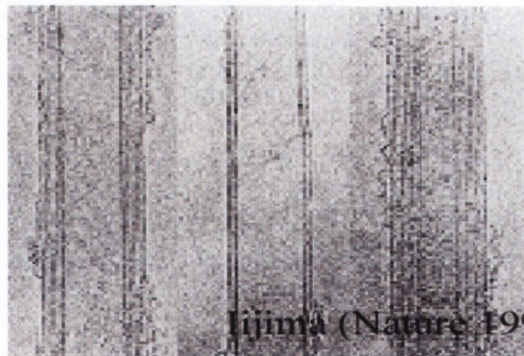


Figure 2.1 TEM picture taken by Iijima

While the first carbon filaments of nanometre dimensions were prepared in France in the 1970s[2], they were not recognised as tubes and were not studied systematically. Iijima's observation that the tubes were hollow, permitting experiments in 1D quantum physics, initiated considerable excitement and research in the field of carbon nanotubes.

2.2.1 Structure of Carbon Nanotubes

A carbon nanotube (CNT) can be visualised as a graphene sheet rolled up into a cylinder. This cylinder can be capped at each end with a half-fullerene molecule. Ideally carbon nanotubes are entirely composed of sp^2 bonded carbon, similar to graphite, where each carbon is arranged in a hexagonal ring and is bonded to three others. Due to the curvature of the tube walls, some of the original planar sp^2 bond vectors of the sheet are bent, picking up some of the characteristics and hence properties of sp^3 type bonds, like those present in diamond.

Carbon nanotubes occur in two distinct forms; single-walled nanotubes (SWNTs), which are composed of just one rolled up graphene sheet and multiwalled nanotubes (MWNTs), which consist of multiple concentric graphene cylinders. Generally, CNT diameters vary between 0.4 and 3 nm for SWNTs and 1.4 and 100 nm for MWNTs[3].

SWNTs exist in different forms that are identified by their chiral vector, C_h

$$C_h = na_1 + ma_2 \quad 2.1$$

where n and m are integers. a_1 and a_2 are the unit vectors of the two-dimensional hexagonal lattice. Carbon nanotubes can act as either metals or semiconductors, depending primarily on this roll up vector, which represents the full circumference of the tube, figure 2.2.

If m is zero, the nanotubes are referred to as "zigzag". If both digits are the same, they are "arm chair". Otherwise they are chiral, producing a mirror image of their structure upon exchange of n and m , examples of these three structural varieties are shown in figure 2.2.

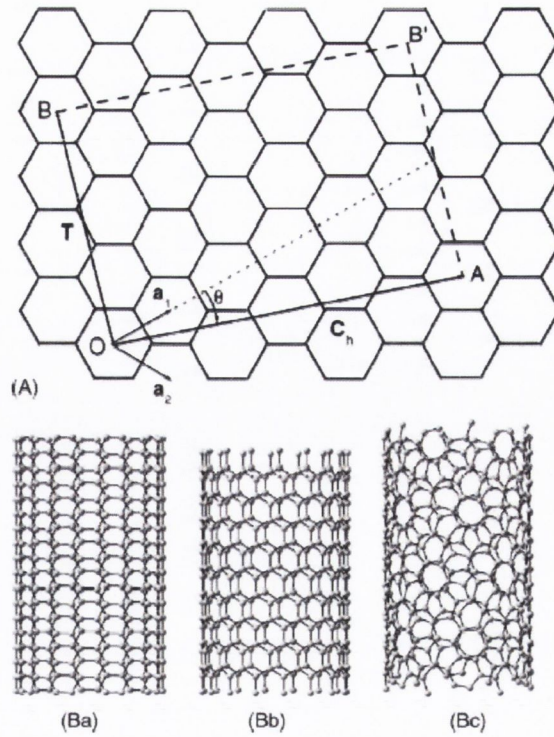


Figure 2.2 (A) Schematic representation of the construction of a nanotube by rolling-up an infinite strip of graphene. (Ba) Armchair Tube. (Bb) Zigzag Tube (Bc) Chiral Tube.

θ is the chiral angle between the chiral vector C_h , and the unit vector a_1 . From the (n, m) values, the chiral angle, θ , and the diameter, d , of a nanotube can be calculated

$$d = \frac{\sqrt{3}}{\pi} a_{c-c} \sqrt{n^2 + nm + m^2} \quad 2.2$$

$$\theta = \text{Tan}^{-1} \frac{\sqrt{3}n}{2m + n} \quad 2.3$$

where a_{c-c} is the carbon-carbon distance in a graphene sheet (1.42 Å[4]).

2.2.2 Mechanical Properties of Carbon Nanotubes

Carbon nanotubes are an extremely high strength material. Carbon-carbon sp^2 bonds are very strong, being shorter and stronger than even the sp^3 bonds in diamond [5]. It is the arrangement of the sp^2 bonds in CNTs that provide them with their unique strength [6], which has been measured experimentally to be in the order of 63 GPa [7]. The tensile strengths of some common materials are listed in table 2.1 for comparison.

Material	Tensile Strength GPa
Aluminium	0.090
Copper	0.200
Iron	0.262
Steel	0.380
Titanium	0.520
Polystyrene	0.052 (max)
Nylon	0.0945 (max)

Table 2.1 Tensile Strengths of some common materials[8].

Mechanical measurements on individual carbon nanotubes are not straight forward due to their size and difficulties in obtaining an individual nanotube for testing. Before experiments could be carried out theoretical studies predicted that their Youngs' modulus was close to 1TPa [9], similar to that of in-plane graphite [10]. To begin with measurements were made in a transmission electron microscope [11] where intrinsic thermal vibrations were used to calculate the Youngs' modulus.

The first direct measurements of Youngs' modulus were made in 1997 by Wong et al. [12] inside an atomic force microscope, they were also successful in measuring an average bending strength of 14GPa. In 2000 Yu et al [7] carried out stress-strain measurements on individual MWNTs inside an electron microscope showing that MWNTs fracture at strains of up to 12%, allowing them to estimate nanotube toughness at around 2232MPa. The Youngs' moduli of some common materials are listed in table 2.2.

Material	Youngs Modulus TPa
Aluminium	0.069
Copper	0.110
Steel	0.270
Titanium	0.107
Polystyrene	0.033 (max)
Nylon	0.038 (max)

Table 2.2 Youngs' Moduli of some common materials[8].

Along with being exceptionally strong and stiff, CNTs are also light weight with a density of approximately 1500kg/m^3 [13]. Perhaps one of the most significant properties of carbon nanotubes is their large aspect ratio, often greater than a thousand, which coupled with the properties previously mentioned suggests them as an ideal filler for the mechanical reinforcement of polymers [14].

MWNTs generally have inferior mechanical properties to SWNTs due to weak inter-wall bonding. The inter-wall interaction strength in multiwalled CNTs should be in the same order as that in graphite, which has a shear strength value in the range of 0.48 MPa [5]. Under stress the failure of the outermost tube occurs followed by pullout of the inner tubes [7], often referred to as telescoping or “sword from sheath” behaviour, figure 2.3.

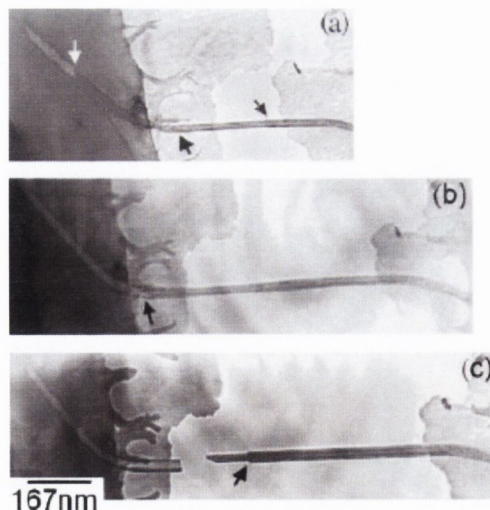


Figure 2.3 Failure of a MWNT demonstrating “Sword from Sheath” behaviour[15].

2.2.3 Electronic Properties of Carbon Nanotubes

Carbon nanotubes are a quasi 1 dimensional materials, having diameters of only a few nanometres and lengths of often up to several microns. Their density of states (DOS) has been calculated as,

$$\text{DOS} = g(E) \propto \frac{1}{\sqrt{E - E_0}} \quad 2.4$$

where E_0 is the energy at the band edge, calculated from the E-k dispersion curve of the energy band diagram. When the density of states $g(E)$ of a carbon nanotube is plotted a series of spikes are present at energies corresponding to the band-edge, where $E = E_0$, figure 2.4. These spikes occur symmetrically about the Fermi level, and are known as van Hove singularities.

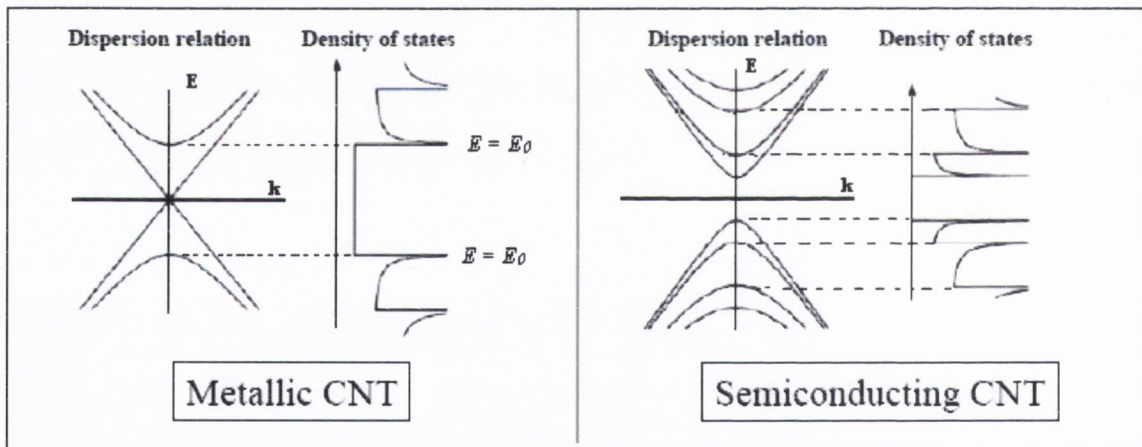


Figure 2.4 Dispersion Relation and Density of States Diagram for a metallic and semiconducting carbon nanotube.

The appearance of van Hove singularities is due to the quantisation of the allowed electronic states around the circumference of a nanotube, where the electrons are confined by the small circumference of the tube. Therefore only certain wave numbers, k , are allowed. The Born-Von Karmen periodic boundary condition is used to calculate the allowed states for a wave around the diameter of a carbon nanotube where,

$$C_h \cdot k = 2\pi j \quad j = 0, 1, 2, \dots \quad 2.5$$

C_h is the chiral vector of the nanotube, k is the wave number and j is an integer. Carbon nanotubes are very long, and can be considered infinite along their length, thus the number of allowed states along the axial direction is continuous. So for every allowed value of k around the tube circumference there are corresponding bands of energy levels along the length of the tube. The lowest level of each of these bands is called E_0 , figure 2.4.

For a given sub band the energy difference between the van Hove peaks in the valence and conductance band, E_g is,

$$E_g = \frac{n 2\gamma a_{cc}}{d} \quad 2.6$$

where n is an integer, the carbon-carbon tight binding overlap energy $\gamma = 2.7$ eV, the carbon lattice constant $a_{cc} = 1.42\text{\AA}$ and $d =$ diameter of the nanotube[16]. Thus E_g is inversely proportional to d . This makes sense as the curvature of a nanotube decreases the diameter increases accordingly and the band gap will reduce, this will eventually result in a flat sheet with no band gap, ie. graphene.

As the band gap energy is dependent on the tube diameter it must also depend its n, m values and so on its chirality. Thus the band gap energy will vary for different types of nanotubes. Nanotubes can be either metallic or semiconducting depending on the size of this energy gap. In general a nanotube will be metallic if,

$$\frac{m - n}{3} = p \quad 2.7$$

where p is an integer. This means 1/3 of nanotubes are metallic and have non zero density of states at the Fermi energy. The other 2/3 are semiconducting and have a zero density of states or an energy gap between the van Hove peaks either side of the Fermi level. For a

semiconducting tube, the separation between these van Hove peaks is referred to as the band gap energy. The value of n between the peaks separated by the Fermi level is 1 so,

$$E_g = \frac{2\gamma a_{cc}}{d} \quad 2.8$$

One of the most important electrical properties of carbon nanotubes is the reduced probability of electron scattering as a result of the limited number of allowed electronic states. This means that the transport is ballistic over distances greater than $1\mu\text{m}$. Ballistic conduction occurs where the distance travelled by the electrons along the tube axis is less than their mean free path and no scattering occurs. The electrons encounter no resistance and dissipate no energy, therefore Joule heating is minimised. This allows high current densities to be tolerated without destruction of the tube. Carbon nanotubes can carry current densities of $100\text{MA}/\text{cm}^2$ [17], in theory 1000 times that of copper.

2.2.4 Production and Synthesis

If carbon nanotubes are to be used in many applications, a cheap, efficient and plentiful supply is of the utmost importance. The three most common methods of CNT production are arc-discharge, laser ablation, and chemical vapour deposition.

In the arc-discharge method which is illustrated in figure 2.5, a current is passed between two graphite electrodes, in a buffer gas causing the evaporation of the anode.

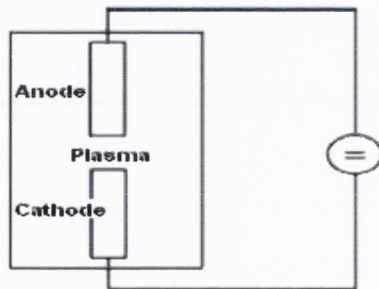


Figure 2.5 Arc-discharge scheme[18]. Two graphite electrodes are used to produce a dc electric arc-discharge in inert gas atmosphere.

Laser ablation involves, the evaporation by a laser of a solid target of graphite, figure 2.6. The graphite target also contains a metal catalyst (Co, Ni) and is placed in a horizontal tube with a flow of inert gas. The pressure is controlled and the temperature in the tube furnace is usually ~ 1200 °C. The nanotubes are deposited on a water-cooled collector outside the furnace.

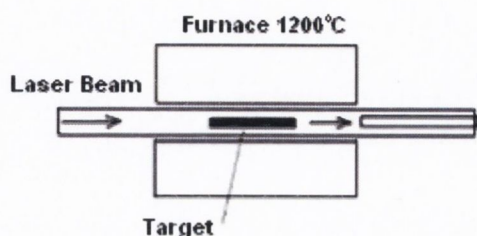


Figure 2.6 Laser-ablation scheme[18].

The growth material for the NTs is a hot expanding plasma of atomic or molecular carbon species and the atomic vapour of the catalyst (usually Fe, Ni,Co) which condense to form nanotubes. At present, laser ablation produces small amounts of cleaner nanotubes, whereas the arc discharge method produces relatively larger quantities (although still in the range of grams) of impure material. These were initially the most widely used methods, but were too expensive and slow and gave insufficient yields to remain dominant.

Chemical vapour deposition (CVD) involves the catalytic pyrolysis of hydrocarbons, providing carbon atoms for nanotube growth, figure 2.7.

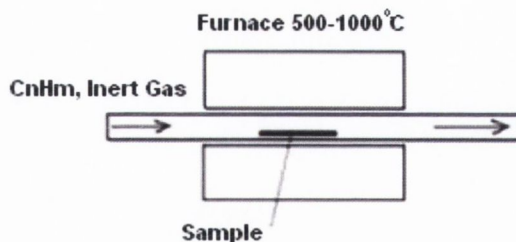


Figure 2.7 Chemical vapour deposition scheme[18].

The hydrocarbon (usually acetylene or methane), and a carrier gas (argon) are heated in a furnace in the presence of catalytic particles (usually Fe, Co, Ni). As the gas is heated, the

hydrocarbons decompose, catalysed by the metal particles. The carbon atoms precipitate and form nanotubes. By choosing the appropriate growth conditions, it is possible to obtain single or multiwalled nanotubes with controlled average diameters and lengths[19]. The catalyst metallicity is crucial for the CNTs growth and generally CNT diameters depend on the catalyst cluster dimensions. The main advantage of CVD over other methods is the low cost associated with large scale production. However, the CNTs produced by the catalytic process are usually thicker than those by arc-discharge, contain more defects and often consist of large aggregates and many impurities[20].

The high-pressure carbon monoxide process (HiPco), developed at Rice University is effectively a CVD process without any substrate [21] and produces single-walled carbon nanotubes from gas-phase reactions of iron pentacarbonyl with carbon monoxide at high pressures (10-100 atm). The product is reported to contain 97% SWNT. Unfortunately, as with all the other SWNT production techniques, metal catalyst, and possibly other impurities are also present.

To date all carbon nanotubes contain defects. Some deviation from the six-membered-ring structure, such as the inclusion of five- or seven- membered rings appear in the carbon network. These stem from the initial formation of the tubes. In general, impurities such as carbon-coated metal, carbon nanoparticles and amorphous carbon are also present.

There are many different methods of nanotube purification [22]. Liquid oxidation[23, 24], gas-phase oxidation[25-28] and electrochemical oxidation [29] have been employed to purify SWCNTs. Microfiltration [30], gel permeation chromatography [31] and centrifugation [32] have also been found effective. Due to the importance of purification in nanotube research, other alternative methods still need to be explored.

The route towards mass production of CNTs has been hampered by a lack of understanding of their exact growth mechanism and kinetics. They remain expensive by industrial standards and the transference of the various production conditions to an industrial scale has not yet been achieved. Nevertheless many commercial nanotube suppliers have recently come on line with the promise of a reliable product at low cost. Already, Cheap Tubes Inc. claims to have the following mission:

We are embracing the commodity status of Carbon Nanotubes. Many of our competitors are unwilling to accept that ultimately CNTs are a commodity. We believe that when a product is a commodity then if features and quality are equal, then price is largest governing factor. We are striving to be the highest volume, lowest cost CNT supplier.

2.2.5 Applications

The properties of carbon nanotubes have prompted much discussion on their application especially when dispersed within polymeric matrices [33]. As yet, scientists have been unable to fully harness the unique attributes exhibited by CNTs at the nano scale and transfer them to the macro scale. Poor dispersion is often cited as a process limitation and the key factor diminishing the mechanical properties of the composite materials [34]. Weak interfacial bonding between the nanotubes and the surrounding polymer matrix also contributes to the poor performance of the composites.

The dispersion of CNTs in polymers is crucial to their successful utilisation in practical applications, however CNTs do not spontaneously disperse in polymers. Unfortunately they are also insoluble in most common organic solvents. The strong attraction between CNTs in a polymer solution is enthalpic in origin and enhanced by their low dimensionality. Attractive forces in graphitic structures are due to their extended pi electron system, which is highly polarisable, and subject to large attractive van der Waals forces. These forces lead to bundles of tubes which are very difficult to disrupt. Extended structures are formed by lateral aggregation of the bundles which further tangle together.

Due to the low entropy of mixing, rigid molecules of high molecular weight require strong attractive interactions with a solvent to disperse. Since the connectivity and rigidity of macromolecules drastically reduces the number of configurations available to them in the dispersed state, mixing becomes a problem. In the case of rigid fillers dispersed into stiff polymers, the problem is compounded in that neither species gains entropy on dispersion.

In certain circumstances, like the case of carbon nanotubes in polymers, thermal energy alone is insufficient to surmount the potential energy barrier to aggregation and specific measures need to be taken. Several methods have been reported to overcome the

problem for CNTs, including the use of surfactants[35], functionalisation of the nanotubes[36], and the use of very specific amide solvents like dimethylformamide (DMF) or N-methylpyrrolidone (NMP)[37].

In spite of the obstacles facing researchers the excellent mechanical and electrical properties of carbon nanotubes make them a good candidate for a wide variety of macro- and micro-application[38]. CNTs are the best known field emitters of any material. This is understandable, given their high electrical conductivity, and the size or sharpness of their tip. The sharpness of the tip also means that they emit at especially low voltage, an important factor for building low-power electrical devices. As previously mentioned carbon nanotubes possess very high current densities. An immediate application of this is in flat-panel displays. Instead of a single electron gun, as in a traditional cathode ray tube display, in CNT-based displays there is a separate electron gun (or even many of them) for each individual pixel in the display. Their high current density, low turn-on and operating voltages, and steady, long-lived behaviour make CNTs very attractive field emitters for this application [17].

There are countless applications for carbon nanotube reinforced polymers which seek to take advantage of their high strengths and inherent lightness particularly in the production of efficient spacecraft and in the automotive industry. Plastics are often used as a replacement for metals. The lack of electrical conductivity in most common plastics can be overcome the addition of conductive fillers, such as carbon black and graphite fibres[8]. The loading required to provide the necessary conductivity using conventional fillers is typically high, and can result in increased weight and degradation of the mechanical properties of the polymer. Carbon nanotubes on the other hand have a higher aspect ratio and so require a lower loading to achieve a given level of conductivity[39]. Applications which could exploit the high conductivity and aspect ratio of CNTs include electromagnetic interference shielding composites, antistatic materials and transparent conductive coatings.

Carbon nanotubes possess desirable characteristics for use as electrodes, in batteries and capacitors. They have a tremendously high surface area which has been reported as high as $1587 \text{ m}^2/\text{g}$ [40], making them highly accessible to the electrolyte and are good conductors of electricity. Research has shown that CNTs have the highest reversible capacity of any carbon material for use in lithium-ion batteries [41].

Carbon nanotubes are also being investigated for biomedical applications as drug carriers, sensors and reinforcement agents for prosthetics. Hydroxyapatite has been used in clinical bone graft procedures for many years but exhibits poor tensile strength and toughness when compared to bone. Carbon nanotubes are currently being investigated as a reinforcing filler for hydroxyapatite but more work needs to be carried out to assess the bioactivity and toxicity of carbon nanotubes and their composites before they can be considered for clinical applications[42].

As carbon nanotubes are a relatively new material there are almost certainly many more unanticipated applications yet to be discovered.

2.3 Polymers

Prior to the early 1920's, chemists doubted the existence of molecules having molecular weights greater than a few thousand. Work by the German chemist Hermann Staudinger, on natural compounds such as rubber and cellulose challenged this view. A Nobel Prize was awarded to him in 1953 for the formulation of a polymeric structure for rubber, based on a repeating isoprene unit. Recognition that polymeric macromolecules make up many important natural materials lead to the creation of many synthetic polymers possessing a variety of properties.

Organic polymers are long, one dimensional macromolecules, made up of repeating identical building blocks that consist mainly of carbon, oxygen, hydrogen and nitrogen atoms. They form a large class of natural and synthetic materials with a variety of properties and purposes. They typically have low densities with mechanical properties usually lower than those of ceramics or metal. However, on the basis of their low densities, their stiffness and strength per mass is often comparable to those of heavier more robust materials. In general polymers are chemically inert. One of their major disadvantages is their lack of electrical conductivity and the fact that they have a tendency to soften or decompose at modest temperatures.

2.3.1 Mechanical Properties of Polymers

The characteristics of a polymer depend on its chemical properties i.e. way the chains bond to each other and also on physical properties like the shape and uniformity of the individual chains. Side groups on a polymer chain can affect its molecular interactions with other chains and influence the materials strength and melting point. In Kevlar strong hydrogen bonds are responsible for its high strength and melting point. Branching and tacticity in polymers influence the way the chains arrange themselves and has considerable influence on their properties. The more entangled a polymer chain, the higher the melt temperature and the lower the percentage crystallinity of the bulk polymer.

Polymers can be grouped into three major classes; plastics, fibres and elastomers, although there is no firm dividing line between these groups. One way of classifying a polymer is to examine a stress-strain plot of the material, figure 2.8. Rigid plastics and fibres are resistant to deformation and are characterised by a high modulus (or stiffness) and low percentage elongation. Elastomers readily undergo deformation and exhibit largely reversible elongations under small applied stresses, they exhibit elasticity.

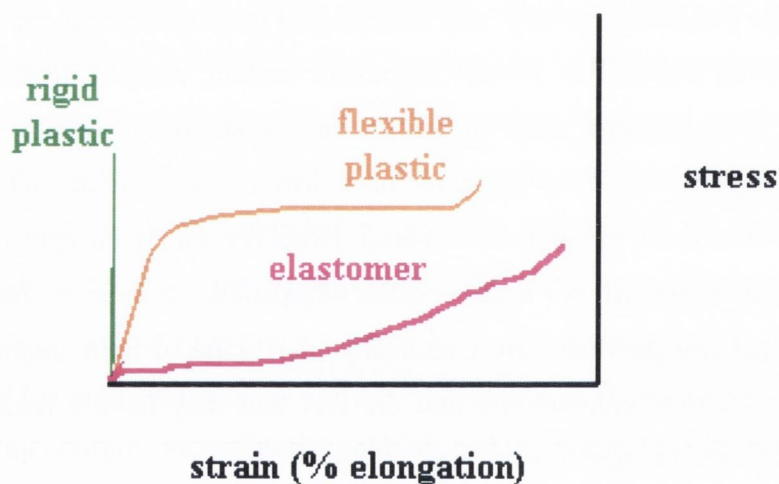


Fig. 2.8 Stress-Strain curves of different polymer types[43].

Plastics are probably the largest class of polymer materials and are usually divided into two groups; thermosets and thermoplastics. Thermoplastics can be remoulded after heating, whereas thermosets cannot due to cross-linked bonds formed during processing.

They may also be further classified as amorphous or crystalline depending on the degree of order present among their chains.

Elastomers are often weaker than plastics but are generally more ductile. They have the ability to undergo large deformations and elastically spring back to their original form. This is a result of crosslinks within the polymer that provide the force to restore the chains to their original conformation after the stress has been removed. Unstressed an elastomer will be amorphous and composed of molecular chains that are highly twisted and coiled. Elastic deformation occurs as these coils untwist under stress, figure 2.9.

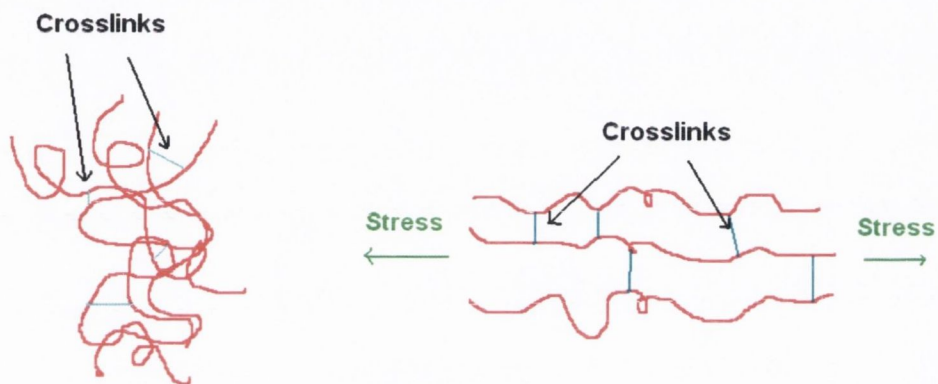


Figure 2.9 Schematic of elastomer chains unstressed and during elastic deformation in response to an applied tensile stress.

Elastomers must be kept above their glass transition temperature to deform in such a way, below it they become brittle.

Polymer fibres are often characterised by a high modulus and low percentage elongation. They are produced by drawing long filaments from the bulk polymer with aspect ratios of at least 100. They are often used in the textile industry in cloths or fabric. Some such as Kevlar can also be employed in composite materials. High tensile strength is desirable in polymer fibres as they are often subjected to considerable stretching, twisting, and abrasion during use.

2.3.2 Electronic Properties of Polymers

The majority of polymers are insulating in nature. Their valence electrons are used up in covalent bonds and so are localised and unable to conduct electricity. In some polymers however this is not the case. In π -conjugated polymers like polyacetylene alternate single and double bonds are present along the polymer backbone. Single bonds consist of overlapping orbitals along the internuclear axis, called σ -bonds. Double bonds consist of a σ -bond and also a parallel π -bond. The π -bond is a result of overlapping orbitals directed perpendicular to the internuclear axis, figure 2.10.

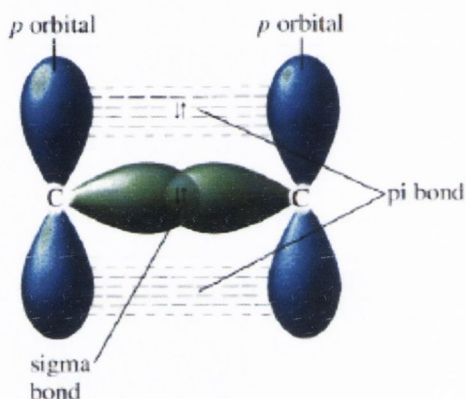


Figure 2.10 Double bond consisting of a σ -bond and a π -bond.

In conjugated polymers the π -electrons can become delocalised and shared along the polymer chain, enabling them to conduct electricity. Other examples of conducting polymers are poly(aniline), poly(phenylenevinylene) and poly(pyrrole). Delocalised bonds in these examples are due mainly to the presence of aromatic rings. The electrical conductivity of conducting polymers is however far below the level required for many applications where metals are currently used.

2.4 Carbon Nanotube Polymer Composites

As discussed in the previous section polymers possess a host of attractive qualities including durability and mouldability. They are lightweight and chemically stable. One of the most attractive properties of polymers is the ease and low cost with which they can be processed. They are often however mechanically lacking for certain applications where particularly high strengths or stiffness are required and are poor conductors of electricity. The role of CNTs in polymer composites is to overcome these issues through mechanical reinforcement or by improving their electrical properties.

2.4.1 Theory of Polymer Matrix Reinforcement

The simplest way to model a fibre reinforced composite is to apply the rule of mixtures. In the rule of mixtures it is assumed that the reinforcing fibres are aligned and span the full length of the composite and that there is perfect stress transfer between the matrix and the fibres[8]. Hence, equal strain occurs for both the fibre and the matrix. In this situation, the Young's modulus of the composite parallel, $Y_{C\parallel}$ and perpendicular, $Y_{C\perp}$, to the fibre direction are:

$$Y_{C\parallel} = \phi_f Y_f + (1 - \phi_f) Y_m \quad \text{and} \quad Y_{C\perp} = \frac{Y_f Y_m}{\phi_f Y_m + (1 - \phi_f) Y_f} \quad 2.9$$

where Y_f and Y_m are the modulus of the fibre and matrix respectively, and ϕ_f is the volume fraction of the fibre.

Naturally this is a simplified situation. The rule of mixtures only applies when the fibres are at least as long as the composites. It cannot be applied to nanostructure reinforced composites as the lengths of the fibres, $\sim 1 \mu\text{m}$, are substantially less than any composite films prepared. Matrix-fibre interfacial stress transfer, τ , must be considered. Nanoparticles are ideal for reinforcement because of their high surface area to volume ratio, which maximises the area available for interaction with the polymer matrix, thus allowing greater

stress transfer. The stress transferred from the matrix to the fibre scales with fibre length, l . At a critical length, l_c , the transferred stress is enough to break the fibre.

For systems where short fibres are used for reinforcement, Cox derived his shear lag theory[44]. It states that for aligned fibres in a composite, the Young's modulus of the composite is

$$Y_C = (\eta_1 Y_f - Y_m) V_f + Y_m \quad 2.10$$

where,

$$\eta_1 = 1 - \frac{\text{Tanh}(a \cdot l / D)}{a \cdot l / D} \quad 2.11$$

η_1 is the length efficiency factor which describes the reduced effective modulus of the reinforcement fibres due to their shorter length, l . D is the diameter, and a is given by

$$a = \sqrt{\frac{-3Y_m}{2Y_f \ln V_f}} \quad 2.12$$

In order to consider a more realistic situation still, the Krenchel orientation efficiency factor [8], η_0 , is introduced for randomly orientated short fibres.

$$Y_C = (\eta_0 \eta_1 Y_f - Y_m) V_f + Y_m \quad 2.13$$

η_0 is equal to 1 for aligned fibres, 3/8 for fibres aligned in the plane and 1/5 for randomly orientated fibres [14]. Similar calculations can be made to derive equations for composite strength [14].

The Halpin-Tsai theory [45] was developed for continuous fibre composites and accounts for a distribution of fibre lengths and orientations in the polymer matrix. The composite modulus Y_C for randomly orientated fibres is

$$Y_C = \frac{3}{8} \left[\frac{1 + \zeta \eta_L V_f}{1 - \eta_L V_f} \right] Y_m + \frac{5}{8} \left[\frac{2 + \eta_T V_f}{1 - \eta_T V_f} \right] Y_m \quad 2.14$$

Where $\zeta = 2l/D$ and

$$\eta_L = \frac{Y_f / Y_m - 1}{Y_f / Y_m + \zeta}, \quad \eta_T = \frac{Y_f / Y_m - 1}{Y_f / Y_m + 2} \quad 2.15$$

Although the Halpin-Tsai theory works well at low volume fractions it is known to underestimate the increase in modulus at high volume fractions [14].

In composite materials the change of Young's modulus with respect to the volume fraction of filler, dY/dV_f , is often used as a marker for reinforcement. To achieve reinforcement in fibre-polymer matrices a large filler aspect ratio is preferred in order to achieve the maximum contact with the polymer with the least amount of filler, so retaining the positive attributes of the host polymer. A good dispersion is also vital as previously mentioned in section 2.2.4. Perhaps most important is the interaction between the fibres and their host. There is little point in adding filler to a polymer if applied stresses are not efficiently transferred from the polymer to the filler particles. Improved interfacial stress transfer can be achieved in carbon nanotube polymer composites by functionalisation of the nanotubes [46], in-situ polymerisation of the polymer with the nanotubes[47], or for semi crystalline polymers by crystallisation around the nanotubes [48].

2.4.2 Mechanical Reinforcement in Carbon Nanotube Polymer Composites

There have been literally thousands of studies on the reinforcement of polymers with carbon nanotubes. In this section a brief overview of the field is presented.

Carbon nanotube composites can be prepared in a variety of ways. Solution processing is perhaps the most common method, where the nanotubes and polymer are mixed together in a solvent before it is evaporated off to form a film. The main advantage

of solution processing is that the nanotube soot or powder is agitated in the solvent encouraging de-bundling and dispersion. The nanotubes are generally dispersed in the solvent or solvent polymer solution using magnetic stirring, shear mixing, reflux or ultrasonication. Sonication can be provided in two forms, mild sonication in a bath or high-power sonication using a tip. Solution processing relies on the efficient dispersion of the nanotubes in the relevant solvent. Solvents are usually chosen based on the solubility of the polymer. As pristine carbon nanotubes do not easily disperse in most solvents a surfactant is often employed to disperse the nanotubes before mixing with the polymer solution [49, 50]. Nanotubes have also been dispersed in polymer solutions while insoluble in the solvent alone[51].

Studies using this method and non-functionalised nanotubes with various polymers [49, 51-56] have shown increases in the Young's Modulus of the composites (which is a marker of mechanical reinforcement) at nanotube loading levels of between 1 and 60 wt %, usually with between a 1 and 3.8 times increase of the Young's modulus. At 1wt% loadings Qian et al. [53] observed an increase in the modulus of polystyrene from 1.62 to 1.69GPa, the tensile strength of their composites also increased from 12.8 to 16MPa. They observed both fracture and pull out of the nanotubes on fracture of the composite suggesting non-uniform bonding. Studies on a methylethyl-methacrylate co-polymer reinforced with MWNTs [57] gave a modulus increase of 3.29 times from 0.71GPa to 2.34GPa. The MWNTs were dispersed using a surfactant before being added to the polymer.

Where sonication was used to disperse MWNTs in polyvinylalcohol (PVA) water solutions [51] the modulus was observed to increase by a factor of 3.6 to 7.04GPa at 0.6% volume nanotubes with a strength enhancement from 81 to 348MPa. Microscopy study indicated nanotube pullout but in this case a layer of polymer was still present around the nanotubes. This suggests the presence of interfacial crystallinity which aids reinforcement.

Melt processing is an alternative preparation method for insoluble polymers and involves mixing nanotubes with a viscous liquid form of polymer by shear mixing. This method is simple and fast and is compatible with industrial processing. It is particularly suitable for use with thermoplastics as they soften when heated. Amorphous polymers can be processed above their glass transition temperature while semi-crystalline polymers must

be heated above their melt temperature to induce sufficient softening. After mixing, samples can be prepared by moulding or extrusion techniques.

Lower increases in Young's Modulus are generally observed for melt processed composites[58-61]. CVD MWNTs melt mixed in polystyrene gave a modulus increase of 2.25 times on the addition of 25wt% nanotubes[59]. The addition of only 0.75wt% SWNTs to polypropylene observing the modulus increase from 0.85GPa to 1.19GPa[60]. Composite fibres are also often prepared by melt processing methods[62, 63] and generally show similarly lower reinforcement levels. The production process for fibres can act to align the nanotubes within the fibre. SWNT and polypropylene were used by Moore et al. [62] to produce fibres that were further drawn to improve nanotube alignment, they observed a 2.29 times increase in the modulus with 1 wt% nanotubes. The poorer reinforcement affects of melt processed composites are in part due to poor nanotube dispersion within the polymer and problems with nanotubes sticking to the walls of the processing equipment.

Composites containing functionalised nanotubes have shown the most positive reinforcement results. The graphene like surface of a carbon nanotube is relatively smooth and so quite difficult for a polymer to adhere to. In addition to this, nanotubes as previously mentioned bundle together, lowering the surface area available to the polymer and providing reinforcement through bundles which have lower mechanical properties than individual tubes. Functionalisation aids both dispersion and interaction between the polymer and the nanotubes in a composite material, and so increases the stress transfer between the nanotubes and their host.

Work by Hwang et al[15] using polymethyl-methacrylate (PMMA) grafted MWNTs in PMMA showed a ten times modulus increase to 29GPa on the addition of 20 wt% CNTs, with an observed dY/dV_f value of 115GPa. The nanotubes failed by "sword from sheath" behaviour suggesting good interfacial stress transfer as the nanotube polymer bond did not fail [37]. Small amounts of hydroxyl functionalised SWNTs were used by Lui et al [64] to reinforce PVA with a reinforcement value (dY/dV_f) of 305 GPa. A reinforcement value of ~380GPa was achieved by Bhattacharyya et al [47] by grafting a protein onto MWNTs and mixing them with PVA.

In addition to these standard methods of composite preparation there are a few alternatives such as coagulation and electro spinning, layer by layer deposition and infiltration methods. Variations on the last two have been made possible in this work through recent advances in dispersion technology.

The basic infiltration method begins as a carbon nanotube film or bucky paper. Bucky papers have traditionally been prepared by the vacuum filtration of a nanotube surfactant water dispersion [65]. This carbon nanotube paper is then taken and soaked in a polymer solution to allow intercalation of the polymer into the considerable free volume (~70%) of the paper [13]. This results in very high volume fraction composite material [66].

2.4.3 Theory of Electrical Conduction in Nanotube Polymer Composites

The majority of polymers are insulating in nature as their bonds are generally arranged in such a way that no electrons are free to conduct electricity. Polymers that are conductive have many uses as they combine the electrical properties of a metal with the low density and processability of a polymer.

Insulating polymers can be made conductive by the addition of a conductive filler. Silver, nickel, platinum, gold, palladium and carbon are all common fillers. One advantage of composites over inherently conductive polymers is that the filler can simultaneously provide mechanical reinforcement along with increased conductivity.

Percolation theories are frequently applied to describe this insulator-to-conductor transition in composites comprising of conductive fillers in an insulating matrix and will be discussed in the following section.

2.4.3.1 Percolation Theory

Percolation theory describes random systems which have a sharp phase transition at which long-range connectivity suddenly appears or disappears[67]. The point at which the

transition occurs is called the percolation threshold. This usually occurs over a small concentration range and depends on many factors including the connectivity of the phases, the size and shape of each phase and the wetting behaviour of the phases.

In order for a current to flow through an insulating polymer the filler particles must form a complete pathway.

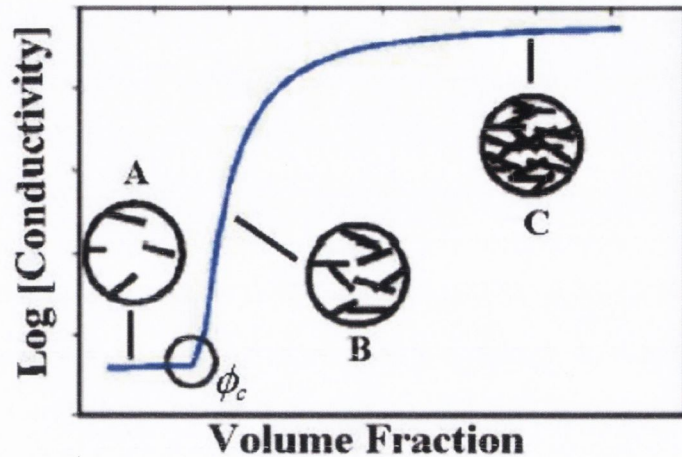


Figure 2.11 Predicted dependence of conductivity on the concentration of filler particles in an insulating matrix. Below the percolation threshold (ϕ_c) **A**, no conducting network exists. Above ϕ_c , **B**, long range conductivity begins to appear and conduction occurs. At **C** multiple conductive paths exist and the conductivity increases slowly with increasing filler content.

For conductive fillers in an insulating polymer matrix, the percolation threshold, ϕ_c , is defined as the filler concentration at which the composite conductivity begins to increase above that of the polymer. Just above ϕ_c the conductivity starts to rise slowly, but as the concentration of filler material, ϕ , is increased further, the conductivity rises sharply as more parallel pathways appear, often by several orders of magnitude. This is illustrated in figure 2.11. This increase in the conductivity of the system can be described by the percolation law in equation 2.16, but this is only valid in the critical region near the percolation threshold, where $|\phi - \phi_c| \ll 1$.

$$\sigma = \sigma_0 (\phi - \phi_c)^t$$

2.16

t is the critical conductivity exponent, and σ_0 is related to the conductivity of the filler. σ_0 is an extrapolation of the percolation law to 100% filler material and is not necessarily equal the conductivity of the pure filler material, as the percolation law is not valid that far from the percolation threshold, ϕ_c . Conductance barriers between the filler particles will reduce the conductivity of the system and have been assigned as the cause of low values for σ_0 [68]. The exponent t is expected to depend on sample dimensionality with calculated values of $t = 1.33$ and $t = 2.0$ in two and three dimensions, respectively[69].

The volume fraction of filler required for percolation depends on the conductivity and importantly on the shape of the filler material [70]. Spherical particles require a higher loading, whereas fibres link up more efficiently and reach percolation at much lower levels. Excluded volume theories have been developed to explain the dependence of the percolation threshold on the geometry of the filler particles. The excluded volume is defined as the volume around an object into which the centre of a similar object is not allowed to enter if overlapping of the two objects is to be avoided [71]. For spheres, it can be shown that V_{ex} is eight times the volume of the sphere, as it relates to twice the radius.

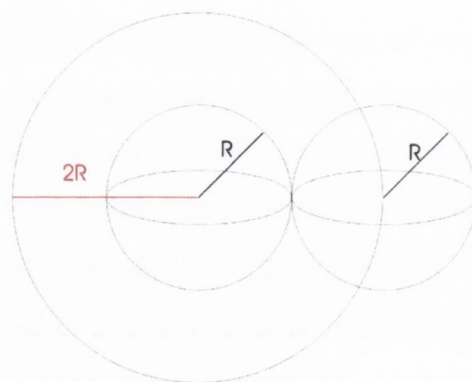


Figure 2.12 Excluded volume of a sphere

In the case of nanotubes, which can be approximated as prolate ellipsoids, the derivation of the excluded volume has dependence on both the nanotube length and diameter [72], this in turn can be related to the percolation threshold as

$$\phi_c \sim 0.6 d/L \qquad 2.17$$

This suggests that due to the high aspect ratio of carbon nanotubes very low percolation thresholds can be expected on their inclusion in an insulating matrix.

2.4.4 Conductivity in Carbon Nanotube Polymer Composites

Extremely low percolation thresholds have been reported for carbon nanotube polymer composites, as low as 2.5×10^{-3} wt% for un-entangled multiwalled-nanotubes (MWNT) in epoxy[39]. The maximum conductivities achieved in that and similar studies are low. Typically maximum values range between 1.4×10^{-5} S/m[73] and 1000 S/m, the latter value for a sample containing 10wt% nanotubes[74]. The vast majority of results have appeared at the lower end of this range, often due to polymer tunnelling barriers[73] which limit inter-tube charge transport. Such low conductivities may not be suitable for many applications that hope to utilise the high electrical conductivity of carbon nanotubes. Nanotube only films have displayed much higher conductivities, like those prepared by Wu et al. who measured values of 6.6×10^5 S/m[75]. The electrical properties of high load composites are therefore of interest and are discussed in chapters 4 and 6.

2.5 Carbon Nanotube Macrostructures

Composites are not the only way in which to arrange carbon nanotubes in a macroscopic form. Several preparation methods take advantage of the fact that nanotubes are inclined to bundle together these include carbon nanotube fibres and carbon nanotubes sheets [76].

2.5.1 Carbon Nanotube Fibres

Macroscopic carbon nanotube fibres have the potential to form high-strength, lightweight, thermally and electrically conducting structural elements. Futuristic applications such as space tethers and the space elevator [77] will require ultra-strong SWNT fibres but many other applications will require multifunctional properties without such high strengths [78]. The potentially good electrical properties of nanotube ropes may be used for highly efficient transmission of electricity over long distances. Their thermal properties may be exploited in microelectronic applications where thermal management is an increasing problem as miniaturization progresses [77].

Continuous fibres consisting predominantly or solely of SWNTs have been produced by solution spinning. Several research groups have used solution spinning to produce bulk quantities of SWNT fibres with lengths of 1 m or above.

The first truly continuous process for making fibres composed primarily or solely of SWNTs was developed by Poulin et al [79]. This process produced fibres composed of a network of SWNTs and a polymer, typically polyvinyl alcohol (PVA) which could be removed by washing and heating. The fibres had an electrical conductivity of 1000S/m. Fibres have also been spun from DNA stabilized SWNT dispersions [80]. A Young's modulus of 19 GPa, and a tensile strength of 130 MPa was achieved in this study; these values are twice those achieved for fibres spun from SWNT-SDS dispersions. However, the electrical resistivity of fibres produced from the DNA-stabilized dispersions was more than 50% higher than that of those produced from the SDS-stabilized suspensions.

Highly aligned fibres consisting solely of SWNTs have also been produced by wet-spinning SWNT superacid dispersions [81, 82]. The direct protonation of singlewall carbon nanotubes in superacids allows them to be dispersed at more than an order of magnitude higher concentration than that typically achieved in surfactants (8wt%). The fibre is formed by pushing the dispersion through a 125 μ m syringe needle into a diethyl ether coagulation bath [82]. A Young's modulus of 120 GPa and tensile strengths of 120 MPa were achieved for these fibres which were on the order of 50 micrometers in diameter and tens of meters in length. These fibres demonstrated conductivities of 5×10^5 S/m.

2.5.2 Carbon Nanotube Bucky Papers

Carbon nanotubes can also be macroscopically arranged in the form of a Bucky paper. A dilute nanotube dispersion of some kind, most commonly a water surfactant dispersion, is filtered through a filter paper leaving behind an entanglement of nanotubes. This residue is a Bucky paper. Bucky Papers are very promising materials [76] having demonstrated actuation properties [83], high conductivities of up to $6.6 \times 10^5 \text{S/m}$ [75] and potential as transparent electrodes [84]. Strengths and Youngs' moduli of up to 15MPa and 2GPa respectively have been observed for these structures [85]. This thesis as a whole is a study of carbon nanotubes in this macroscopic form.

2.6 Conclusions

As discussed in the previous sections carbon nanotubes are both interesting and very promising for material scientists. However problems involving their dispersion and adequate stress transfer in polymer matrices need to be addressed.

Chapters 4 and 6 of this thesis concern themselves with the study of high volume fraction composites prepared through the vacuum filtration of a nanotube polymer dispersion, a one step version of the previously described infiltration method. The advantage of this new method is that neither a surfactant nor second soaking step is required.

In chapter 5 the control factors of the mechanical and electrical properties of Bucky paper are investigated.

Chapter 6 also investigates a layer by layer deposition method. This consists of thin alternate layers of nanotube dispersion and polymer solution being deposited one on top of the other. This method also facilitates composites of high nanotube volume fractions.

2.7 References

- [1] S. Iijima, *Nature* **1991**, 354, 56.
- [2] A. Oberlin, M. Endo, T. Koyama, *Journal of Crystal Growth* **1976**, 32, 335.
- [3] N. T. V. G. M. P. Dimitrios Tasis, *Chemistry - A European Journal* **2003**, 9, 4000.
- [4] J. P. Lu, *Phys. Rev. Lett. JI - PRL* **1997**, 79, 1297.
- [5] Y. Min-Feng, *Journal of Engineering Materials and Technology* **2004**, 126, 271.
- [6] J. M. Xu, *Infrared Physics & Technology* **2001**, 42, 485.
- [7] M.-F. Yu, O. Lourie, M. J. Dyer, K. Moloni, T. F. Kelly, R. S. Ruoff, *Science* **2000**, 287, 637.
- [8] W. D. Callister, *Materials & Design* **1991**, 12, 59.
- [9] J. P. Lu, *Journal of Physics and Chemistry of Solids* **1997**, 58, 1649.
- [10] B. T. Kelly, *Physics of Graphite*, London: Applied Science **1981**.
- [11] M. M. J. Treacy, T. W. Ebbesen, J. M. Gibson, *Nature* **1996**, 381, 678.
- [12] E. W. Wong, P. E. Sheehan, C. M. Lieber, *Science* **1997**, 277, 1971.
- [13] J. N. Coleman, W. J. Blau, A. B. Dalton, E. Munoz, S. Collins, B. G. Kim, J. Razal, M. Selvidge, G. Vieiro, R. H. Baughman, *Applied Physics Letters* **2003**, 82, 1682.
- [14] J. N. Coleman, U. Khan, W. J. Blau, Y. K. Gun'ko, *Carbon* **2006**, 44, 1624.
- [15] G. L. Hwang, Y. T. Shieh, K. C. Hwang, *Advanced Functional Materials* **2004**, 14, 487.
- [16] J. W. G. Wilder, L. C. Venema, A. G. Rinzler, R. E. Smalley, C. Dekker, *Nature* **1998**, 391, 59.
- [17] B. Q. Wei, R. Vajtai, P. M. Ajayan, *Applied Physics Letters* **2001**, 79, 1172.
- [18] V. N. Popov, *Materials Science and Engineering: R: Reports* **2004**, 43, 61.
- [19] Z. Zhang, C. Dewan, S. Kothari, S. Mitra, D. Teeters, *Materials Science and Engineering B* **2005**, 116, 363.
- [20] W. A. de Heer, A. Châtelain, D. Ugarte, *Science* **1995**, 270, 1179.
- [21] J. B. Michael, A. W. Peter, T. C. Daniel, K. A. Smith, E. S. Richard, "Gas-phase production of carbon single-walled nanotubes from carbon monoxide via the HiPco process: A parametric study", **2001**.
- [22] R. Saito, G. Dresselhaus, M. S. Dresselhaus, *Physical Properties of Carbon Nanotubes*, Imperial College Press, London **1998**.
- [23] G. S. Duesberg, J. Muster, H. J. Byrne, S. Roth, M. Burghard, *Applied Physics A: Materials Science & Processing* **1999**, 69, 269.
- [24] M. Holzinger, A. Hirsch, P. Bernier, G. S. Duesberg, M. Burghard, *Applied Physics A: Materials Science & Processing* **2000**, 70, 599.
- [25] T. W. Ebbesen, P. M. Ajayan, H. Hiura, K. Tanigaki, *Nature* **1994**, 367, 519.
- [26] E. Dujardin, E. T. W., K. Ajit, T. M. M. J., *Advanced Materials* **1998**, 10, 611.
- [27] J. L. Zimmerman, R. K. Bradley, C. B. Huffman, R. H. Hauge, J. L. Margrave, *Chem. Mater.* **2000**, 12, 1361.
- [28] A. C. Dillon, T. Gennett, K. M. Jones, J. L. Alleman, P. A. Parilla, M. J. Heben, *Advanced Materials* **1999**, 11, 1354.
- [29] M. Monthieux, B. W. Smith, B. Burteaux, A. Claye, J. E. Fischer, D. E. Luzzi, *Carbon* **2001**, 39, 1251.
- [30] I. W. Chiang, B. E. Brinson, R. E. Smalley, J. L. Margrave, R. H. Hauge, *J. Phys. Chem. B* **2001**, 105, 1157.

- [31] H. Hu, B. Zhao, M. E. Itkis, R. C. Haddon, *J. Phys. Chem. B* **2003**, *107*, 13838.
- [32] J. Zhang, H. Zou, Q. Qing, Y. Yang, Q. Li, Z. Liu, X. Guo, Z. Du, *J. Phys. Chem. B* **2003**, *107*, 3712.
- [33] R. H. Baughman, A. A. Zakhidov, W. A. de Heer, *Science* **2002**, *297*, 787.
- [34] R. Andrews, M. C. Weisenberger, *Current Opinion in Solid State and Materials Science* **2004**, *8*, 31.
- [35] Z. X. Jin, S. H. Goh, G. Q. Xu, Y. W. Park, *Synthetic Metals* **2003**, *135-136*, 735.
- [36] N. O. V. Plank, R. Cheung, *Microelectronic Engineering* **2004**, *73-74*, 578.
- [37] S. Giordani, S. D. Bergin, V. Nicolosi, S. Lebedkin, M. M. Kappes, W. J. Blau, J. N. Coleman, *J. Phys. Chem. B* **2006**, *110*, 15708.
- [38] R. H. Baughman, A. A. Zakhidov, W. A. de Heer, *Science* **2002**, *297*, 787.
- [39] J. K. W. Sandler, J. E. Kirk, I. A. Kinloch, M. S. P. Shaffer, A. H. Windle, *Polymer* **2003**, *44*, 5893.
- [40] M. Cinke, J. Li, B. Chen, A. Cassell, L. Delzeit, J. Han, M. Meyyappan, *Chemical Physics Letters* **2002**, *365*, 69.
- [41] B. Gao, C. Bower, J. D. Lorentzen, L. Fleming, A. Kleinhammes, X. P. Tang, L. E. McNeil, Y. Wu, O. Zhou, *Chemical Physics Letters* **2000**, *327*, 69.
- [42] A. A. White, S. M. Best, I. A. Kinloch, *Int. J. Appl. Ceram. Technol.* **2007**, *4*, 1.
- [43] G. After Odian, *Principles of Polymerisation*, Wiley, New York **1991**.
- [44] H. L. Cox, *British Journal of Applied Physics* **1952**, *3*, 72.
- [45] J. L. K. J. C. Halpin Affdl, *Polymer Engineering & Science* **1976**, *16*, 344.
- [46] R. Blake, Y. K. Gun'ko, J. Coleman, M. Cadek, A. Fonseca, J. B. Nagy, W. J. Blau, *J. Am. Chem. Soc.* **2004**, *126*, 10226.
- [47] S. Bhattacharyya, C. Sinturel, J. P. Salvetat, M. L. Saboungi, *Applied Physics Letters* **2005**, *86*, 113104.
- [48] K. P. Ryan, M. Cadek, V. Nicolosi, S. Walker, M. Ruether, A. Fonseca, J. B. Nagy, W. J. Blau, J. N. Coleman, *Synthetic Metals* **2006**, *156*, 332.
- [49] A. Dufresne, M. Paillet, J. L. Putaux, R. Canet, F. Carmona, P. Delhaes, S. Cui, *Journal of Materials Science* **2002**, *37*, 3915.
- [50] O. Probst, E. M. Moore, D. E. Resasco, B. P. Grady, *Polymer* **2004**, *45*, 4437.
- [51] J. N. Coleman, *Advanced Functional Materials* **2004**, *14*, 791.
- [52] M. S. P. Shaffer, A. H. Windle, *Advanced Materials* **1999**, *11*, 937.
- [53] D. Qian, E. C. Dickey, R. Andrews, T. Rantell, *Applied Physics Letters* **2000**, *76*, 2868.
- [54] M. Cadek, J. N. Coleman, V. Barron, K. Hedicke, W. J. Blau, *Applied Physics Letters* **2002**, *81*, 5123.
- [55] B. Safadi, R. Andrews, E. A. Grulke, *Journal of Applied Polymer Science* **2002**, *84*, 2660.
- [56] J. N. Coleman, K. P. Ryan, M. Cadek, V. Nicolosi, S. Walker, M. Ruether, A. Fonseca, J. B. Nagy, W. J. Blau, *Synthetic Metals* **2006**, *156*, 332.
- [57] C. Velasco-Santos, A. L. Martinez-Hernandez, F. Fisher, R. Ruoff, V. M. Castano, *Journal of Physics D: Applied Physics* **2003**, *36*, 1423.
- [58] Z. Jin, K. P. Pramoda, G. Xu, S. H. Goh, *Chemical Physics Letters* **2001**, *337*, 43.
- [59] R. Andrews, D. Jacques, D. Qian, T. Rantell, *Acc. Chem. Res.* **2002**, *35*, 1008.
- [60] M. A. L. Manchado, L. Valentini, J. Biagiotti, J. M. Kenny, *Carbon* **2005**, *43*, 1499.

- [61] W. E. Dondero, R. E. Gorga, *Journal of Polymer Science, Part B: Polymer Physics* **2006**, *44*, 864.
- [62] Eric M. Moore, D. L. Ortiz, V. T. Marla, R. L. Shambaugh, B. P. Grady, *Journal of Applied Polymer Science* **2004**, *93*, 2926.
- [63] R. Haggemueller, H. H. Gommans, A. G. Rinzler, J. E. Fischer, K. I. Winey, *Chemical Physics Letters* **2000**, *330*, 219.
- [64] L. Liu, A. H. Barber, S. N. H. , D. Wagner, *Advanced Functional Materials* **2005**, *15*, 975.
- [65] J. Liu, A. G. Rinzler, H. Dai, J. H. Hafner, R. K. Bradley, P. J. Boul, A. Lu, T. Iverson, K. Shelimov, C. B. Huffman, F. Rodriguez-Macias, Y.-S. Shon, T. R. Lee, D. T. Colbert, R. E. Smalley, *Science* **1998**, *280*, 1253.
- [66] C. J. Frizzell, M. in het Panhuis, D. H. Coutinho, K. J. Balkus, A. I. Minett, W. J. Blau, J. N. Coleman, *Physical Review B* **2005**, *72*.
- [67] R. Zallen, *The Physics of Amorphous Solids*, Wiley, New York **1983**.
- [68] D. S. McLachlan, C. Chiteme, C. Park, K. E. Wise, S. E. Lowther, P. T. Lillehei, E. J. Siochi, J. S. Harrison, *Journal of Polymer Science, Part B: Polymer Physics* **2005**, *43*, 3273.
- [69] D. Stauffer, A. Aharony, *Introduction to Percolation Theory*, Taylor & Francis, **1991**.
- [70] I. Balberg, *Physical Review B* **1985**, *31*, 4053.
- [71] I. Balberg, *Physical Review B* **1998**, *57*, 13351.
- [72] I. Balberg, C. H. Anderson, S. Alexander, N. Wagner, *Physical Review B* **1984**, *30*, 3933.
- [73] B. E. Kilbride, J. N. Coleman, J. Fraysse, P. Fournet, M. Cadek, A. Drury, S. Hutzler, S. Roth, W. J. Blau, *Journal Of Applied Physics* **2002**, *92*, 4024.
- [74] R. Ramasubramaniam, J. Chen, H. Y. Liu, *Applied Physics Letters* **2003**, *83*, 2928.
- [75] Z. C. Wu, Z. H. Chen, X. Du, J. M. Logan, J. Sippel, M. Nikolou, K. Kamaras, J. R. Reynolds, D. B. Tanner, A. F. Hebard, A. G. Rinzler, *Science* **2004**, *305*, 1273.
- [76] M. Zhang, S. Fang, A. A. Zakhidov, S. B. Lee, A. E. Aliev, C. D. Williams, K. R. Atkinson, R. H. Baughman, *Science* **2005**, *309*, 1215.
- [77] B. I. Yakobson, R. E. Smalley, *Am. Scientist* **1997**, *85*, 324–337.
- [78] R. H. Baughman, *Science* **2000**, *290*, 1310.
- [79] B. Vigolo, A. Penicaud, C. Coulon, C. Sauder, R. Pailler, C. Journet, P. Bernier, P. Poulin, *Science* **2000**, *290*, 1331.
- [80] J. N. Barisci, M. Tahhan, G. Wallace, S. Badaire, T. Vaugien, M. Maugey, P. Poulin, *Advanced Functional Materials* **2004**, *14*, 133.
- [81] V. A. Davis, L. M. Ericson, A. N. G. Parra-Vasquez, H. Fan, Y. Wang, V. Prieto, J. A. Longoria, S. Ramesh, R. K. Saini, C. Kittrell, W. E. Billups, W. W. Adams, R. H. Hauge, R. E. Smalley, M. Pasquali, *Macromolecules* **2004**, *37*, 154.
- [82] L. M. Ericson, H. Fan, H. Peng, V. A. Davis, W. Zhou, J. Sulpizio, Y. Wang, R. Booker, J. Vavro, C. Guthy, A. N. G. Parra-Vasquez, M. J. Kim, S. Ramesh, R. K. Saini, C. Kittrell, G. Lavin, H. Schmidt, W. W. Adams, W. E. Billups, M. Pasquali, W.-F. Hwang, R. H. Hauge, J. E. Fischer, R. E. Smalley, *Science* **2004**, *305*, 1447.
- [83] U. Vohrer, I. Kolaric, M. H. Haque, S. Roth, U. Detlaff-Weglikowska, *Carbon* **2004**, *42*, 1159.

- [84] M. Rowell, A. T. Mark, D. M. Michael, P. Hans-Jurgen, D. Gilles, S. Niyazi Serdar, H. Liangbing, G. George, *Applied Physics Letters* **2006**, *88*, 233506.
- [85] P. G. Whitten, G. M. Spinks, G. G. Wallace, *Carbon* **2005**, *43*, 1891.

Chapter 3

Materials and Methods

3.1 Introduction

This chapter includes a brief description of the materials used throughout this thesis and outlines the experimental methods used to characterise them, and the nanotube (NT) and NT/Polymer films prepared from them.

3.2 Polymers

As discussed in section 2.3 polymers can be grouped into three major classes, plastics, fibres and elastomers. Two very different polymers were chosen for study in this work. The first was the thermoplastic polystyrene and the second was the elastomer polyurethane.

3.2.1 Polystyrene

Polystyrene $[\text{CH}_2\text{CH}(\text{C}_6\text{H}_5)]_n$ is a long chain non-conjugated hydrocarbon with every second carbon connected to a phenyl group (figure 3.1).

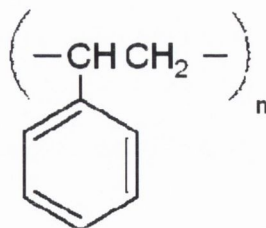


Figure 3.1 Chemical structure of polystyrene

In ordinary atactic polystyrene the phenyl groups are randomly distributed on both sides of the chain. This random positioning prevents the chains from ever aligning with sufficient regularity to achieve any crystallinity, so the plastic has no melting temperature, T_m . Polystyrene is a thermoplastic polymer meaning that it will soften when heated above its glass transition temperature (T_g), can be shaped and, on cooling, will harden into the form of its container or mould. Importantly, this is a repeatable process. Solid polystyrene is transparent, rigid and electrically insulating. The typical mechanical properties of polystyrene are shown in table 3.1. Polystyrene (PS) with a molecular weight of 350,000g/mol was purchased from Aldrich for use in this work.

3.2.2 Polyurethane

Polyurethane $[(-R_1-NHCOOR_2OOCHN-)_n]$ is a thermosetting elastomer, where R can be any organic molecule, figure 3.2.

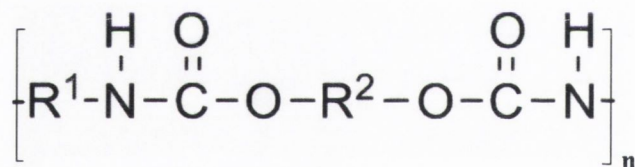


Figure 3.2 Chemical structure of polyurethane

It is an amorphous polymer which behaves as an elastomer above its glass transition temperature which is far below room temperature. An urethane linkage is produced by reacting an isocyanate group, $-N=C=O$ with a hydroxyl group, $-OH$. Polyurethanes are produced by the polyaddition reaction of a polyisocyanate and a polyalcohol (polyol) in the presence of a catalyst and other additives. Polyurethane is opaque, flexible and electrically insulating. The typical mechanical properties of polyurethane are listed in table 3.1. A polyurethane dispersion, in the form of a waterborne emulsion with particle size <3 microns was provided by Hydrosize[®] Technologies, Inc. (www.hydrosize.com).

Polymer	Youngs' Modulus GPa	Tensile Strength MPa	Strain at Break %	Toughness MPa
Polystyrene [1]	2.28-3.28	35.9-51.7	1.2-2.5	~0.21*
Polyurethane [2]	0.002	32.8	700	20-60

Table 3.1 Mechanical properties of polystyrene and polyurethane

3.3 Carbon Nanotubes

The properties of carbon nanotubes have already been discussed in chapter 2. Several varieties of unfunctionalised and functionalised tubes were used during the course of this work. Their names, production method, supplier and functionality are listed below in table 3.2.

Name	Production Method	Supplier	Functionality
Purified HiPCO SWNT	HiPCO	www.cnanotech.com	N/A
As Prepared (AP) Elicarb SWNTs	CVD	www.thomas-swan.co.uk	N/A
Annealed Elicarb SWNT	CVD	www.thomas-swan.co.uk	N/A
Nanolab DWNTs	CVD	www.nano-lab.com	N/A
Swent SWNTs	CVD	www.swnano.com	N/A
AP-SWNT	CVD	www.carbonsolution.com	N/A
P2-SWNT	CVD	www.carbonsolution.com	Lowly-COOH
P3-SWNT	CVD	www.carbonsolution.com	Highly-COOH (4-6 atomic% COOH [3])
P5-SWNT	CVD	www.carbonsolution.com	Octadecylamine (ODA)
P7-SWNT	CVD	www.carbonsolution.com	Polyethylene glycol (PEG)
P8-SWNT	CVD	www.carbonsolution.com	Polyaminobenzene Sulfonic Acid (PABS)

Table 3.2 Carbon nanotube supplier and information.

* Toughness value of Polystyrene from own work. Unavailable in literature.

3.4 Solvent Choice

As was previously mentioned in chapter two pristine nanotubes do not disperse in most common solvents. The noncovalent attachment of surfactants[4] is often used to facilitate dispersion. Surfactants have been found to form micelles around SWNTs, following a high power sonication step. The energy from the sonic tip disrupts the van der Waals forces that hold the NTs together and they debundle. The surfactants have a polar head group and an apolar tail. The head group is soluble in water and the tails are attracted to the surface of the nanotubes forming micelles. These micelles act as a protective sheath around the SWNTs shielding them from the solvent and preventing the rebundling that normally occurs due to the large surface energy difference between nanotube surface and the solvent[5].

When the use of a surfactant is not desirable specific amide solvents have been found to disperse carbon nanotubes [6], one of these is N-methyl-2-pyrrolidone (NMP). In this study by Giordani et al., it was found that using this solvent good quality SWNT dispersions could be routinely fabricated without the need for ultracentrifugation and that these dispersions were stable against both sedimentation and aggregation. AFM studies show that the nanotube bundle diameters tend to decrease with concentration until very small bundles are found at low concentrations[6]. The first polymer that was chosen for study in this work was polystyrene which is soluble in NMP.

When carbon nanotubes are functionalised it allows them to be dispersed in other solvents[7]. In this study the polyethylene glycol and the polyaminobenzene sulfonic acid functionalised nanotubes could be dispersed in water[8]. Where water was not an adequate solvent with which to disperse the carbon nanotubes organic solvents were used. The carboxylic acid functionalised nanotubes were dispersed in NMP. The octadecylamine nanotubes were dispersed in chloroform.

3.4.1 N-methyl-2-pyrrolidone (NMP)

N-methyl-2-pyrrolidone (NMP) is a solvent containing a 5-membered lactam structure, figure.3.3. It has a boiling point of 202 °C [9] and was purchased from Aldrich.

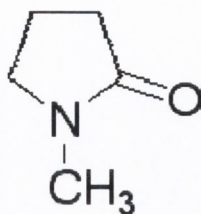


Fig.3.3 Chemical structure NMP.

3.4.2 Chloroform

Chloroform (CHCl₃) is a common lab solvent with a boiling point of ~60.5 °C [9] and was purchased from Aldrich.

3.5 Sonication

Throughout this work nanotube dispersions were prepared using ultrasonication. A sonic tip (or horn) provides sufficient energy to the nanotubes to break the van der Waals interactions between them (which are the cause of bundling[10]) and facilitate dispersion.

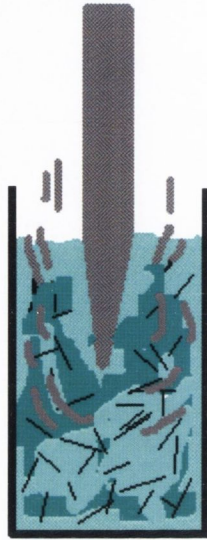


Fig.3.4 Schematic of NT dispersion through ultrasonication.

Dispersions were typically exposed to a sonication power of 120W at 60KHz for a few minutes. Mild sonication was also used by placing the dispersions in a sonic bath often for longer periods of time.

3.6 Buchner Filtration

Buchner filtration was used to prepare all the NT containing films described in chapters 4, 5 and 6. A schematic of the apparatus is shown in figure 3.5.

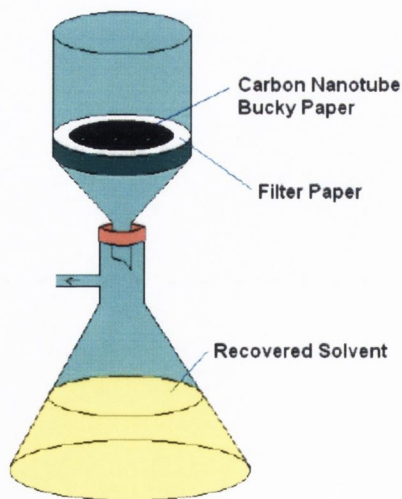


Fig. 3.5 Buchner filtration apparatus

A teflon filter paper is placed on the porous sintered glass of the Buchner funnel. The NT dispersion is poured onto the filter paper and a vacuum pulls the solvent through the filter leaving behind a mesh of entangled NTs.

3.7 Thermogravimetric Analysis

Thermogravimetric Analysis (TGA) is a technique often used to determine the thermal stability of a material. A sample is placed in a furnace on a sensitive balance and heated at a chosen rate. The furnace environment is controlled by air or nitrogen purging. A characteristic curve is obtained displaying mass against temperature. The mass of the sample decreases as the temperature increases due to oxidation. The derivative of this curve may show more than one distinct peak, especially in composite materials. Each peak may be assigned to a process involving a material in the composite and the area under the curve can be used to calculate the filler to matrix mass ratio of the composite.

In Chapters 4 and 6 a Perkin Elmer Thermogravimetric analyser Pyris 1 was used to calculate the nanotube mass fraction, m_f , of each composite film.

3.8 UV-Vis Absorbance Spectroscopy

Ultraviolet and visible (UV-vis) absorbance spectroscopy monitors the attenuation of a beam of light as it interacts with a sample. It is governed by the Beer-Lambert Law (eqn. 3.1) where the Absorbance, A , is related to the incident and transmitted intensities.

$$\frac{I}{I_0} = e^{-A} \quad 3.1$$

The Beer-Lambert law states that the absorbance of a solution is directly proportional to the solution's concentration. Thus UV/VIS spectroscopy can be used to determine the concentration of a solution.

On examining a NT or any other type of dispersion, the absorbance, A , is equal to αCl , where α is the extinction coefficient, C is the concentration and l is the length of the

cuvette. If the initial concentration of the NT dispersion is known, changes due to sedimentation over time or by an acceleration of this process by centrifugation result in a change in the value of A . As the path length l and extinction coefficients α do not change, the change in A is therefore proportional to the change in concentration C of the dispersion. In Chapter 6 a Cary 6000i UV-Vis Spectrometer was used to find post-centrifuge NT dispersion concentrations.

3.9 Raman Spectroscopy

Raman spectroscopy is a fingerprinting technique that gives information about the vibrational frequencies of a material and hence can be used to identify its composition. When monochromatic light is shone on a sample not all light is scattered at the same frequency as the incident light. The oscillating electric field of the incident wave can induce an oscillating dipole moment in the material and although the majority of the light is elastically (Rayleigh) scattered, some is Raman shifted to a higher or lower frequency. This occurs when the incident photons exchange energy with molecules in the sample. Whether a sample is Raman active or inactive depends on the polarisability of its electron cloud. For instance water is highly polar and hence its polarisability does not change as its molecules vibrate. Strong Raman scatterers have distributed electron clouds such as pi-bonds which are easily polarised. This change in polarisability is what causes a material to be Raman active. Raman spectroscopy is therefore a useful tool for the examination of CNTs. Several distinctive modes are observed for carbon nanotubes and are shown in figure 3.6.

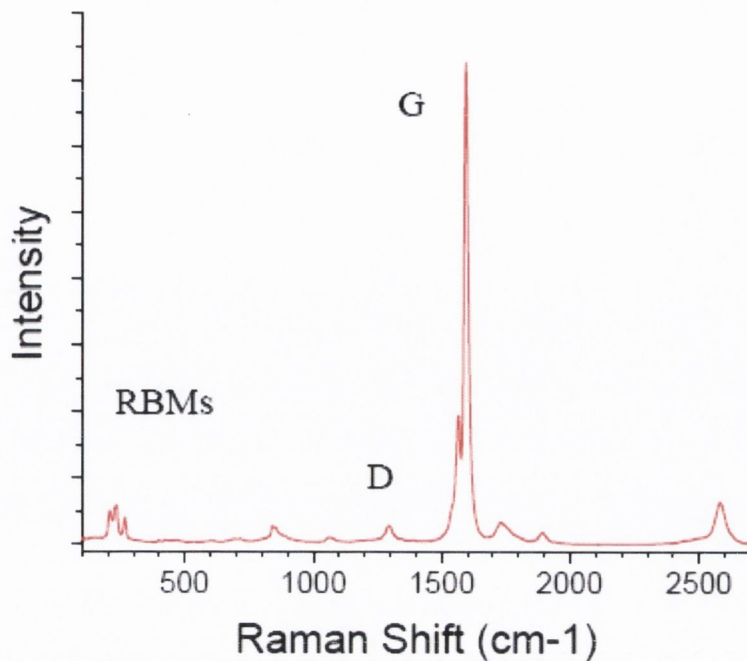


Figure 3.6 Typical Raman spectra for single-walled carbon nanotubes.

Raman active peaks are observed for SWNTs in the low frequency area of a Raman spectrum and are referred to as radial breathing modes (RBM). The RBM frequency is inversely proportional to the diameter of the tube, making it an important feature for determining the diameter distribution of a sample. Its absence in other graphitic forms makes it a useful diagnostic for confirming the presence of SWNTs in a sample.

The D- band is called a defect mode as it indicates the presence of sp^3 hybridised carbon. It usually occurs at 1280 cm^{-1} . The relative strength and width of the D band mode gives a qualitative measurement of how large a fraction of graphitic material and nanotubes with defects are present in a sample.

The G band is a tangential shear mode of carbon atoms. In graphite, there is one single G mode at $\sim 1580\text{ cm}^{-1}$. In carbon nanotubes, the single G band transforms into several modes due to the confinement of wave-vectors along the circumference. The quality of a carbon nanotube sample is often evaluated by comparing the D to G band intensity. For high quality samples, without defects and amorphous carbon, the D/G ratio is often below a couple of percent[11, 12]

In Chapter 5 Raman spectroscopy was carried out on various kinds of CNTs using a Horiba Jobin Yvon LabRam HR with the 633nm excitation wavelength laser.

3.10 Scanning Electron Microscopy

Scanning Electron Microscopy (SEM) involves scanning an electron beam across a sample line by line to build up an image of the sample. The basic principle of SEM is that a stream of electrons is formed and accelerated towards a specimen using a positive electrical potential. A cold field emission source is used as the electron source. A tip acts as a cathode and is usually made of an electrochemically etched length of single crystal tungsten wire. When a voltage is applied to the anode and intense field is experienced at the tip. This results in a potential barrier small enough for conduction electrons to tunnel out of the tungsten into the vacuum. A second anode is provided to accelerate the electrons to the desired total accelerating voltage, figure 3.7.

The beam is then confined and focused using metal apertures and magnetic lenses. When the beam hits the sample a detector monitors the backscattered secondary electrons emitted and converts them into a voltage which is applied to the grid of a cathode ray tube.

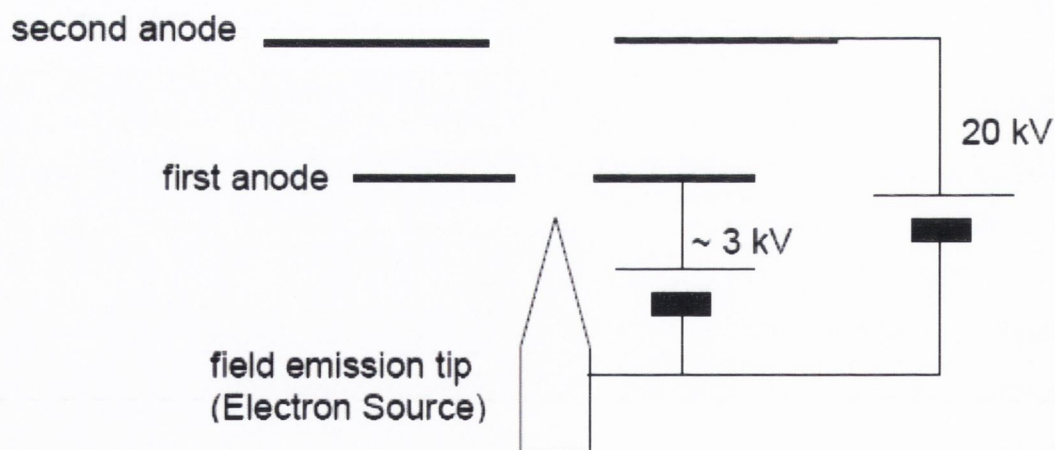


Fig.3.7 Scheme of a cold emission gun. The proximity of the first anode (the extraction anode) and the sharpness of the tip bring an intense electric field at the tip, capable of extracting the electrons by tunnelling; the second anode further accelerates the electrons.

The obtained images have a characteristic three-dimensional appearance and are useful for judging the surface structure of a sample. As samples are inundated by an influx of electrons, a charge will tend to accumulate unless the specimen is earthed. This is typically achieved by coating objects with a nanometer thick layer of gold.

In Chapters 4, 5 and 6 Scanning Electron Microscopy was performed on uncoated NT and NT/Polymer films using a Hitachi S-4300 Field Emission Scanning Electron Microscope.

3.11 Tensile Testing

Tensile testing is a direct way to characterise the mechanical properties of a material by applying an increasing force (stress) and measuring the elongation (strain) incurred. Alternatively the elongation can be incremented and the force required to achieve the strain can be measured. Deformation where stress (σ) and strain (ϵ) are proportional is called elastic deformation and is non-permanent elongation. Hookes law states that for elastic materials, stress is proportional to the strain at loads less than the yield point of the material. This constant of proportionality is Young's modulus (Y) and is calculated from the linear part of a stress/strain curve. The stress corresponds to the force per unit area (N/m^2) while strain is dimensionless – this means Y has the unit of stress (Pa). Other useful parameters are the toughness (T) and the ultimate tensile strength (σ_t). Ultimate tensile strength is the maximum stress applied before fracture of the sample. Toughness is calculated from the area under the stress strain curve and is the energy absorbed per unit volume at fracture.

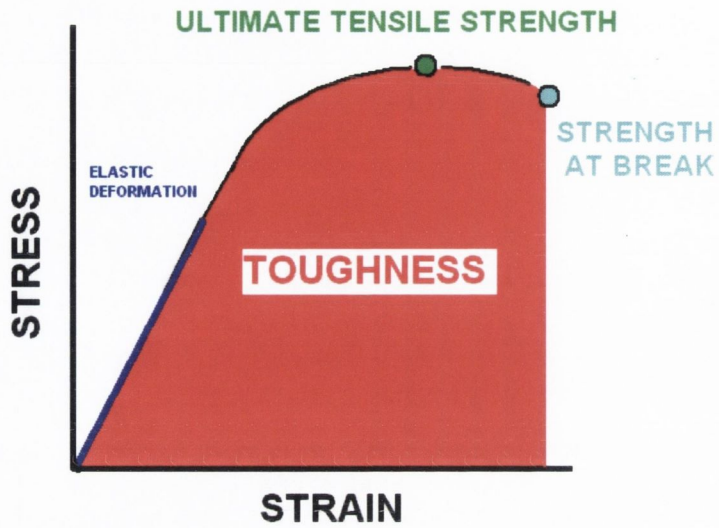


Figure 3.8 Illustrative stress-strain curve.

In chapters 4, 5 and 6 mechanical testing was performed using a Zwick tensile tester Z100 with a 100 N load cell.

3.12 References

1. Callister, W.D., *Materials science and engineering: An introduction (2nd edition)*. Materials & Design, 1991. **12**(1): p. 59.
2. www.hydosize.com.
3. www.carbonsolutions.com.
4. Liu, J., et al., *Fullerene Pipes*. Science, 1998. **280**(5367): p. 1253-1256.
5. O'Connell, M.J., et al., *Band Gap Fluorescence from Individual Single-Walled Carbon Nanotubes*. Science, 2002. **297**(5581): p. 593-596.
6. Giordani, S., et al., *Debundling of Single-Walled Nanotubes by Dilution: Observation of Large Populations of Individual Nanotubes in Amide Solvent Dispersions*. J. Phys. Chem. B, 2006. **110**(32): p. 15708-15718.
7. Tasis, D., et al., *Soluble Carbon Nanotubes*. Chemistry - A European Journal, 2003. **9**(17): p. 4000-4008.
8. Zhao, B., et al., *Synthesis and Characterization of Water Soluble Single-Walled Carbon Nanotube Graft Copolymers*. J. Am. Chem. Soc., 2005. **127**(22): p. 8197-8203.
9. www.sigmaaldrich.com.
10. Thess, *Uniform ropes of carbon nanotubes*. Science, 1996. **273**(5274): p. 405c-0.
11. Dillon, A.C., et al., *Systematic inclusion of defects in pure carbon single-wall nanotubes and their effect on the Raman D-band*. Chemical Physics Letters, 2005. **401**(4-6): p. 522-528.
12. Doorn, S.K., et al., *Raman Spectroscopy and Imaging of Ultralong Carbon Nanotubes*. J. Phys. Chem. B, 2005. **109**(9): p. 3751-3758.

Chapter 4

Carbon Nanotube Polystyrene Composites:

The observation of percolation-like scaling, far from the percolation threshold, in high volume fraction, high conductivity composite films.

4.1 Introduction and Relevant Background Literature

As has been discussed in Chapter 2 carbon nanotubes are ideal fillers in conducting and reinforced composites. In this chapter CNT polystyrene composites have been prepared and tested both mechanically and electrically. The emphasis of discussion is on the electrical results. Chapters 5 and 6 will focus more on the mechanical properties of bucky papers and bucky composites.

There have been many studies on low volume fraction composites where the addition of a very small amount of nanotubes substantially modifies the electrical properties of polymer matrices[1-9]. The critical filler concentration needed to achieve electrical conductivity, the percolation threshold, has been reported to be as low as 1.3×10^{-3} vol% for inorganic nanowires in PMMA[7] and 2.5×10^{-3} wt% for un-entangled multiwalled-nanotubes (MWNT) in epoxy[9]. However, the maximum conductivities achieved in these low volume fraction composites are commensurate with low nanotube loading levels. Typical maximum values range between 1.4×10^{-5} S/m[3] and 1000 S/m, the latter value for a sample containing 10wt% nanotubes[10]. The vast majority of results have appeared at the low end of this range, probably due to ever-present polymer tunnelling barriers[3] which limit inter-tube charge transport. Such conductivities are small relative to those observed for nanotube-only films, prepared by the vacuum filtration of a nanotube

dispersion, which display values up to 6.6×10^5 S/m[11]. Fewer studies have appeared on composites with volume/weight fractions above 20%[12-14], due to severe difficulties in maintaining nanotube dispersion.

In polymer nanotube composites mechanical reinforcement is often initially observed at low nanotube loading levels. Above a certain point aggregation of the nanotubes occurs changing the behaviour of the system and so affecting the properties of the composite. This effect can be seen in the work of Blond et al[15] on the addition of multi-walled nanotubes to Poly(methyl methacrylate), figure 4.1.

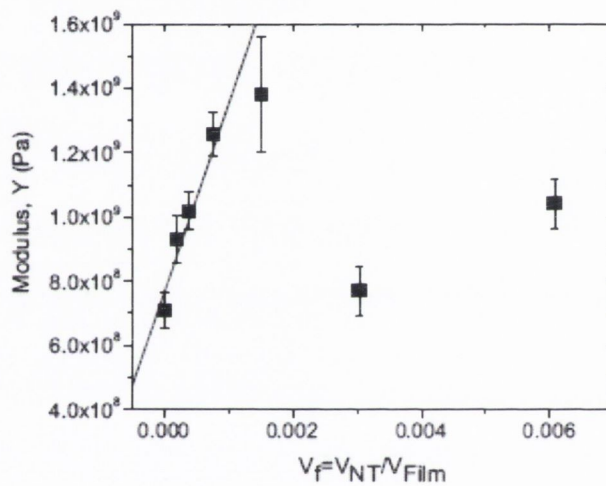


Fig.4.1 Youngs' modulus as a function of nanotube volume fraction in PMMA-MWNT composites[15]

Often carbon nanotube polymer films are cast from solution. A high polymer concentration is required, typically around 30mg/mL[15], this allows the preparation of free standing films suitable for comprehensive testing. In order to achieve a high volume fraction composite, a high nanotube concentration is then also necessary. However this means that the issue of nanotube aggregation becomes a serious problem making it virtually impossible to fabricate high mass fraction composites where the nanotubes remain well dispersed[16].

In this and subsequent chapters advantage has been taken of recent advances [16] in nanotube dispersion research. Giordani et al[16] have reported that SWNTs can be

dispersed in N-methyl-2-pyrrolidone (NMP), without aggregation at concentrations below ~ 0.02 mg/ml. They measured the absorbance of the supernatants of different nanotube NMP dispersions after a centrifugation process which removed aggregates. The mass fraction of nanotube material removed by centrifugation was, χ_{Agg} . This value was plotted against the original concentration of their dispersions. At high concentration, the fraction of material removed by centrifugation approaches one, but falls off gradually to close to zero for the low concentration samples. Visual inspection confirmed that centrifugation had removed the aggregates. The fact that $\chi_{\text{Agg}} \approx 0$ at low concentration would suggest that good dispersions can be obtained at low nanotube concentrations in NMP.

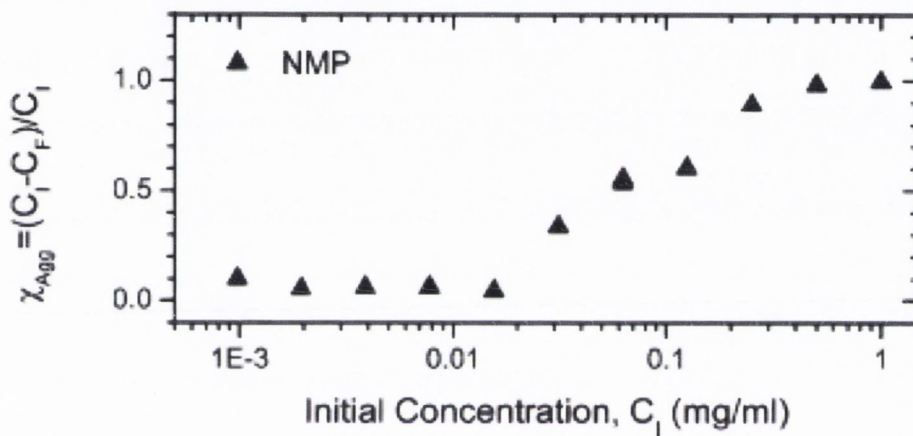


Figure 4.2 Fraction of the nanotube mass contained in large aggregates as a function of initial concentration[16].

In this work polymer has been added to similar dispersions to give composite dispersions which display minimal aggregation. However, these cannot be deposited to form films by the usual means, as the large solvent volumes involved are prohibitive. If a typical drop cast film were to be prepared using such low concentrations it would involve dropping several hundred layers. This combined with the high boiling point of NMP which is 202°C [17] makes the usual method of solution casting highly impractical.

In this chapter extremely high mass fraction polymer-nanotube composite films were prepared in a simple and straightforward way, achieving nanotube mass fractions of

between 22% and 82%. These films have extremely high conductivities, varying between ~ 100 and ~ 7000 S/m for the lowest and highest nanotube content composites respectively. The latter value is close to that measured for pure nanotube control films (mass fraction 100%) of ~ 9000 S/m. Furthermore, when the nanotube mass fraction is transformed into nanotube volume fraction (including the effect of film porosity) we observe percolation-like scaling of the conductivity with volume fraction. The conductivity scales with the volume fraction as a power law with exponent 2.2, extremely close to the value of 2.0 predicted by percolation theory[18] for three dimensional systems. More surprisingly, this scaling persists from the lowest nanotube content sample right up to the nanotube only film in contrast with the expectation that percolation-scaling breaks down at higher volume fractions.

In Section 4.2 of this chapter a method for producing relatively thick films of very high volume fraction nanotube content, commonly referred to as “Bucky Papers”, is described. Sections 4.3 to 4.5 investigate the composition, morphology and thermal properties of these films. Results of tensile testing are included in section 4.6. Finally the electrical results are presented in section 4.7 with further discussion in section 4.8.

4.2 Film Fabrication

Dispersions were prepared by adding purified HiPCO SWNTs to solutions of polystyrene (PS) in NMP at various mass fractions and sonicating for 3 min using a high-power ultrasonic tip.

To achieve a nanotube concentration of 0.0875mg/ml, one that reduces NT bundling while remaining practical, an initial dispersion of 0.35mg/ml was diluted twice, sonicating for 1 minute between steps. The dispersion concentration of 0.0875mg/ml involved using 400ml of NMP. The diluted dispersions underwent a further 4hrs sonication in a low-power ultrasonic bath followed by 1 minute under the sonic tip. The dispersions were then vacuum filtered through a Teflon filter paper (pore size= $0.45\mu\text{m}$), washed with dionised water and methanol and dried at ambient temperature for 12 hrs in a vacuum oven. The filtration times for the dispersions were between several hours and three days depending on the amount of the polymer that was included. It should be noted that much polymer was lost during filtration. The films were free standing when peeled from the filter paper and were

cut into strips of width 2.2mm and lengths of several centimetres using a non-shear method. A photograph of the nanotube only bucky paper is shown in figure 4.3.

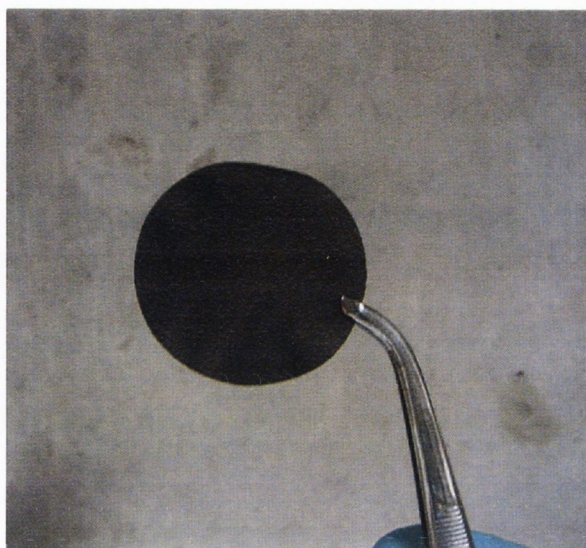


Figure 4.3 A Carbon Nanotube Bucky Paper

A polystyrene only film was also prepared by diluting PS at high concentrations and dropping 4 layers onto a teflon boat. A polystyrene only film cannot be prepared by Buchner filtration as the polymer chains can pass through the pores of the filter paper.

4.3 Porosity Measurements

The dimensions and masses of all films were measured using a digital micrometer and a microbalance. Film thicknesses ranged from 50 μm to 290 μm . The density of each film, ρ_{film} , was calculated. Porosity, P , was calculated from $P = 1 - \rho_{film} / \rho_{NT}$, where the nanotube density was taken to be $\rho_{NT} = 1500 \text{ kg/m}^3$ [19]. The porosities of the prepared films ranged from 54 to 78%.

4.4 Thermogravimetric Analysis of Composite Films

Thermogravimetric analysis (TGA) was employed to calculate the nanotube mass fraction, m_f , of each film as not all the polymer in the original dispersion remained part of the final film. Neglecting the region of the mass versus temperature curve where the solvent

is removed from the sample, the normalized nanotube peak was subtracted from the original composite curve. This new curve was integrated along with the original composite curve and the ratios of their areas used to find the percentage polystyrene present in the composite and so in turn the nanotube mass fraction.

A second method of analysis was also employed to ensure accuracy. Purified HiPCO nanotubes contain an amount of residual catalyst material from their production, namely iron, Fe. The ratio of nanotube to iron content should be constant throughout the nanotube soot. Considering both the reference NT only film and a composite film the relation between the nanotubes present and the remaining catalyst material should be the same, equation 1.

$$\frac{M_{\text{NT in Composite}}}{M_{\text{Fe in Composite}}} = \frac{M_{\text{NT in Reference}}}{M_{\text{Fe in Reference}}} \quad 4.1$$

The amount of nanotubes in the composite is the mass of the composite minus the mass of the polymer present. (All values of mass were taken after the point where all solvent had burned off)

$$\frac{\text{Total } M_{\text{Composite}} - M_{\text{Polymer in Composite}}}{M_{\text{Fe in Composite}}} = \frac{M_{\text{NT in Reference}}}{M_{\text{Fe in Reference}}} \quad 4.2$$

Simply by rearranging equation 4.2 the mass of polymer in the composite can be found.

$$\text{Total } M_{\text{Composite}} - \left(\frac{M_{\text{NT in Reference}}}{M_{\text{Fe in Reference}}} \right) M_{\text{Fe in Composite}} = M_{\text{Polymer in Composite}} \quad 4.3$$

Both methods consistently agree within 2 % of each other. Composites were found to have nanotube mass fractions between 22% and 82%.

To achieve low nanotube mass fractions, large excesses of PS had to be used to counter polymer loss during film formation by filtration, figure 4.4.

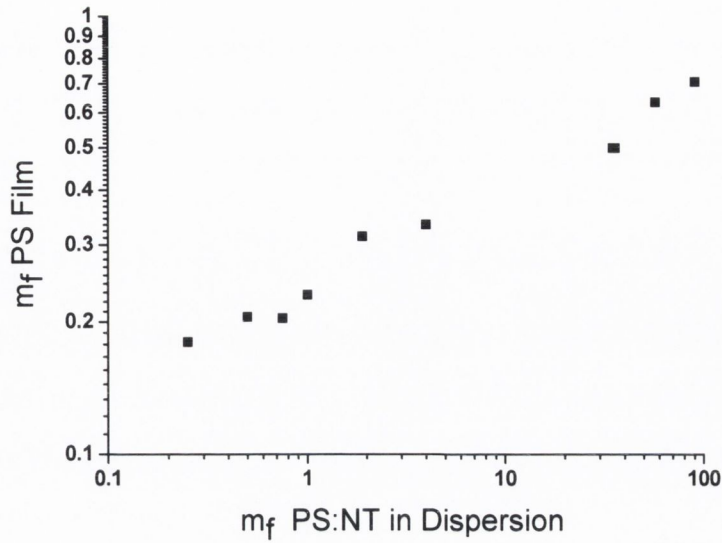


Figure 4.4 PS mass fraction film as a function of mass fraction PS:NT ratio of dispersion.

A representative TGA curve of the nanotube $m_f = 0.77$ composite along with the nanotube only reference film and the drop cast polystyrene film shown in figure 4.5.

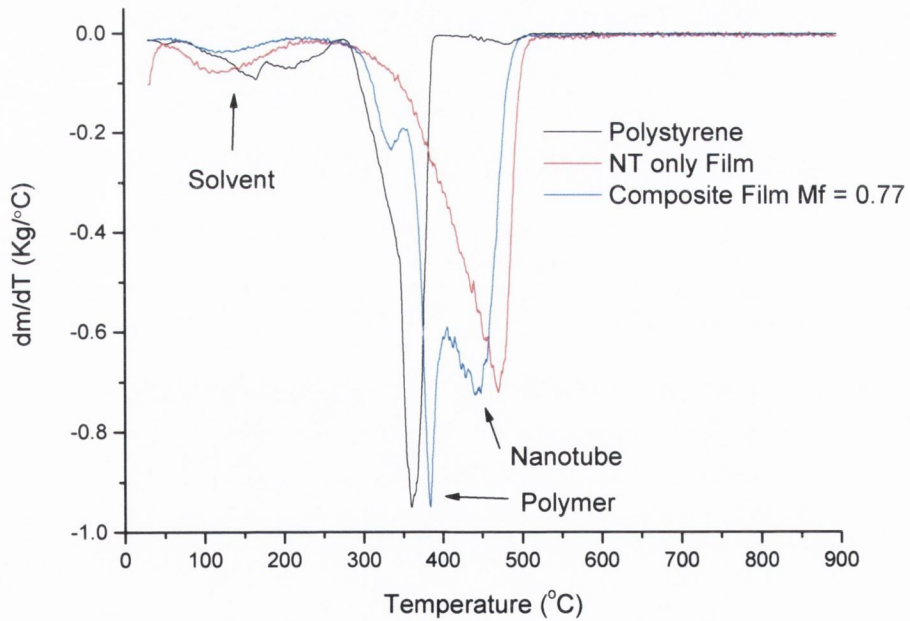


Figure 4.5 Derivative TGA curves of polystyrene, nanotube only and composite films.

From the TGA curves a small amount of trapped solvent can be seen, an average of $4.0\% \pm 2.4\%$. This is probably a combination of both NMP and water, and is to be expected when dealing with such porous material.

4.5 Scanning Electron Microscopy of Composite Films

Scanning electron microscopy (SEM) images were taken of all films, the software package Image Tool was used to analyse them. An image of the surface of one of the composite films ($m_f=0.77$) is shown in figure 4.6A. For comparison purposes, an image of the nanotube only bucky paper is shown in figure 4.6B.

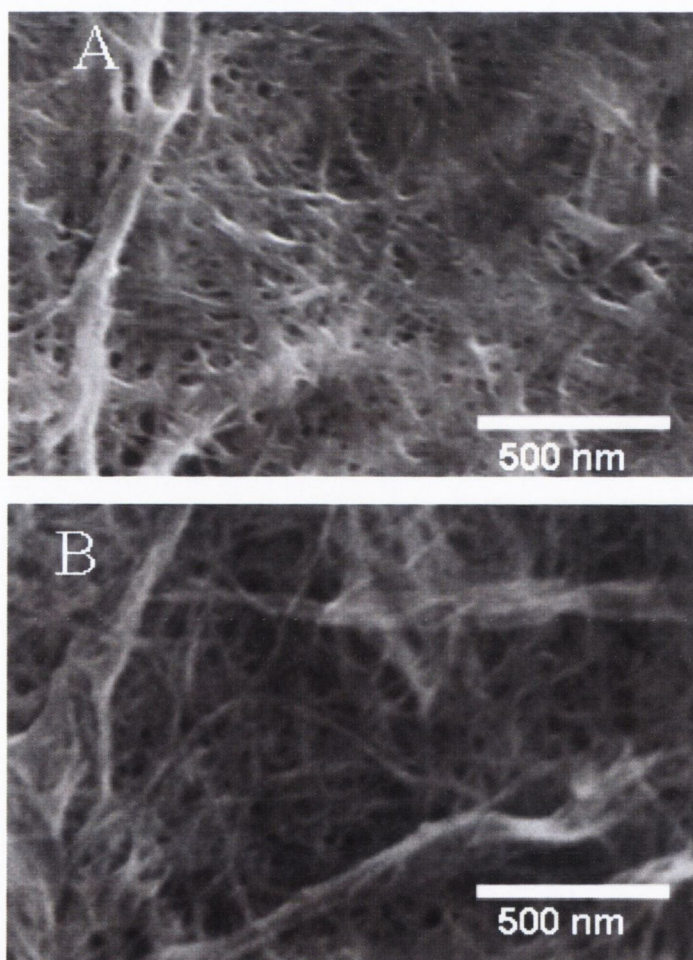


Figure 4.6. SEM images of A) a high volume fraction composite film ($m_f=0.77$), B) a film of nanotube-only Bucky paper.

It can be seen that the nanotube-only film consists of a network of bundles with a mean diameter of 13 ± 3 nm. At the nanotube concentrations used to prepare these films, AFM measurements show that the typical bundle size in solution is approximately 8nm[16]. The fact that the bundles observed in the film are slightly larger shows that slight aggregation occurs during film formation. However, this effect is relatively small. As the bundles in NMP dispersions are known to have lengths of >1 micron [16], these diameters mean that the bundles have aspect ratios of at least 75. It is also clear from this image that these films contain large numbers of irregular pores with diameters in the range 10-100nm. This is in agreement with previous measurements on bucky paper and indicates significant porosity[20]. The importance of the porosity of the films will be discussed further in section 4.8.

It may be noted that it would be possible to significantly reduce the bundle size in solution by working at lower concentrations. Recent work has shown that mean bundle diameters of ~ 2 nm can be achieved in NMP at concentrations below 5×10^{-3} mg/ml[16]. However, fabrication of thick films from solutions of such low concentrations becomes more problematic because as the concentration is lowered very long filtration times are required to filter off the excess solvent. In addition, working with low concentration dispersions, attaining reproducible high power sonication on the litre scale becomes a problem. The Ultra Sonic Processor used throughout this work can handle a maximum volume of 25ml at any one time.

While the image of the composite surface (4.6A) looks similar to that of the nanotube only film, there are some significant differences. The 1-dimensional objects making up the film are much less well defined compared to those found in the nanotube only sample. This is largely because they have large diameters, with means between 13 and 22 nm, depending on the polymer content of the film. In addition, while pores are still visible, they are smaller compared to the nanotube-only film with typical diameters in the 10-30 nm range. Both of these differences can be explained by the presence of a polymer coating on the SWNT bundles of the composite film. However, the combination of thicker objects and narrower pores would suggest that the coating forms in the drying phase.

4.6 Mechanical Analysis of Composite Films

Stress-strain measurements were made of all nanotube containing films using a Tensile Tester with a 100 N load cell and cross-head speed of 0.5 mm/min (Figure 4.8). Measurements were also made of the drop cast polystyrene film for comparison.

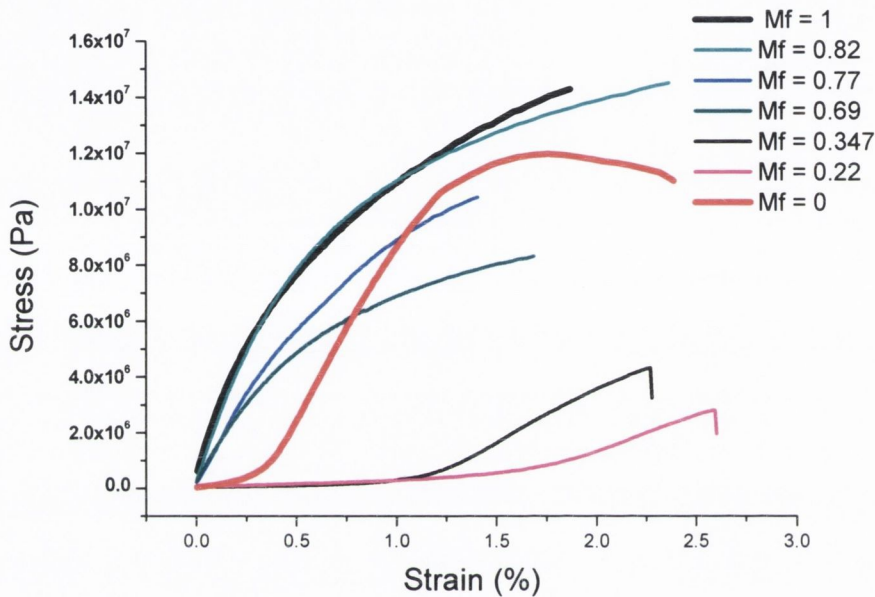


Figure 4.8 Selected Representative Stress Strain Curves of Composite and non-composite films.

The nanotube only film (in black) shows behaviour typical of a thermoplastic polymer, very similar to that of polystyrene itself, with reasonably high strengths and little elongation. The high mass fraction composites appear similar in behaviour to the polymer and nanotube samples. The low mass fraction composites however appear to perform worse than either of their component materials.

From these stress strain curves it was possible to deduce the stiffness (Young's Modulus, Y), Strength at Break (σ_B), Toughness (T) and Strain at break (Ductility) of the films.

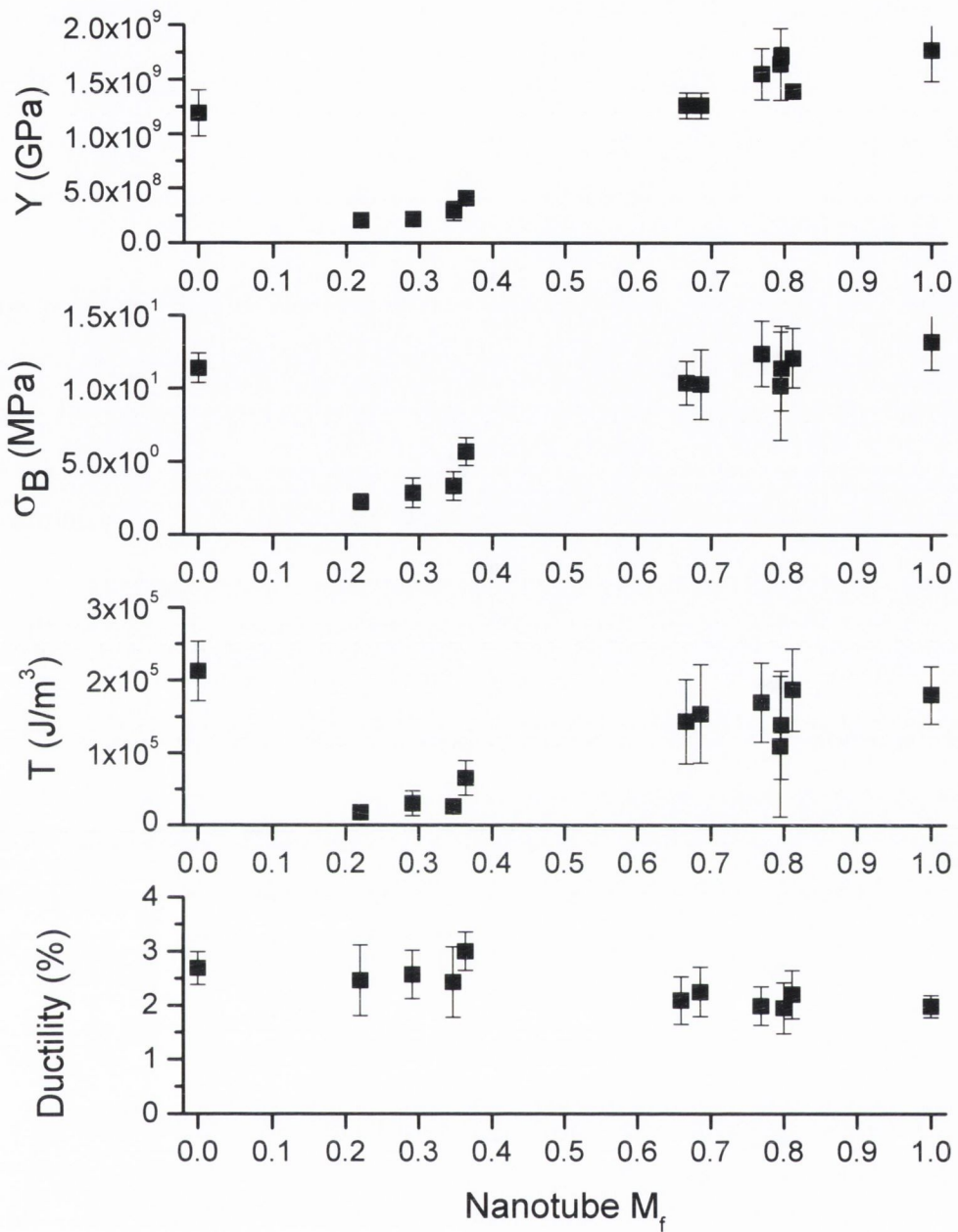


Figure 4.9 Youngs' Modulus of of Composite and non-composite films.

The mechanical results show very modest reinforcement of the polystyrene, when the composites are compared to the drop cast polystyrene only film. The Youngs Modulus increases slightly to a value of 1.72 GPa, 45 % above that of polystyrene itself. The same can be said of the ultimate tensile strength which increases by 9%, the toughness however

actually shows a slight decrease and the strain at break remains pretty much unaffected. At lower nanotube mass fraction the case is worse still with the composite properties actually being below that of polystyrene. Similarly, low reinforcement values been found by other authors [21, 22].

There may be two reasons for these low reinforcement values. Firstly, as was seen from the SEM images in section 4.5, the polymer layer probably does not form in the dispersion but in the drying phase, meaning that the composite consists of nanotubes bonded to each other by weak Van der Waal interactions surrounded by an over cover of polystyrene that is absent at the nanotube cross-over junctions. This may indicate poor interaction between the nanotubes and their host polymer, which is a constant problem in nanotube polymer reinforcement[23]. Often the use of a surfactant is blamed for this lack of interaction [24]. There was no surfactant used to disperse the nanotubes in this case but the affect of the solvent used is worth considering. It has been shown that nanotube dispersibility is maximised in solvents whose surface energy matches that of graphitic surfaces, such as NMP[25]. The disadvantage of this enhanced dispersibility is that the NMP can form a barrier around the nanotubes and so hinder good stress transfer to the host matrix[26]. We know from the TGA measurements in section 4.4 that in spite of washing with both water and methanol a certain amount of trapped solvent remains.

These results strongly suggest that there is little stress transfer between the polystyrene and nanotubes and consequently poor reinforcement of the polymer.

From this piece of work two main questions arouse. The first being *“what makes a good bucky paper in the first place (mechanically speaking)?”* and also *“how is it possible to increase stress transfer within a composite bucky paper?”*. These two questions provided the motivation for the work in chapters 5 and 6 respectively.

4.7 Electrical Measurements of Composites Films

Bulk, in-plane, electrical measurements were carried out on the films by painting silver electrodes onto the ends of the strips. All strips were cut to the same length. Current-voltage (I-V) measurements were made using a Keithley Model 2400 sourcemeter over the range of 0 to 3 Volts with a 0.03V increment. All curves were Ohmic in the voltage range studied. A plot of current density versus field for selected films is shown in figure 4.10. The resistance calculated from the slope of the I-V curves matched well to that measured using the method described below.

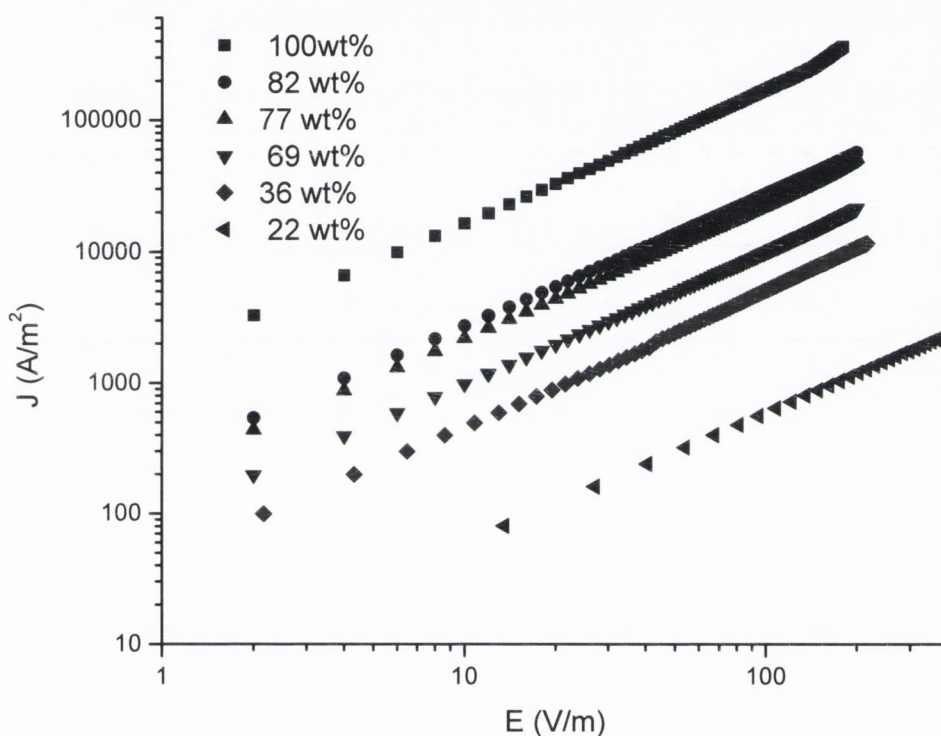


Figure 4.10 Current Density versus Field for selected nanotube loading levels

Resistance (R_T) measurements were made as a function of length (l), as shown in figure 4.11 by measuring the resistance, cutting the end off the strip, repainting the end with silver paint, re-measuring the resistance and repeating. This method was used as opposed to

4-probe measurements to ensure uniform current flow through the entire cross section of these (thick, see section 4.3) films.

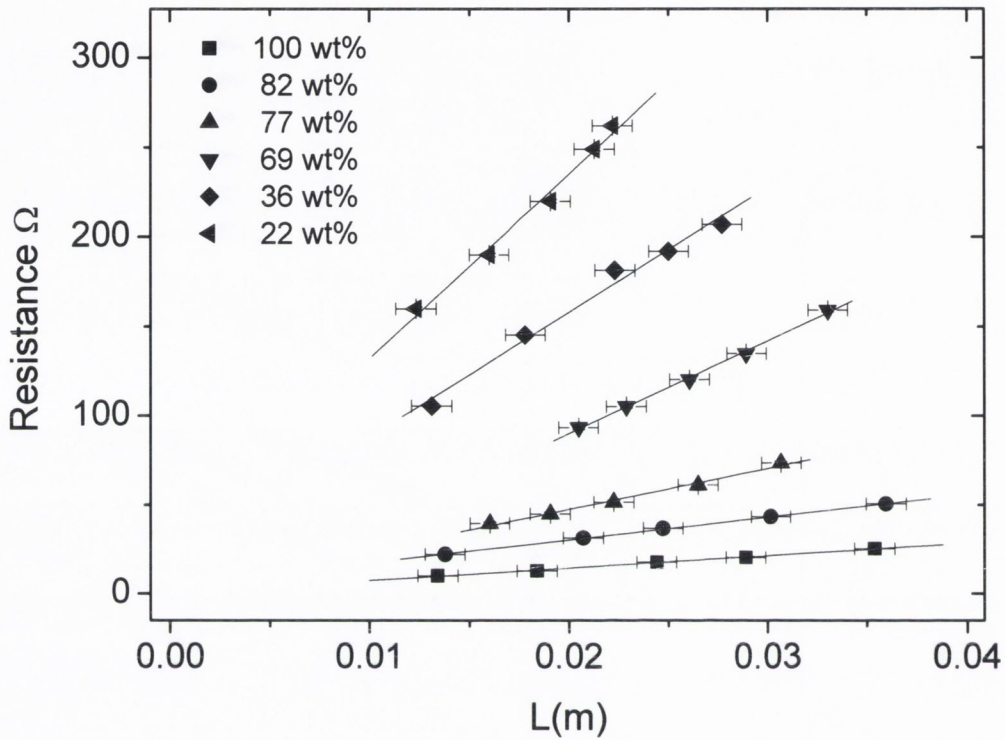


Figure 4.11 Resistance versus sample length for selected nanotube loading levels. The straight lines are fits to equation 4.4.

The total measured resistance of a strip of the film is a combination of its actual resistance and the added resistance due to the contacts (silver paint). The resistance scaled linearly with strip length as described by equation 4.4

$$R_T = \frac{1}{\sigma A} l + R_C \tag{4.4}$$

Where σ is the bulk conductivity, A is the strip cross-sectional area and R_C is the contact resistance. The contact resistance was close to zero in all cases. The slope of these lines was used to find σ , which is plotted as a function of nanotube mass fraction in figure 4.12a.

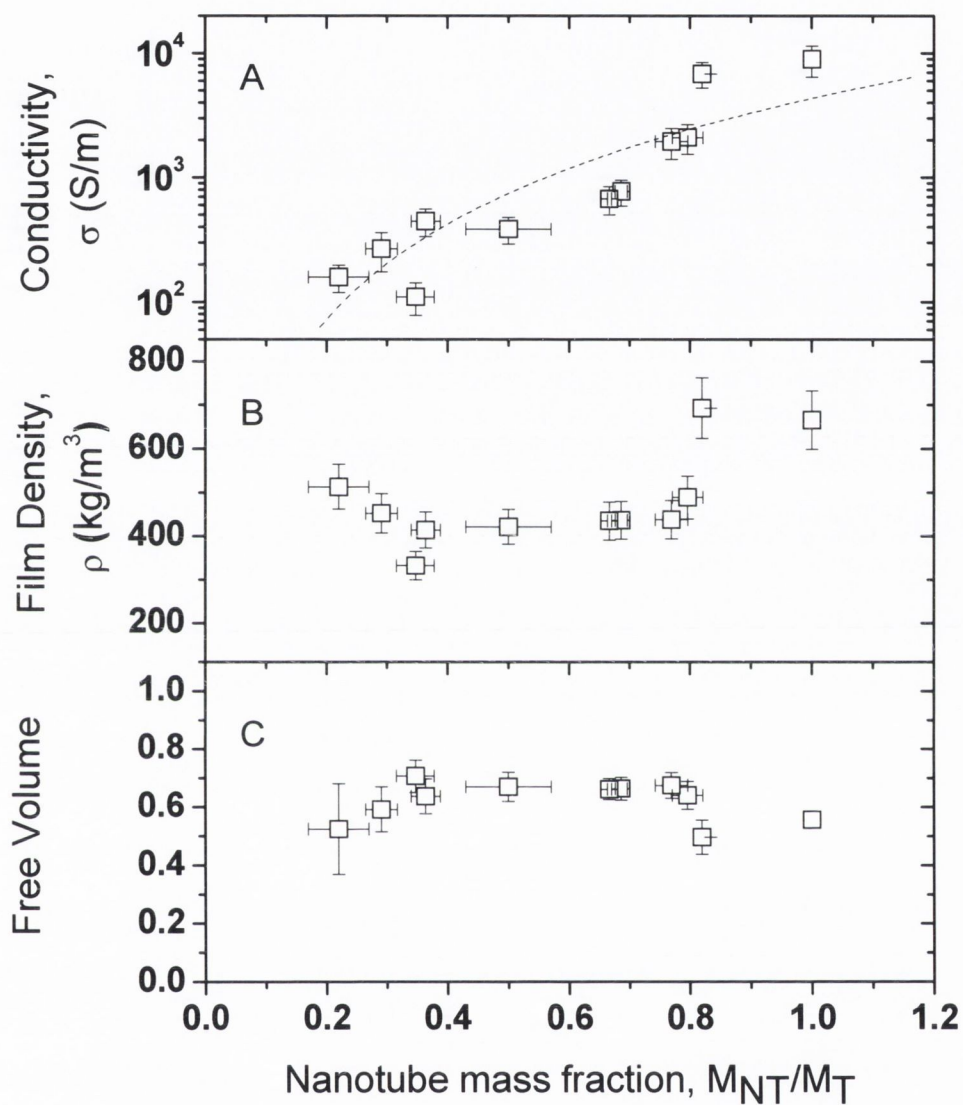


Figure 4.12. a) DC conductivity versus nanotube mass fraction, the curved line is to fit equation 4.5 b) Film density versus nanotube mass fraction. c) Free volume versus nanotube mass fraction.

Conductivities ranged from ~100S/m for papers of ~22wt% NT up to ~10⁴S/m for the nanotube-only bucky paper. These values compare well with the most conductive composites found in the literature. In comparison, polyacrylonitrile/SWNT composite films with 40wt% nanotubes display conductivities of 1.5×10⁴ S/m[12] and maximum conductivities of 2.5×10³ S/m were measured for composites of 80wt% MWNT, coated with polyaniline[14].

The conductivity, σ , of a percolative system is generally described as a function of volume fraction, p , (as opposed to mass fraction) by the scaling law[27]

$$\sigma = \sigma_0 \left[\frac{p - p_c}{1 - p_c} \right]^t \approx \sigma_0 p^t \quad 4.5$$

where σ_0 is related to the conductivity of the filler, p_c is the percolation threshold and t is the conductivity exponent. The left side of 4.5 is a special case of a more general effective media equation and holds when $p > p_c$ and when $|\sigma_{\text{polymer}}| \rightarrow 0$ [27]. If p_c is very small, then $p - p_c \sim p$, even at reasonably low volume fractions. As discussed previously in section 4.5 the bundles present in these films are expected to have aspect ratios greater than 75. This allows us to predict the percolation threshold to be <1vol%[28]. Thus, we might expect the approximation $\sigma \approx \sigma_0 p^t$ to hold when p is greater than a few percent; ie for all loading levels studied here. (It should be pointed out that due to this approximation it is impossible to calculate the percolation threshold from this data.) However, it is crucial to note that, in general, percolation scaling expressions are only valid near the percolation threshold. Thus we might expect the approximation stated above to hold at intermediate volume fractions but to break down at high volume fractions.

For these composites we can most easily quantify the nanotube content in terms of mass fraction (as opposed to volume fraction) as measured by thermogravimetry. Equation 4.5 has been fitted to the conductivity versus nanotube mass fraction data in figure 4.12a. While percolation scaling laws are often applied to data expressed in terms of mass fraction, we note that this procedure is not strictly correct unless the mass fraction is proportional to the volume fraction ie. at low nanotube content or when the polymer and

nanotube densities are equal. The poor quality of the fit can be partly explained by the fact that m_f and p are not proportional at the high NT loading levels used here. However there is also another reason. The measured density of the films (figure 4.12b) is much lower than the density of either PS ($\sim 1100 \text{ kg/m}^3$) or of SWNTs ($\sim 1500 \text{ kg/m}^3$), indicating that the films are porous in nature, in agreement with the SEM observations in section 4.5. This porosity must be accounted for when calculating the volume fraction, p , from m_f .

The fractional volume taken up by pores ($V_{\text{pore}}/V_{\text{Total}}$) can be calculated as follows:

$$\frac{V_{\text{Pore}}}{V_{\text{Film}}} = \frac{V_{\text{Film}} - V_{\text{NT}} - V_{\text{Polymer}}}{V_{\text{Film}}}$$

$$\frac{V_{\text{Pore}}}{V_{\text{Film}}} = 1 - \left(\frac{V_{\text{NT}}}{V_{\text{Film}}} + \frac{V_{\text{Polymer}}}{V_{\text{Film}}} \right)$$

$$\frac{V_{\text{Pore}}}{V_{\text{Film}}} = 1 - \left(\frac{m_{\text{NT}}}{\rho_{\text{NT}}} \cdot \frac{\rho_{\text{Film}}}{m_{\text{Film}}} + \frac{m_{\text{Polymer}}}{\rho_{\text{Polymer}}} \cdot \frac{\rho_{\text{Film}}}{m_{\text{Film}}} \right)$$

$$\frac{V_{\text{Pore}}}{V_{\text{Film}}} = 1 - \left(\frac{\rho_{\text{Film}}}{\rho_{\text{NT}}} M_f + \frac{\rho_{\text{Film}}}{\rho_{\text{Polymer}}} (1 - m_f) \right) \quad 4.6$$

where ρ_{Total} , ρ_{NT} , and ρ_{Poly} are the film, nanotube and polymer densities respectively. This is illustrated in figure 4.12c. The largest free volume is found for the films furthest away from either pure NT or pure PS composition. It is not clear why this should be the case but may be related to the mechanism of deposition of polymer on the nanotubes during the drying phase and the fact that at high polymer contents, significant amounts of polymer get washed through the filter.

The nanotube m_f and measured film density values can be used to calculate the true nanotube volume fraction, $p = V_{\text{NT}}/V_{\text{Film}}$, from

$$p = \frac{V_{NT}}{V_{Film}} = \frac{\rho_{Film}}{\rho_{NT}} m_f \quad 4.7$$

giving values in the range 7.5vol% to 38vol% for the composites and 44vol% for the (porous) nanotube-only film.

Shown in figure 4.13 is the conductivity versus this true nanotube volume fraction, p . The conductivity scales with p as predicted by equation 4.5. Moreover, this scaling extends right up to the bucky paper sample at $p=0.44$. This is an exciting and wholly unexpected observation. Percolation scaling laws are only strictly valid close to the percolation threshold. That the scaling continues to apply right up to the nanotube only film is an important result which we will address in more detail in section 4.9.

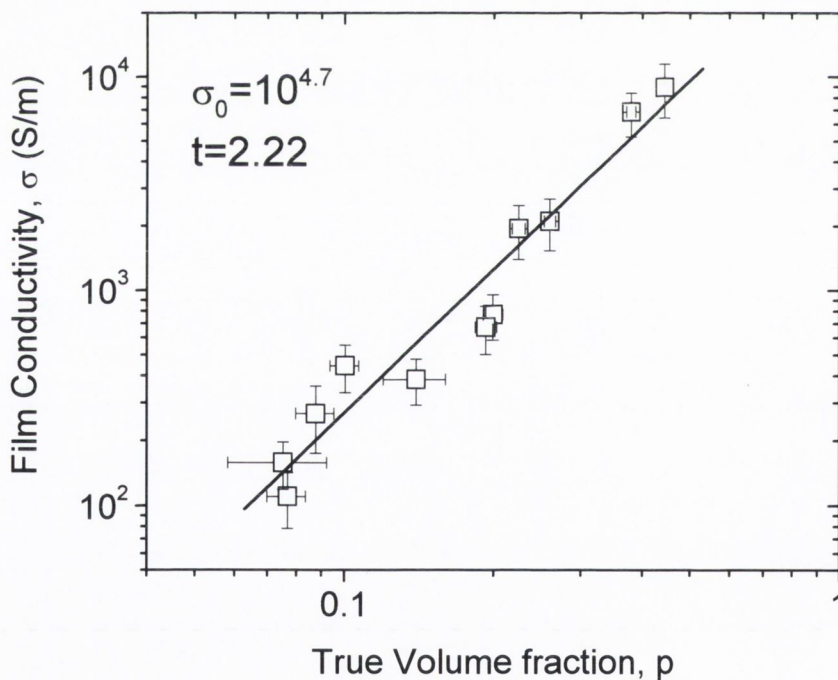


Figure 4.13 DC conductivity versus nanotube volume fraction, calculated having accounted for the film porosity. The straight line is a fit to equation 4.5.

Fitting equation 4.5 to the data gives a value of $\text{Log}(\sigma_0/\text{Sm}^{-1})=4.7\pm 0.2$. This value represents the extrapolated conductivity of a non-porous nanotube only film and is significantly below the in-plane conductivity of graphite[29], suggesting that charge transport is limited by inter-nanotube charge transfer. The power law exponent $t=2.2\pm 0.2$ agrees well with the universal scaling value of $t=2$. The fact that t is not significantly greater than 2 also suggests that inter-nanotube polymer tunnelling barriers do not limit the conductivity[30], as is the case in most composites[3]. That the bundles are not separated by polymer tunnelling barriers shows that the polymer coatings observed in figure 4.5A cannot simply coat individual bundles but must coat the network as a whole, allowing intimate contact between bundles at junction sites. This supports the idea that the coating forms during the drying phase.

In previous studies, percolation scaling has never been observed at volume fractions approaching the pure nanotube based material. Shaffer et al.[31] observed an exponential increase in conductivity up to a conductivity of 10^2 S/m at 60wt% MWNTs in PVA. Percolation scaling has been observed up to 15vol% MWNT polyurethane composites with maximum conductivities of 2000S/m[32]. Composites based on PMMA and SWNT have shown scaling for nanotube concentrations of up to 10 wt% with maximum conductivities of 1700S/m[33], figure 4.14A. The highest loading level at which scaling was still observed was 40wt% for a MWNT/PMMA composite with a maximum conductivity of 3000S/m[13], figure 4.14B.

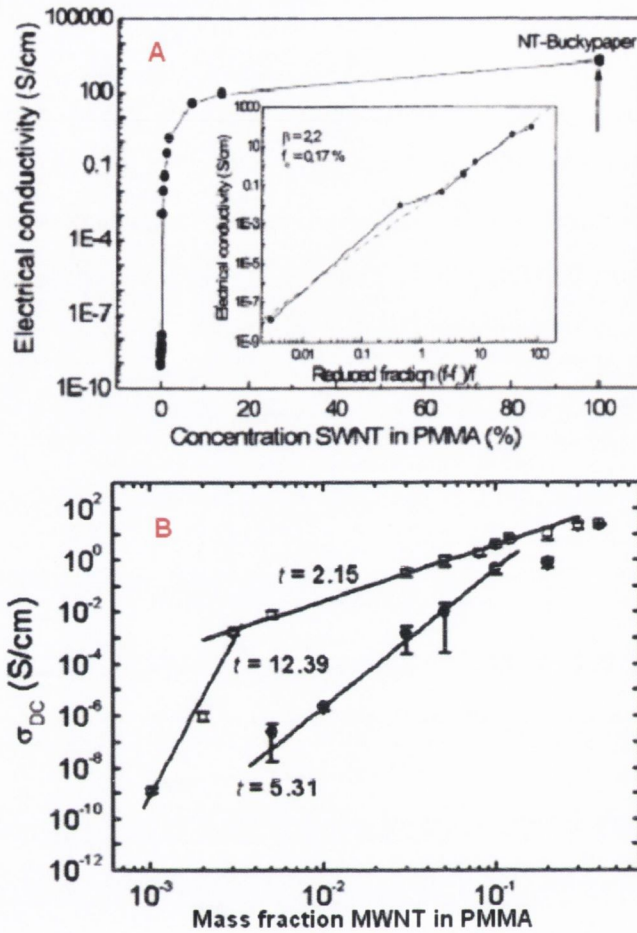


Fig. 4.14 A: Electrical conductivity as a function of SWNT concentration in PMMA[33] B: Electrical conductivity as a function of nanotube mass fraction in PMMA[13]

While scaling right up to $p=1$ has been observed for 2-dimensional systems of nanoparticles[34], it is thought that this is the first time scaling has been observed right up to the filler only material for rod-like fillers.

4.8 Discussion and Conclusion

Percolation-like scaling at high volume fractions has not previously been observed partly due to the difficulty in preparing high nanotube-content samples. However, it must be stressed that such scaling can only be observed in composites where the filler particles come into intimate contact at junction sites as mentioned above. Otherwise, as is generally observed in polymer-nanotube composites, the fillers (nanotubes) tend to be separated by a

polymer layer that acts as a tunnelling barrier, hindering inter-filler electron transport[3]. By definition, these barriers are not present in the filler-only material leading to different inter-filler charge transfer mechanisms for composites and filler only material. Thus, observation of continuous scaling up to the nanotube-only film, confirms the absence of polymer tunnelling barriers in these high-content composites.

The fact that the composite conductivity scales right up to the nanotube-only bucky paper shows the conductivity of these composites is limited only by the conductivity of the nanotube networks themselves. Thus, it may be possible to increase the conductivity of these composites at all volume fractions by taking steps designed to produce more conductive nanotube-only films. For example, it might be possible to use intrinsically more conductive nanotube material (higher proportion of metallic tubes) or to prepare films from smaller bundles by working at lower concentration[16]. Such efforts would increase composite conductivity by effectively increasing σ_0 . Conductivities of up to 10^4 S/m for the pure NT non-composite films have been observed. While not exceptional, this value compares fairly well with current literature values. Films of SWNT, originally dispersed in oleum, have shown conductivities of 10^4 S/m[35]. However, carbon nanotube sheets, transfer-printed onto a polyethyleneterephthalate substrate, have demonstrated conductivities as high as 2×10^5 S/m [36], while ultra-thin SWNT films prepared by Wu et al. gave conductivities of 6.6×10^5 S/m[11]. By combining the processing techniques used to prepare these very high conductivity nanotube films with the composite formation methods described here, it should be possible to make composites with conductivity as high as 10^5 S/m thus paving the way for applications such as composite electrodes.

In conclusion, a novel method has been used to produce high mass fraction polymer-nanotube composite films that display extremely high conductivity. When the conductivity was plotted versus true volume fraction, percolation scaling was observed right up to the nanotube only bucky paper. This unexpected result shows that, in these systems at least, percolation scaling persists even at very high volume fractions. In addition, unlike most composites, the conductivity is limited by the conductivity of the nanotube network and not the presence of polymer tunnelling barriers.

4.9 References

1. Grunlan, J.C., et al., *Water-based single-walled-nanotube-filled polymer composite with an exceptionally low percolation threshold*. *Advanced Materials*, 2004. **16**(2): p. 150-+.
2. Jiang, X.W., Y.Z. Bin, and M. Matsuo, *Electrical and mechanical properties of polyimide-carbon nanotubes composites fabricated by in situ polymerization*. *Polymer*, 2005. **46**(18): p. 7418-7424.
3. Kilbride, B.E., et al., *Experimental observation of scaling laws for alternating current and direct current conductivity in polymer-carbon nanotube composite thin films*. *Journal Of Applied Physics*, 2002. **92**: p. 4024-4030.
4. Makeiff, D.A. and T. Huber, *Microwave absorption by poly aniline-carbon nanotube composites*. *Synthetic Metals*, 2006. **156**(7-8): p. 497-505.
5. Martin, C.A., et al., *Formation of percolating networks in multi-wall carbon-nanotube-epoxy composites*. *Composites Science and Technology*, 2004. **64**(15): p. 2309-2316.
6. McLachlan, D.S., et al., *AC and DC percolative conductivity of single wall carbon nanotube polymer composites*. *Journal of Polymer Science, Part B: Polymer Physics*, 2005. **43**(22): p. 3273-3287.
7. Murphy, R., et al., *Observation of extremely low percolation threshold in Mo6S4.5I4.5 nanowire/polymer composites*. *Scripta Materialia*, 2006. **54**(3): p. 417-420.
8. Sandler, J., et al., *Development of a dispersion process for carbon nanotubes in an epoxy matrix and the resulting electrical properties*. *Polymer*, 1999. **40**(21): p. 5967-5971.
9. Sandler, J.K.W., et al., *Ultra-low electrical percolation threshold in carbon-nanotube-epoxy composites*. *Polymer*, 2003. **44**(19): p. 5893-5899.
10. Ramasubramaniam, R., J. Chen, and H.Y. Liu, *Homogeneous carbon nanotube/polymer composites for electrical applications*. *Applied Physics Letters*, 2003. **83**(14): p. 2928-2930.
11. Wu, Z.C., et al., *Transparent, conductive carbon nanotube films*. *Science*, 2004. **305**(5688): p. 1273-1276.
12. Guo, H., et al., *Structure and properties of polyacrylonitrile/single wall carbon nanotube composite films*. *Polymer*, 2005. **46**(9): p. 3001-3005.
13. Kim, H.M., et al., *Electrical conductivity and electromagnetic interference shielding of multiwalled carbon nanotube composites containing Fe catalyst*. *Applied Physics Letters*, 2004. **84**(4): p. 589-591.
14. Konyushenko, E.N., et al., *Multi-wall carbon nanotubes coated with polyaniline*. *Polymer*, 2006. **47**(16): p. 5715-5723.
15. Blond, D., et al., *Enhancement of modulus, strength, and toughness in poly(methyl methacrylate)-based composites by the incorporation of poly(methyl methacrylate)-functionalized nanotubes*. *Advanced Functional Materials*, 2006. **16**(12): p. 1608-1614.

16. Giordani, S., et al., *Debundling of Single-Walled Nanotubes by Dilution: Observation of Large Populations of Individual Nanotubes in Amide Solvent Dispersions*. J. Phys. Chem. B, 2006. **110**(32): p. 15708-15718.
17. www.sigmaaldrich.com.
18. Stauffer, D. and A. Aharony, *Introduction to Percolation Theory*. 1991: Taylor & Francis.
19. Coleman, J.N., et al., *Improving the mechanical properties of single-walled carbon nanotube sheets by intercalation of polymeric adhesives*. Applied Physics Letters, 2003. **82**(11): p. 1682-1684.
20. Frizzell, C.J., et al., *Reinforcement of macroscopic carbon nanotube structures by polymer intercalation: The role of polymer molecular weight and chain conformation*. Physical Review B, 2005. **72**(24).
21. Chang, T.E., et al., *Conductivity and mechanical properties of well-dispersed single-wall carbon nanotube/polystyrene composite*. Polymer, 2006. **47**(22): p. 7740-7746.
22. Qian, D., et al., *Load transfer and deformation mechanisms in carbon nanotube-polystyrene composites*. Applied Physics Letters, 2000. **76**(20): p. 2868-2870.
23. Coleman, J.N., et al., *Small but strong: A review of the mechanical properties of carbon nanotube-polymer composites*. Carbon, 2006. **44**(9): p. 1624-1652.
24. Liu, L., et al., *Mechanical Properties of Functionalized Single-Walled Carbon-Nanotube/Poly(vinyl alcohol) Nanocomposites*. Advanced Functional Materials, 2005. **15**(6): p. 975-980.
25. Bergin, S.D., et al., *Exfoliation in Ecstasy: Liquid crystal formation and chirality dependent debundling observed for single wll nanotubes dispersed in the liquid drug Butyrolactone*. Nanotechnology, 2007. **in press**.
26. Khan, U., et al., *The effect of solvent choice on the mechanical properties of carbon nanotube-polymer composites*. Composites Science and Technology, 2007. **67**(15-16): p. 3158-3167.
27. McLachlan, D.S., et al., *The correct modelling of the second order terms of the complex AC conductivity results for continuum percolation media, using a single phenomenological equation*. Physica B-Condensed Matter, 2003. **338**(1-4): p. 256-260.
28. Garboczi, E.J., et al., *Geometrical Percolation-Threshold of Overlapping Ellipsoids*. Physical Review E, 1995. **52**(1): p. 819-828.
29. Kaye, G.W.C. and T.H. Laby, *Tables of Physical and Chemical Constants*. 16th ed. 1995: Longman.
30. Balberg, I., *Limits on the continuum-percolation transport exponents*. Physical Review B: Condensed Matter and Materials Physics, 1998. **57**(21): p. 13351-13354.
31. Shaffer, M.S.P. and A.H. Windle, *Fabrication and Characterization of Carbon Nanotube/Poly(vinyl alcohol) Composites*. Advanced Materials, 1999. **11**(11): p. 937-941.
32. Koerner, H., et al., *Deformation-morphology correlations in electrically conductive carbon nanotube thermoplastic polyurethane nanocomposites*. Polymer, 2005. **46**(12): p. 4405-4420.

33. Skakalova, V., U. Dettlaff-Weglikowska, and S. Roth, *Electrical and mechanical properties of nanocomposites of single wall carbon nanotubes with PMMA*. Synthetic Metals, 2005. **152**(1-3): p. 349-352.
34. Dunbar, A.D.F., et al., *Morphological differences between Bi, Ag and Sb nanoparticles and how they affect the percolation of current through nano-particle networks*. European Physical Journal D, 2006. **39**(3): p. 415-422.
35. Sreekumar, T.V., et al., *Single-wall carbon nanotube films*. Chemistry of Materials, 2003. **15**(1): p. 175-178.
36. Zhou, Y.X., L.B. Hu, and G. Gruner, *A method of printing carbon nanotube thin films*. Applied Physics Letters, 2006. **88**(12).

Chapter 5

The factors controlling the Mechanical and Electrical properties of nanotube films (bucky papers)

5.1 Introduction and Relevant Background Literature

As previously mentioned, the outstanding thermal[1], electrical[2] and mechanical[3] properties of carbon nanotubes have made them the most studied of all nano-materials in recent years. Their low density, high aspect ratio, exceptional strength and stiffness and high conductivity suggest them as an especially promising material for many mechanical and electronic applications.

However it has been extremely difficult to turn this potential into a recipe for practical structural materials. The main reason for this is that, although strong, nanotubes are of course very small. Thus any real structural material will be fabricated from arrays or networks of nanotubes[4] or from composites of nanotubes embedded in a matrix. In either case, the resulting mechanical properties will depend strongly on the stress transfer either between nanotubes or from the matrix to the nanotubes. The conductivity of these structures will depend on the number of conductive paths through the film and on the typical number of inter-bundle junctions encountered on a given path.

This has resulted in macroscopic nanotube based materials with mechanical and electrical properties far inferior to those of the nanotubes themselves. For example, fibres fabricated from nanotubes alone have demonstrated strengths many times lower than the strengths of the individual nanotubes[5].

As mentioned already in relation to composites, single wall nanotubes tend to bundle together due to van der Waals interactions between them [6]. Although individual nanotubes are strong, nanotube bundles are weak and exhibit low shear

moduli[7]. Thus, nanotube networks or fibres made from bundles are expected to have different properties to those made from individual nanotubes. In composite materials, aggregation of nanotubes into bundles acts to decrease the nanotube surface area available to make contact with the chosen polymer, inhibiting their reinforcement capabilities[8] and in the case of conducting composites, raising the percolation threshold[9].

A number of studies have looked at the mechanical properties of macroscopic materials fabricated solely from carbon nanotubes. These materials include sheets[4], films[1, 10-12] and fibres[5, 13]. A very wide range of mechanical properties have been measured with strengths ranging of ~5MPa for bucky papers[12] to 1GPa for fibres[5]. The common factor between these materials is that they are held together by van der Waals interactions between nanotubes or nanotube bundles. However, other than nanotube alignment, it is not clear what factors control the mechanical properties.

Electronically, much work is underway to develop thin, flexible films of carbon nanotubes for applications such as transparent electrodes[4, 14-20]. Little work has been done on the effect of the morphological properties of the films on the conductivity.

Nanotubes films, commonly known as bucky papers, are always porous and always built from networks of bundles, not individual nanotubes. The porosity tends to vary from film to film as does the bundle size. These properties are expected to significantly affect the DC conductivity and the mechanical properties of the films. Any attempt to maximize the DC conductivity or film robustness must first optimise the morphological properties of the film.

From the work on polystyrene nanotube composites in chapter 4, it was clear that investigation was necessary into the control factors that influence the mechanical and electrical properties of carbon nanotube bucky paper.

In this chapter, carbon nanotube films were prepared by the vacuum filtration of a range of pristine and functionalised carbon nanotube dispersions. Stress-strain measurements show that the mechanical properties depend primarily on the morphology of the nanotube network, specifically on the number density of inter-bundle junctions which can be derived in terms of porosity and bundle diameter. Little dependence was seen on the graphitisation of the nanotubes themselves. DC conductivity measurements were also made, demonstrating that the film conductivity increases with increasing nanotube graphitisation and is inversely proportional to film porosity and bundle size. The conductivity scales approximately with the inter-

nanotube junction density but more accurately with the product of the junction density and Raman G:D band ratio.

5.2 Film Fabrication

A range of commercially available nanotubes were used in this study. Purified HiPCO SWNTs, as prepared and annealed Elicarb SWNTs, Nanolab DWNTs and Swent SWNTs were purchased and used as supplied. As-prepared (AP) SWNTs, along with several varieties of functionalised SWNTs were purchased from Carbon Solutions Inc and used as supplied. In all cases NMP[6] was used as a solvent unless otherwise specified. The nanotube functionalities were (acronyms in round brackets)[solvents used in square brackets] carboxylic acid, both lightly and heavily functionalised (-low-COOH, -high-COOH)[NMP], octadecylamine (ODA) [chloroform], poly-aminobenzene-sulfonic-acid (PABS) [water] and poly-ethylene-glycol (PEG) [water].

Dispersions were prepared by adding the SWNTs to the appropriate solvent at a concentration of 0.33mg/ml and sonicating for 3 min using a high-power ultrasonic tip (GEX600, 120W, 60kHz). To achieve a nanotube concentration of 0.08mg/ml, which, as mentioned previously in chapter 4, minimises NT bundling[21] while still remaining practical, the initial dispersions were diluted twice, sonicating for 1 min between steps. These diluted dispersions underwent a further 4hrs sonication in a low-power ultrasonic bath, followed by 1 min under the sonic tip. They were then vacuum filtered through a Teflon filter paper (pore size=0.45 μ m), washed with deionised water and acetone and dried at ambient temperature for 12 hrs in a vacuum oven. The films were free standing after being peeled from the filter paper and were cut into strips of width 2.2mm and lengths of several centimetres. Film thicknesses ranged from 11 μ m to 22 μ m. Porosity measurements were made as described in chapter 4, the values obtained along with other physical measurements are listed in Table 5.1.

5.3 Film Analysis

It might be expected that the properties of nanotubes films would depend on two main factors: the properties of the nanotubes themselves and the topological properties of the nanotube network. SEM was used in order to explore the topological properties of

the network along with careful measurements of the film porosity. Direct measurement of the mechanical properties of the nanotubes themselves is less straightforward. However nanotube strength, stiffness and conductivity are sensitive to the population of defects present. Thus the defect content as measured qualitatively by Raman spectroscopy may be used as a proxy for nanotube mechanical properties and conductivity.

The electrical characterisation and analysis of these films was undertaken by Philip Lyons and Dr. Sukanta De.

5.3.1 Scanning Electron Microscopy of Carbon Nanotube Films

Scanning electron micrographs of SWNTs films prepared from Hipco SWNTs, Elicarb annealed SWNTs, Carbon Solutions ODA functionalised SWNTs and Carbon Solutions PEG functionalised SWNTs are shown in the Fig. 5.1. These images are typical of nanotube films in general.

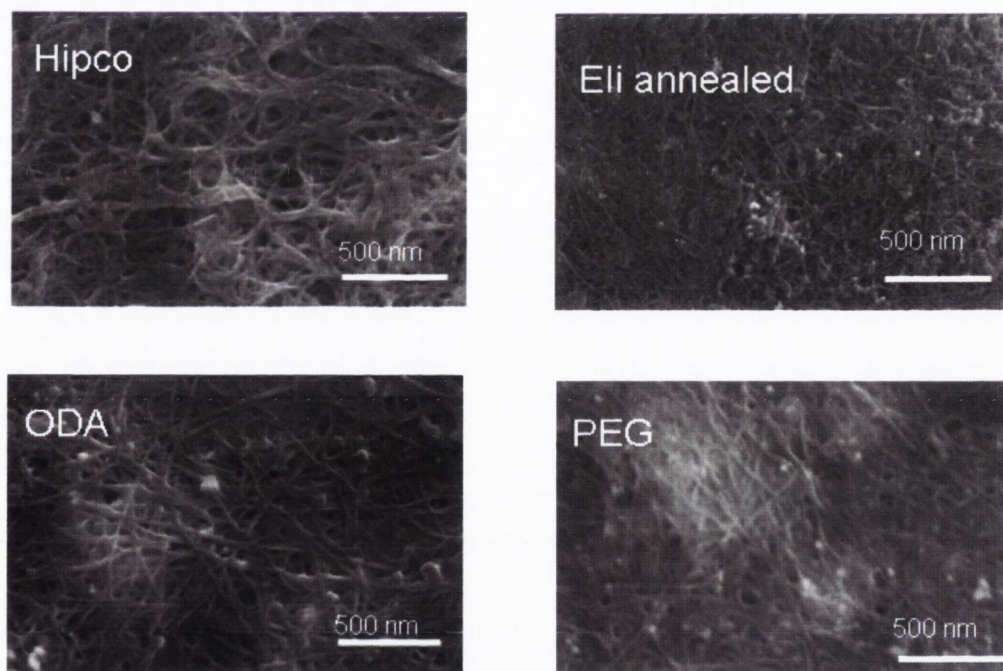


Fig.5.1 SEM images of surfaces of nanotube films prepared from (top left) Hipco SWNTs, (top right) Elicarb annealed SWNTs (bottom left) Carbon Solutions ODA functionalised SWNTs and (bottom right) Carbon Solutions PEG functionalised SWNTs.

The film surfaces consist of randomly orientated porous entanglements of nanotube bundles. The mean size of the nanotube bundles measured from the SEM images are given in table 5.1 and range from 9.8nm for the SWNT-high-COOH film to 21nm for the SWNT-low-COOH film. These means are slightly overestimated as the SEM used here does not have the resolution to see bundles with diameters below ~4nm. It can be seen that all films are porous. The porosity was calculated from the measured densities of the films and varied from 42% for the SWeNT sample to 72% for the SWNT-PABS film. This range encompasses previous values observed for bucky paper prepared from surfactant dispersions[12].

5.3.2 Raman Spectroscopy of Nanotube films

Raman spectroscopy was carried out on the films using a 633nm excitation wavelength laser to investigate the intrinsic properties of the various types of nanotubes. For each film, Raman measurements were made on five different regions of the films. In all cases the spectra were similar within a given film. The five spectra were then averaged to give a final representative Raman spectrum, and are offset for clarity. The representative spectra are shown in fig. 5.2.

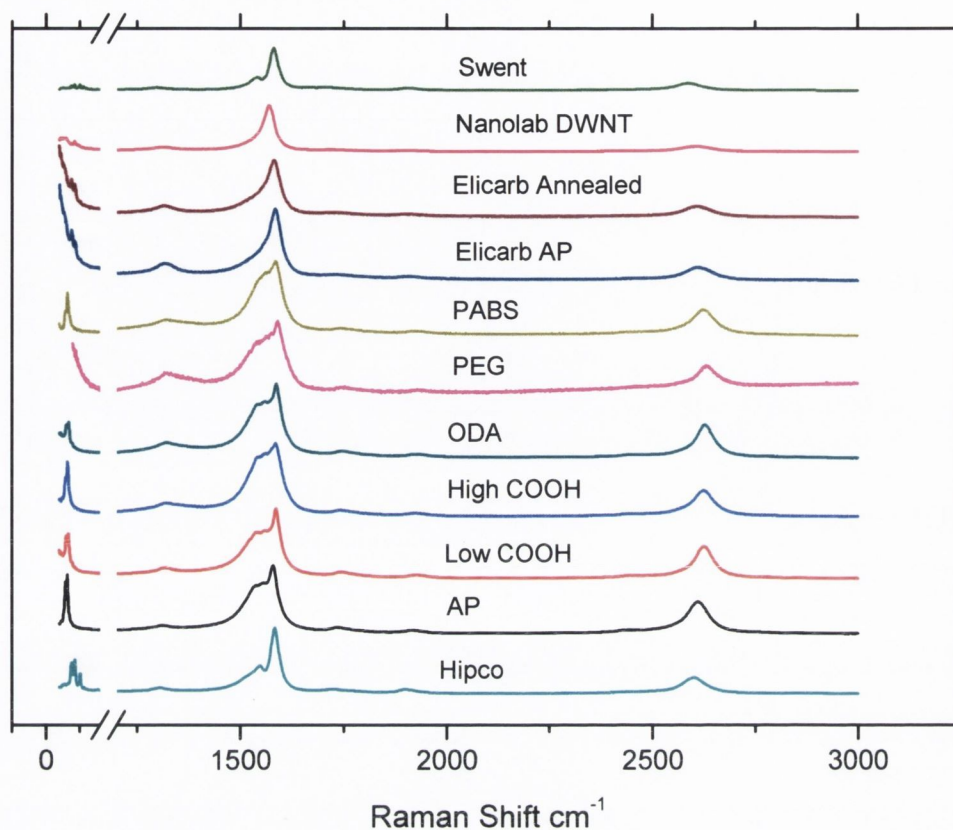


Fig 5.2. Raman Spectra of NT films studied in this work

Raman spectra of carbon nanotubes exhibit two strong bands at approximately 1280 cm^{-1} and 1580 cm^{-1} that are known as the D-band and G-bands respectively [22]. While the G band is associated with the tangential modes of pure sp^2 hybridised graphitic carbon, the D-band corresponds to the presence of deviations from the hexagonal lattice, such as sp^3 type defects. Thus the ratio of intensities of the G and D bands, $I_{G/D}$, is a crude measure of the perfection of the nanotubes. These intensity ratios have been measured for all nanotube films studied and range from 12.3 for the SWeNT nanotubes to 3.2 for the SWNT-PEG film. Overall, the $I_{G/D}$ ratio was smaller for functionalised nanotubes compared to the AP and Hipco tubes. Complete G:D band ratios can be found in table 5.1.

5.3.3 Mechanical Analysis of Carbon Nanotube Films

Stress strain curves were measured, as in chapter 4, for each film type with representative curves plotted in fig 5.3. The four main mechanical parameters were again obtained from these curves: the Youngs' modulus, Y , the toughness, T (energy required to break per volume), the strength at break, σ_B , and strain at break, ϵ_B .

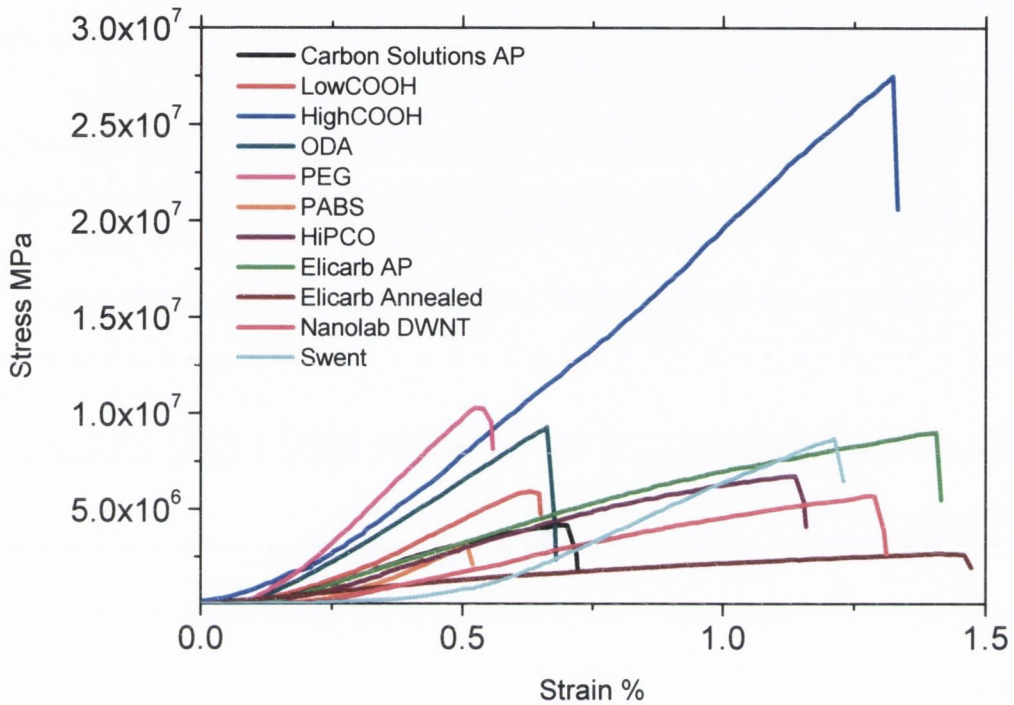


Fig 5.3. Representative Stress Strain curve for each film type.

The ranges of values measured were: modulus (1-3 GPa), strength (2-30 MPa), toughness (4×10^3 - 2×10^5 J/m³) and strain at break (1-2%). In general, these values do not differ greatly to those observed for weak, brittle thermoplastic polymers such as polystyrene[23]. However, there is a significant deviation in each of the properties over the range of tube types studied. It is of interest to ascertain the reasons for these deviations as this will lead to an understanding of the maximisation of the mechanical properties of nanotube based solids.

When considering a nanotube film, the topological properties of the network affect the properties of the film. This is because the structure of the film determines the number and nature of nanotube-nanotube junctions. As these junctions are responsible

for the transfer of stress between nanotubes and are essentially what hold the film together, we expect their properties to significantly affect the mechanical properties of the film.

It is not straightforward to measure directly the global topology of the film or even the nature and distribution of the junctions. However, two film properties that are strongly coupled to the properties of the network and can easily be measured are the film porosity and mean bundle diameter.

Also, the mechanical properties of the nanotubes themselves might be expected to influence the mechanical properties of the films. Well-graphitised SWNT have moduli and strengths of up to 1TPa and 60GPa respectively[24]. However, the presence of defects can result in significant reductions in both strength and modulus[25]. Thus, one might expect the mechanical properties of nanotube films to depend on the density and nature of defects associated with the nanotubes themselves. While we cannot measure this directly, we can crudely quantify the presence of defects through the Raman G/D ratio shown in section 5.3.2.

Thus, we expect the mechanical properties of the nanotube films to vary with film porosity, P , mean bundle diameter, D , and Raman Intensity ratio, $I_{G/D}$. Values for Y , σ_B , T and ϵ_B calculated from the stress-strain curves were each plotted individually as a function of P , D and $I_{G/D}$ and are shown in figures 5.4 to 5.7.

Examining first of all the strength at break, σ_B , versus P , D and $I_{G/D}$ in figure 5.4 we find unsurprisingly, that σ_B falls off as the bundle size and porosity values increase (the black arrows are not a fit to the data). This makes sense as we would expect increasing bundle size and porosity to reduce the number of bundle junctions within the film and so decrease the effective number of van der Waals interactions between adjacent NT bundles. Surprisingly though the σ_B displayed no clear trend with $I_{G/D}$. This suggests that the film strength is not affected by variations in the defect populations, and hence the strength, of the tubes themselves.

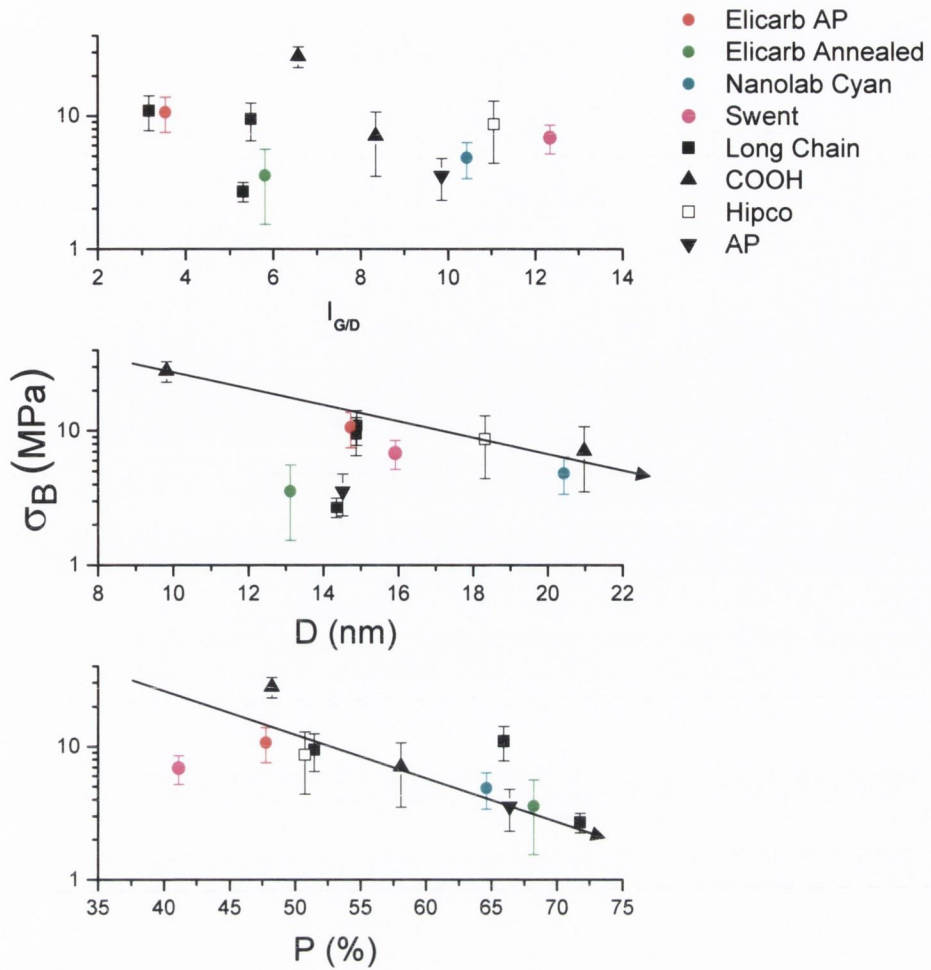


Fig. 5.4 Strength at break as a function of $I_{G/D}$, Bundle Size, D , and Porosity, P .

Looking at the toughness and strain at break data in figures 5.5 and 5.6 respectively, similar trends are evident. These mechanical parameters decreased as both P and D increased. In addition, like the σ_B , both T and ϵ_B proved invariant with $I_{G/D}$.

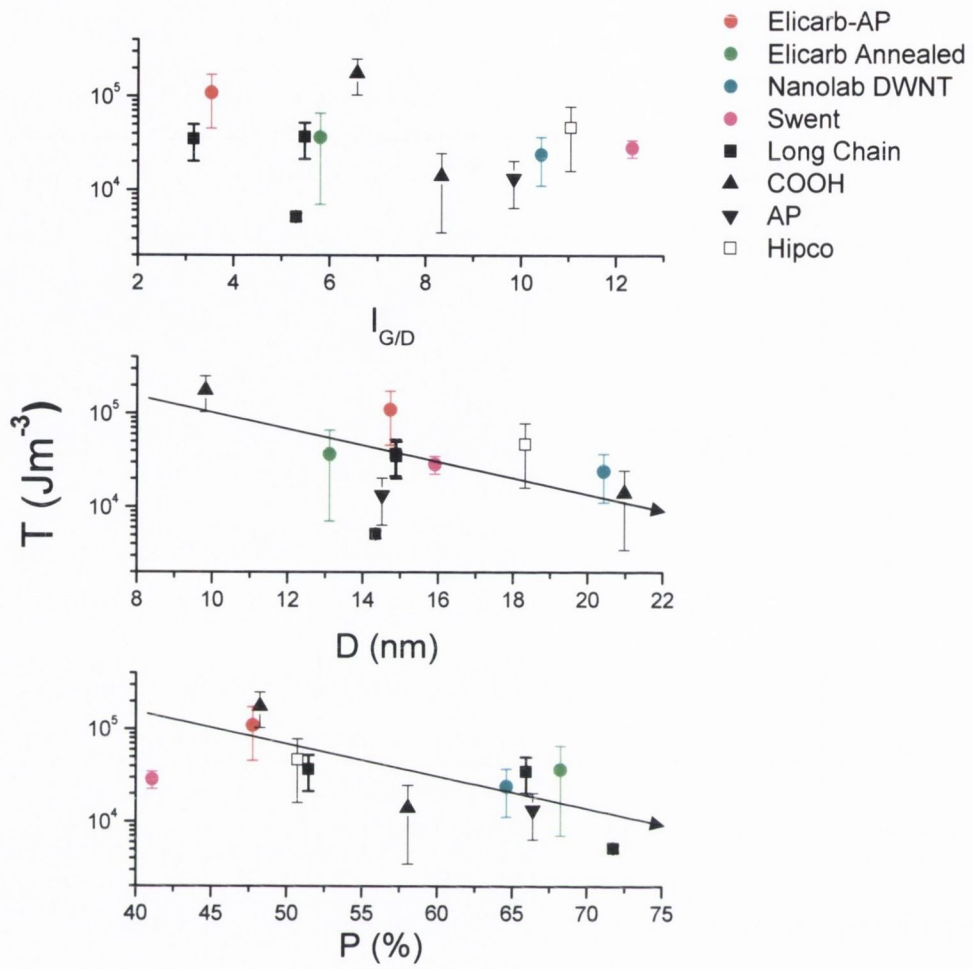


Fig. 5.5 Toughness, T , as a function of $I_{G/D}$, Bundle Size, D , and Porosity, P .

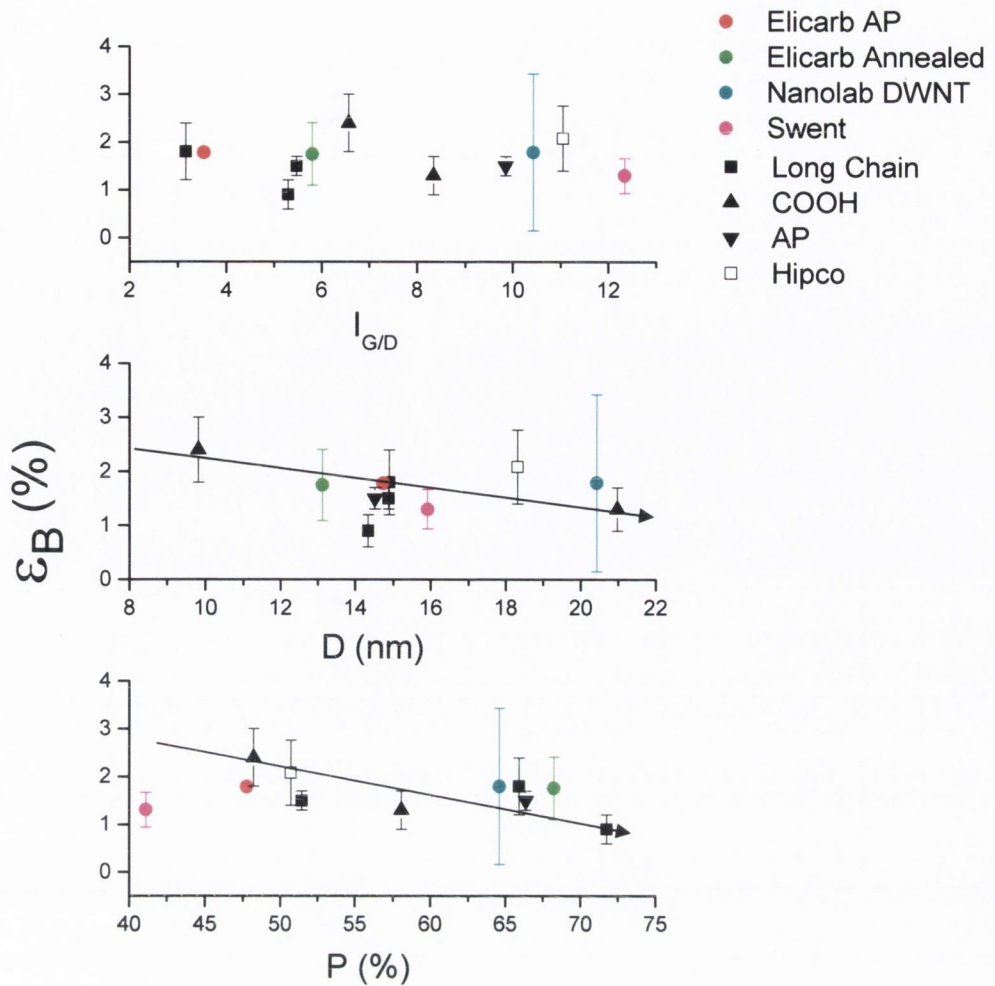


Fig. 5.6 Strain at break, ϵ_B as a function of $I_{G/D}$, Bundle Size, D, and Porosity, P.

The only exception to this trend was the Young's modulus (fig.5.7), which decreased consistently with increasing I_G/I_D from 2 GPa for the SWNT-PEG to 0.6 GPa for the SWNT-AP. Taken as a whole, these results mean that the mechanical properties of the nanotubes themselves have relatively little impact on the mechanical properties of the films. Much more important is the film morphology, with porous films made from high diameter bundles displaying much poorer properties. This strongly suggests that the number of inter-bundle junctions may be an important parameter.

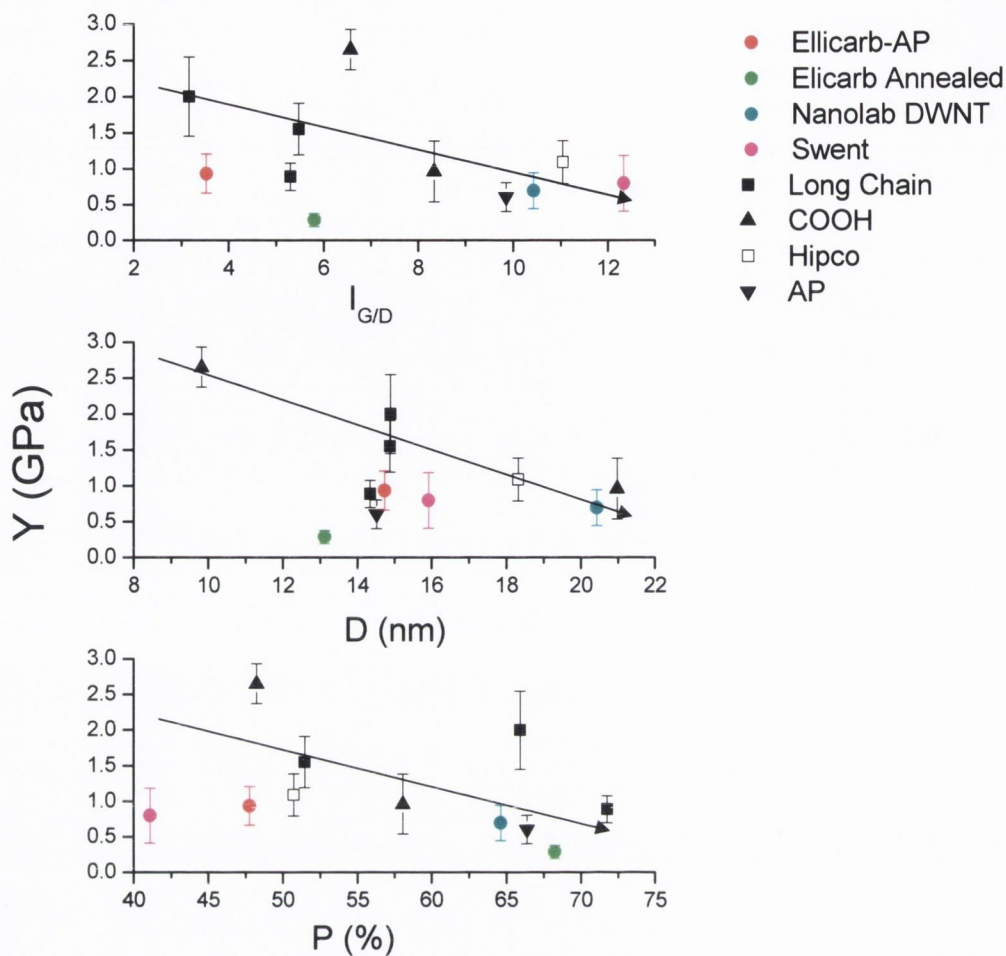


Fig.5.7 Youngs' modulus as a function of $I_{G/D}$, Bundle Size, D, and Porosity, P.

The scatter present in all these plots may be accounted for by the fact that the mechanical properties of the films are most likely controlled by a combination of the bundle size and porosity. Plotting the mechanical properties versus a combined parameter, which is a function of both P and D should reduce this scatter.

5.3.4 Electrical Characterisation of Carbon Nanotube Films

Direct current conductivity measurements were made for the nanotube films (by Philip Lyons and Sukanta De). The bulk conductivity was calculated by measuring the film resistance as a function of film length as describes in chapter 4 [26]. In all cases the contact resistance was close to zero. The conductivity of the films ranged from $6.35 \times 10^2 \text{ Sm}^{-1}$ for the SWNT-PABS film up to $1.56 \times 10^4 \text{ Sm}^{-1}$ for the HiPCO SWNT film. Notably, the highly carboxylic acid functionalised SWNTs displayed a reasonably high conductivity ($1.3 \times 10^4 \text{ Sm}^{-1}$) despite their high levels of functionalisation. This is probably because their $-\text{COOH}$ functionalities are predominately at the tube ends[27] and so have limited effect on charge transport through the tube bodies.

Similar reported bucky paper conductivities have appeared in literature[28]. However, much higher conductivity values of up to $6 \times 10^5 \text{ Sm}^{-1}$, have been reported for thin nanotube films[20] as previously mentioned in chapter 4. The discrepancy between this value and those obtained in this study are most likely due to differences in film morphology.

Two main factors control charge transport through nanotube films; the conductivity of the tubes themselves and the ability of carriers to tunnel from tube to tube. To simplify things, variations in metal/semiconductor populations were neglected along with the effects of slightly different diameter distributions for different tube types. Within this approximation, the conductivity of the nanotubes themselves is controlled by the defect population associated with a given tube type[29], which can be obtained from Raman data. The rate of tunnelling across a given tube-tube junction is controlled by the junction width and the electronic properties of the tubes and so the mean tunnelling rate is controlled by the distribution of the junctions. This is not easy to control for a given sample of nanotubes. However, the number of junctions that a carrier must traverse, on average, when travelling through a nanotube film depends on how the nanotubes are arranged within the film ie the film morphology which can be described by the porosity and mean bundle size.

A plot of film conductivity as a function of I_G/I_D is shown in figure 5.8C. Although the data is quite scattered, the conductivity tends to be larger for films made from tubes with higher I_G/I_D , ie. higher structural perfection. This is unsurprising as the conductivity of individual carbon nanotubes has been shown[29] to be heavily dependant on the presence of defects in the graphitic structure.

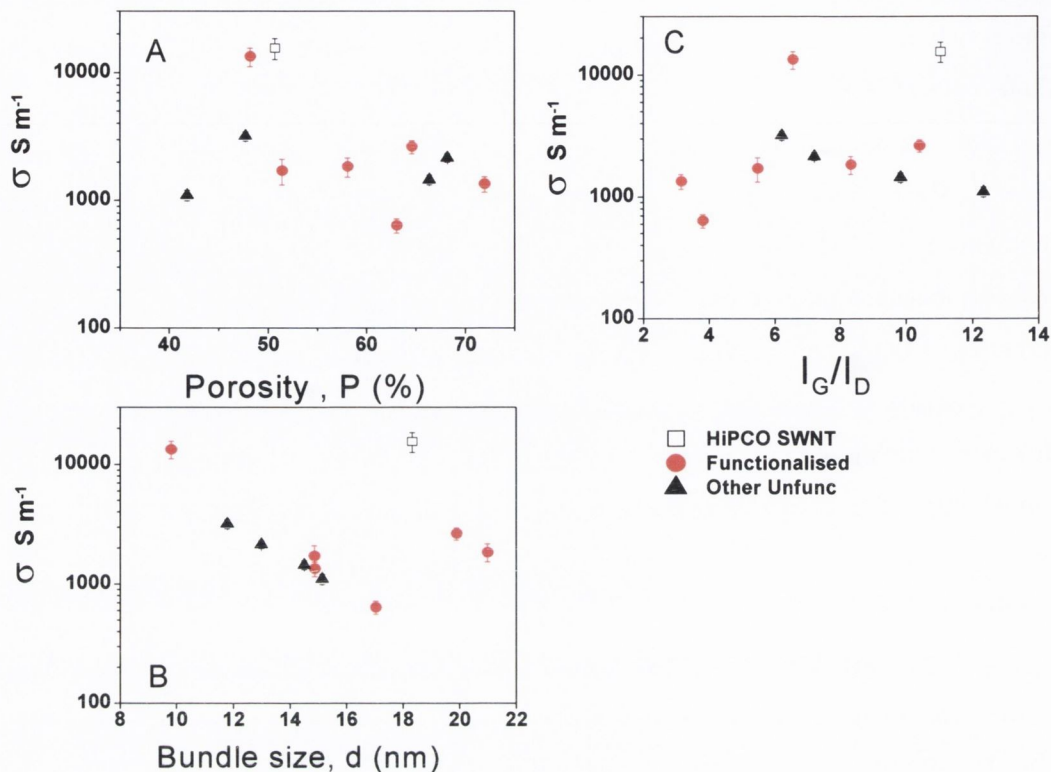


Figure 5.8 Dependence of film conductivity on both nanotube properties (I_G/I_D) and network properties, Porosity and Bundle Size.

Film conductivity is plotted as a function of porosity and bundle size in figure 5.8 A and B respectively. While the data displays considerable scatter, there is a trend towards decreasing conductivity with increasing porosity. Qualitatively, this trend makes sense as a sparser network (more porous) would certainly be expected to be less conductive. Conductivity also decreases with increased bundle size. Hecht et al recently predicted that the conductivity of thin nanotube film should scale approximately as $1/D^2$, based on an analysis of the dependence of the number of junctions in a system on the level of bundling[30].

However, more detailed analysis of the conduction process would have to consider the number of conducting pathways through the film. This is less than straightforward and would require detailed knowledge of the arrangement of bundles within the film. However we can postulate that the number of conductive paths is related to the number density of inter-nanotube junctions.

5.4 Further Analysis and Discussion with consideration of Inter-Nanotube Junction Density

5.4.1 Analyses of Mechanical Results

As discussed above, it is suspected that the number of inter-nanotube junctions is the key factor in both the mechanical and electrical properties of bucky paper films. We can estimate the number of junctions per unit volume of film, N_J , by calculating the number of bundles per unit volume. This parameter is of course related to the film density and the bundle diameter. Multiplying by half the mean number of junctions per bundle, α , gives:

$$N_J = \frac{\alpha \rho_{film} / \rho_{NT}}{2 \pi D^2 L / 4} = \alpha \frac{2(1-P)}{\pi D^2 L} \quad 5.1^*$$

where L is the mean bundle length. The mean number of junctions per bundle, α is halved to avoid double counting of junctions. α can be estimated by using the film density to calculate the average mass in a shell of thickness D surrounding a test bundle. The approximation is made that this mass is concentrated in bundles that are in contact with the test bundle. Approximating the volume of one bundle intersecting the shell (at right angles) by a triangular prism gives the volume of intersection as $\sim(3D^3)/2$. Averaging over all angles of intersection gives a mean volume of intersection of $\sim(3\pi D^3)/4$. Then by dividing the average mass within the shell by the average intersecting volume per bundle, $\rho_{NT}3\pi D^3/4$, the number of bundles within the shell and hence the number of junctions can be estimated as:

$$\alpha \approx \frac{\rho_{film}}{\rho_{NT}} \frac{8L}{3D} = (1-P) \frac{8L}{3D} \quad 5.2^*$$

Calculating α , assuming $L \approx 1\mu\text{m}$, gives values ranging from 73 to 160 junctions per bundle for the -low-COOH and HIPCO samples respectively. Combining this with the previous equation, gives an expression for the number of junctions per unit volume:

* Derived by Johnathan Coleman

$$N_J \approx \frac{16}{3\pi} \frac{(1-P)^2}{D^3} \quad 5.3^*$$

The junction density was found to vary from $2.7 \times 10^{22} \text{ m}^{-3}$ for the Nanolab DWNT tubes to $2.8 \times 10^{23} \text{ m}^{-3}$ for the as-prepared Elicarb sample.

If the number of junctions per unit volume is a key factor, it would be expected that some or all of the mechanical parameters scale with $(1-P)^2 / D^3$. Shown in figure 5.9 are plots of Y , σ_B , T and ϵ_B as a function of junction number density, $N_J \approx 1.7(1-P)^2 / D^3$.

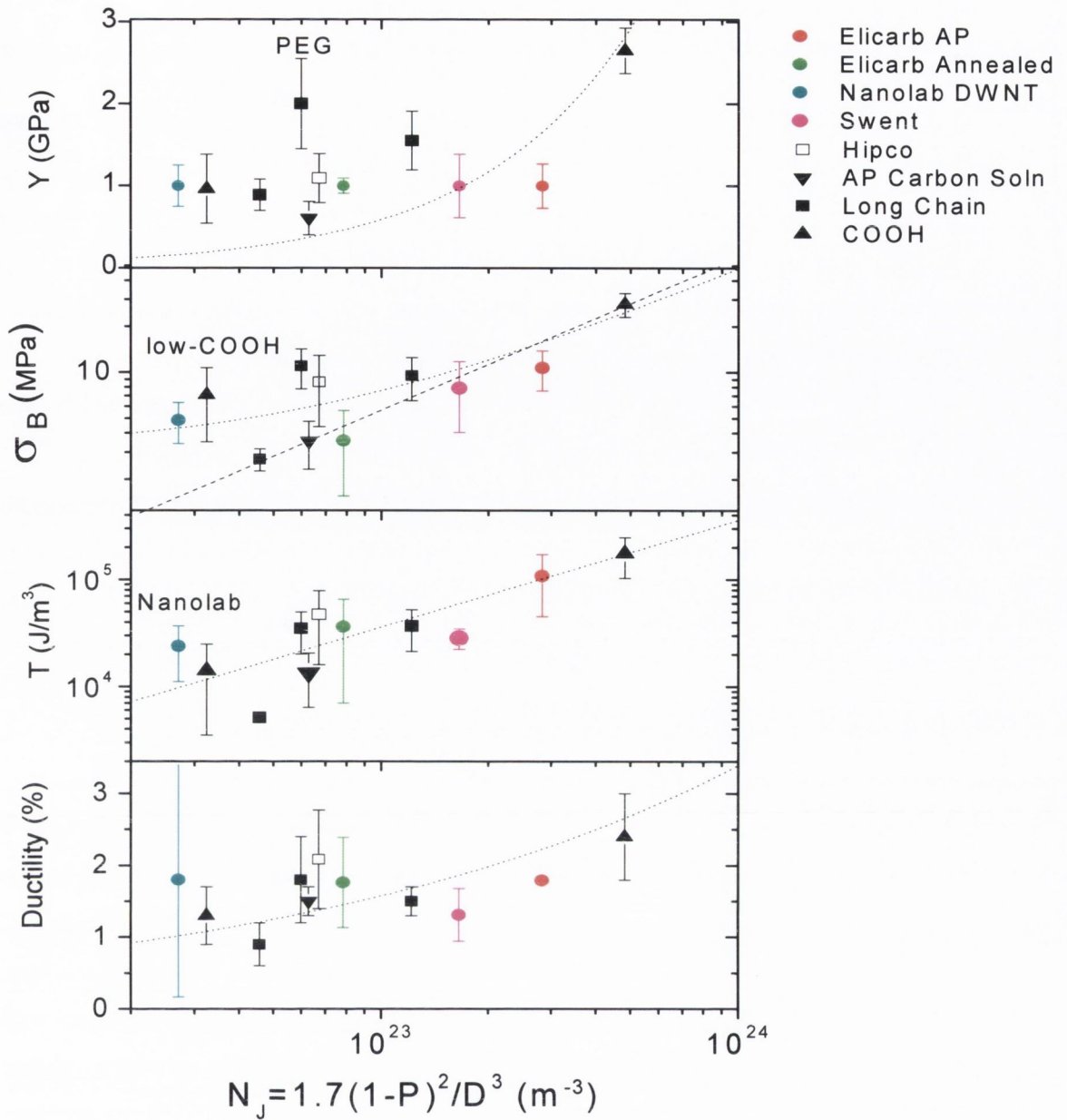


Fig. 5.9 Youngs Modulus (Y), Strength at Break (σ_B), Toughness (T) and Ductility versus the combined parameter of $[1-P]/D^2$ of functionalised and pristine NT films.

No overall relationship is apparent between the Young's modulus and N_j . The dotted line shows a linear trend for comparison. While the functionalised nanotubes may display a weak dependence with N_j , overall the data is too scattered to confirm a definite relationship. This is almost certainly because the modulus, unlike the other parameters scaled with $I_{G/D}$ as well as with the morphological parameters (fig 5.7).

However, in the case of σ_B , the dependence is close to linear as evidenced by the dashed linear fit line. It should be noted that three of the samples with low N_J lie slightly above the fit line (Nanolab DWNT, low-COOH and PEG). Interestingly, these samples lie on a linear fit *with intercept* (dotted line). For the toughness, the dependence is also linear, with the regression line well fitting all the data. Even the ductility tends to increase weakly with the junction number density.

In the case of the tensile strength, the analysis can be taken a step farther. We might speculate that fracture involves the rupture of junctions in a volume, $V_R \sim AL$, where A is the film cross-section area and L is the mean bundle length. We speculate that, on fracture, every bundle in this volume has half its junctions with other bundles severed. Taking the average force to break a junction as f_J , we can write the film strength as

$$\sigma \sim \frac{1}{A} f_J \frac{N_J AL}{2} = \frac{f_J L}{2} \times \frac{1.7(1-P)^2}{D^3} \quad 5.4$$

Approximating the mean bundle length to be $1\mu\text{m}$, and using the fit to the tensile strength data in fig 5.8 we can estimate $f_J \sim 113\text{pN}$. If we assume that the application of this force leads to an opening of the gap between bundles to $\sim 1\text{nm}$ just before fracture, then we can calculate the fracture energy to be $\sim 0.7\text{eV}$ per junction. This compares well with the value of $\sim 0.9\text{ eV}$ per junction calculated assuming a nanotube surface energy[31] of 70mJ/m^2 and a junction cross section of 1 nm^2 (almost certainly an overestimate). In fact, the agreement between the estimation of junction fracture energy from the mechanical measurements with that from surface energy considerations is remarkable given the approximate nature of the calculations.

Attempting a similar calculation for the toughness of the film in terms of the work done breaking junctions, w_J (estimated above at $0.7\text{-}0.9\text{ eV}$), gives the expression:

$$T \sim \frac{w_J L}{2l} \times N_J \quad 5.5$$

where l is the gauge length of the film ($\sim 0.02\text{ m}$). Substituting in $w_J \sim 0.9\text{eV}$ gives a value of $dT/dN_J \approx 3.6 \times 10^{-24}\text{ J}$, a value much smaller than the measured value (3.6×10^{-24}

¹⁹J). While this discrepancy is larger than expected, it is consistent with the fact that most of the work of fracture is done deforming the network, not just breaking junctions.

We can also try to understand the weak dependence of the strain at break on N_J . The number of junctions per unit length is $N_J^{1/3}$. If we assume that strain involves the motion of junctions, then a given extension, $l-l_0 \sim N_J^{1/3}l\Delta$ where l is the gauge length and Δ is the junction displacement under strain. The strain at break is then

$$\varepsilon_B \approx N_J^{1/3} \Delta_{\max} \quad 5.6$$

This expression has been fitted to the strain at break data in figure 5.8 giving a reasonable fit. From the fit we get $\Delta_{\max} \sim 0.34$ nm. This means that the junctions are not free to move very far before failure occurs somewhere in the film. It is not clear whether or not it is significant that Δ_{\max} is so close to the van der Waals distance. However it may not be as one would expect the junction to move along the bundle under strain, not away from the bundle.

5.4.2 Analyses of Electrical Results

As discussed above, we expect the network conductivity to depend on both the nanotube conductivity and the network morphology. However, if the nanotubes themselves are much less resistive than the junctions we might expect the conductivity to be dominated by the network properties. In this scenario, the conductivity would be expected to scale with N_J . Shown in fig 5.10A is a plot of σ versus N_J which demonstrates reasonable scaling. However, from fig 5.8C, we know that variations in the defect population and hence variation in the nanotube conductivity result in variations in the film conductivity. This means that unlike the mechanical properties the conductivity should scale with a parameter which includes contributions from both nanotube and network properties. The simplest way to do this is to look for scaling of the conductivity with the combined parameter: $I_G/I_D \times N_J$, shown in figure 5.10B. This graph displays convincing scaling of the conductivity with $I_G/I_D \times N_J$, indicating that, in addition to depending on the conductivity of the individual nanotubes, the film conductivity depends on the morphological properties of the network, or more specifically the junction number density.

So higher conductivity is achieved for lower porosity films and/or films produced from smaller bundles. High conductivity films are generally made from ultra-centrifuged dispersions which consist mainly of individual nanotubes and very small bundles. This translates into low values of D and hence high conductivities. In this work no attempt was made to exfoliate the nanotubes, resulting in large D values and so lower conductivities.

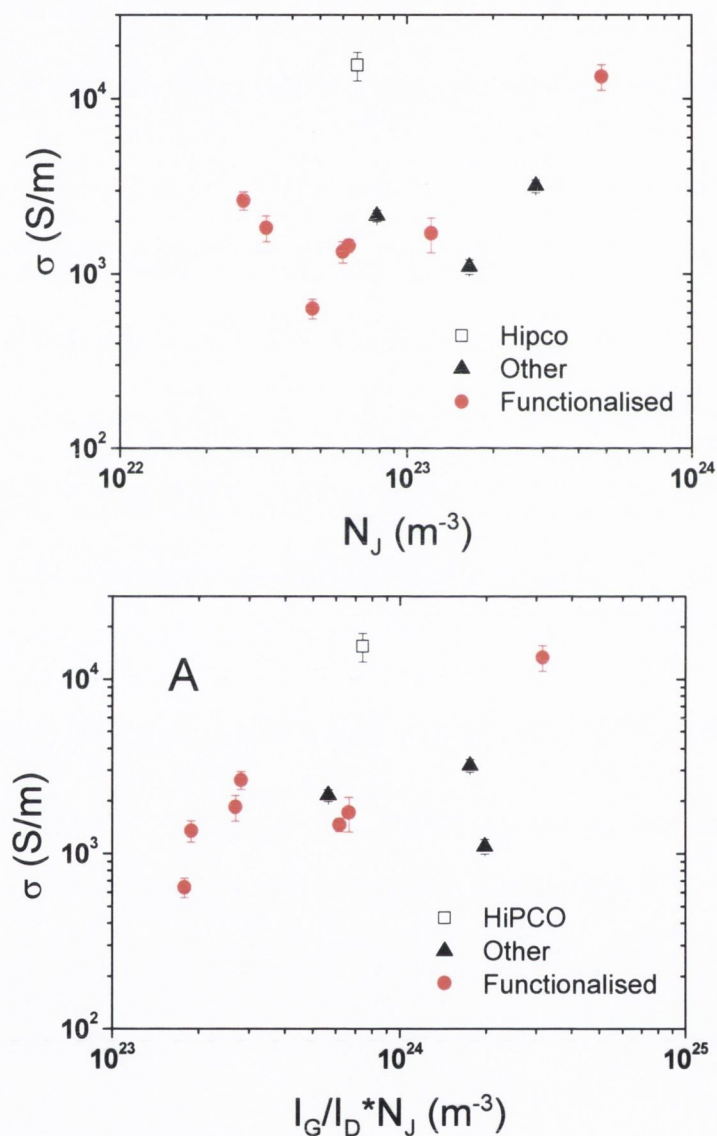


Figure 5.10 Semi-empirical scaling laws for conductivity of nanotube films. A) Approximate scaling of conductivity with number density of inter-nanotube junctions. B) Scaling of conductivity with the product of the junction number density and the Raman ratio.

Lastly, it is important to consider the effect of the functional groups on the properties of the films. In general, the mechanical properties for all the films studied, including those fabricated from functionalised nanotubes, lie close to the $(1-P)^2/D^3$ trend lines. The obvious exceptions are the SWNT-PEG and SWNT-low-COOH films. These materials display strengths slightly above where we might expect according to the analysis. However, the general scaling with $(1-P)^2/D^3$ suggests that film morphology considerations are far more important than any interactions between functional groups of adjacent bundles. This is not so surprising as the functional groups attached to these sort of nanotubes are expected to be predominately at the ends[32]. Furthermore, the agreement between the estimation of junction fracture energy from mechanical measurements with that from surface energy considerations suggests that inter-bundle interactions are similar to graphite-graphite van der Waals interactions rather than interactions between functional groups. In addition, the fact that the mechanical properties in general do not scale with the defect content confirms that the junctions are much weaker than the nanotubes themselves as one would expect.

While the excess stiffness of the SWNT-PEG samples may be due to some entanglement of PEG chains associated with neighbouring bundles, it is felt that this is a small effect in these samples. However, if one wished to enhance this effect, it would be necessary to use nanotubes with a high degree of functionality along their bodies, leading to increased entanglement in the region of junctions. However, the large degrees of functionalisation required might very well reduce the mechanical properties of the nanotubes themselves to a level which could influence the film strength. The ideal situation would be to covalently attach cross-linking molecules that join adjacent nanotubes only at junctions. This would significantly increase junction strength while minimising the degradation of nanotube strength.

Overall, considering the data to hand, it is felt that the role of the functionalities is to influence the dispersibility of the nanotubes during the preparation stage, thus controlling the bundle size. The bundle size most likely then sets the porosity which, coupled with the bundle size, controls the junction number density

5.5 Conclusion

In conclusion the morphological, mechanical and electrical properties of a range of nanotube films made from a selection of commercially available nanotubes were measured. Strong correlation was observed between the mechanical and electrical properties of the films and the film morphology. The defect population as indicated by the Raman G/D ratio correlated strongly with the electrical properties, but only weakly with the mechanical properties.

It has been shown that the number density of inter-bundle junctions is related to both the film porosity and the mean bundle diameter. Both the film strength and toughness scale linearly with junction number density while the strain at break scales sub-linearly. Each of these trends can be explained by simple models. These results underline the importance of morphology to the mechanical properties of nanotube films. It is likely that these findings also apply to recently reported nanotube fibres[5, 13] and sheets[33]. Reasonable scaling of the conductivity with the junction number density has also been observed. However, much better scaling is observed when the conductivity is plotted against the product of the Raman ratio and the junction number density. This demonstrates that the properties of both nanotubes and the network are important for high conductivity films.

This work illustrates that if highly conductive films are required, very conductive, defect free nanotubes are needed which have been extensively exfoliated and arranged into dense films, if mechanical robustness is required the same controls apply but with far less emphasis on the graphitisation of the nanotubes themselves.

SWNTs	Solvent	Y GPa	σ_B MPa	ϵ_B %	T kJm ⁻³	G/D	P %	D nm	σ 10 ³ S/m
As Prepared	NMP	0.6± 0.2	3.5± 1.0	1.5± 0.2	13± 7	9.85	66.4±7 .2	14.5± 3.08	1.449± 0.126
Purified, low- COOH	NMP	0.9± 0.4	7.1± 4	1.3± 0.4	14± 10	8.34	58± 9.04	21± 6.65	1.832± 0.308
Purified, high- COOH	NMP	2.6± 0.3	28± 5	2.4± 0.6	176± 70	6.57	48.2±8 .04	9.8± 3.31	13.353± 2.232
Purified, -ODA	CHCl ₃	1.6± 0.4	9.5± 3.0	1.5± 0.2	37± 15	5.47	51.5± 7.1	14.9± 3.01	1.704 0.386
Purified, - -PEG	Water	2.0± 0.6	11± 3	1.8± 0.6	35± 15	3.16	65.9±8 .2	14.9± 3.63	1.341± 0.187
Purified, - -PABS	Water	0.9± 0.2	2.7± 0.5	0.9± 0.3	5± 0.5	5.3	71.8± 5.9	14.3± 4.54	0.635± 0.081
HipCo	NMP	1.0± 0.3	8.6± 4	2.1± 0.68	47± 31	11.1	50.7±. 5.9	18.3± 5.3	15.54± 2.89
Elicarb- AP	NMP	0.932 ±0.27	10.8± 3.18	1.79± 0.003	109± 63.6	3.5	47.8 ± 5.04	14.74± 3.72	3.187± 0.271
Elicarb- Annealed	NMP	0.289 ±0.09	3.6± 2.05	1.76± 0.66	36.4± 29.4	5.8	68.2±5 .9	13.1± 2.99	2.151± 0.165
Nanolab	NMP	0.695 ±0.25	4.9± 1.48	1.8± 1.6	24± 12.9	10.4 3	64.6±7 .4	20.4± 3.9	2.625± 0.311
SWent	NMP	0.795 ±0.39	6.94± 1.7	1.31± 0.37	28.4± 6.1	12.3 4	44.1±5 .7	15.9± 2.6	1.1± 0.104

Table 5.1. Mechanical and Electrical Properties of NT films.

5.6 References

1. Coleman, J.N., et al., *Improving the mechanical properties of single-walled carbon nanotube sheets by intercalation of polymeric adhesives*. Applied Physics Letters, 2003. **82**(11): p. 1682-1684.
2. Baughman, R.H., A.A. Zakhidov, and W.A. de Heer, *Carbon nanotubes - the route toward applications*. Science, 2002. **297**(5582): p. 787-792.
3. Coleman, J.N., et al., *Small but strong: A review of the mechanical properties of carbon nanotube-polymer composites*. Carbon, 2006. **44**(9): p. 1624-1652.
4. Zhang, D.H., et al., *Transparent, conductive, and flexible carbon nanotube films and their application in organic light-emitting diodes*. Nano Letters, 2006. **6**(9): p. 1880-1886.
5. Motta, M., et al., *Mechanical Properties of Continuously Spun Fibers of Carbon Nanotubes*. Nano Lett., 2005. **5**(8): p. 1529-1533.
6. Giordani, S., et al. *Effect of solvent and dispersant on the bundle dissociation of single-walled carbon nanotube*. 2005. Dublin, Ireland: International Society for Optical Engineering, Bellingham WA, WA 98227-0010, United States.
7. Miko, C., et al., *Effect of electron irradiation on the electrical properties of fibers of aligned single-walled carbon nanotubes*. Applied Physics Letters, 2003. **83**(22): p. 4622-4624.
8. Cadek, M., et al., *Reinforcement of Polymers with Carbon Nanotubes: The Role of Nanotube Surface Area*. Nano Lett., 2004. **4**(2): p. 353-356.
9. Zhang, B., et al., *Preparation and characterization of gas-sensitive composites from multi-walled carbon nanotubes/polystyrene*. Sensors and Actuators B: Chemical, 2005. **109**(2): p. 323-328.
10. Baughman, R.H., et al., *Carbon nanotube actuators*. Science, 1999. **284**(5418): p. 1340-4.
11. Whitten, P.G., G.M. Spinks, and G.G. Wallace, *Mechanical properties of carbon nanotube paper in ionic liquid and aqueous electrolytes*. Carbon, 2005. **43**(9): p. 1891-6.
12. Frizzell, C.J., et al., *Reinforcement of macroscopic carbon nanotube structures by polymer intercalation: The role of polymer molecular weight and chain conformation*. Physical Review B, 2005. **72**(24).
13. Li, Y.-L., I.A. Kinloch, and A.H. Windle, *Direct Spinning of Carbon Nanotube Fibers from Chemical Vapor Deposition Synthesis*. Science, 2004. **304**(5668): p. 276-278.
14. Aguirre, C.M., et al., *Carbon nanotube sheets as electrodes in organic light-emitting diodes*. Applied Physics Letters, 2006. **88**(18).
15. Artukovic, E., et al., *Transparent and flexible carbon nanotube transistors*. Nano Letters, 2005. **5**(4): p. 757-760.
16. Cao, Q., et al., *Transparent flexible organic thin-film transistors that use printed single-walled carbon nanotube electrodes*. Applied Physics Letters, 2006. **88**(11).
17. Gruner, G., *Carbon nanotube films for transparent and plastic electronics*. Journal of Materials Chemistry, 2006. **16**(35): p. 3533-3539.
18. Li, J., et al., *Organic light-emitting diodes having carbon nanotube anodes*. Nano Letters, 2006. **6**(11): p. 2472-2477.

19. Pasquier, A.D., et al., *Conducting and transparent single-wall carbon nanotube electrodes for polymer-fullerene solar cells*. Applied Physics Letters, 2005. **87**(20).
20. Wu, Z.C., et al., *Transparent, conductive carbon nanotube films*. Science, 2004. **305**(5688): p. 1273-1276.
21. Giordani, S., et al., *Debundling of Single-Walled Nanotubes by Dilution: Observation of Large Populations of Individual Nanotubes in Amide Solvent Dispersions*. J. Phys. Chem. B, 2006. **110**(32): p. 15708-15718.
22. Dresselhaus, M.S., et al., *Raman spectroscopy of carbon nanotubes*. Physics Reports, 2005. **409**(2): p. 47-99.
23. Callister, W.D., *Materials science and engineering: An introduction (2nd edition)*. Materials & Design, 1991. **12**(1): p. 59.
24. Yu, M.-F., et al., *Strength and Breaking Mechanism of Multiwalled Carbon Nanotubes Under Tensile Load*. Science, 2000. **287**(5453): p. 637-640.
25. Sammalkorpi, M., et al., *Mechanical properties of carbon nanotubes with vacancies and related defects*. Physical Review B (Condensed Matter and Materials Physics), 2004. **70**(24): p. 245416.
26. Blighe, F., et al., *Advanced Materials* (In press), 2007.
27. Zhao, B., H. Hu, and R C. Haddon, *Synthesis and Properties of a Water-Soluble Single-Walled Carbon Nanotube-Poly (-aminobenzene sulfonic acid) Graft Copolymer*. Advanced Functional Materials, 2004. **14**(1): p. 71-76.
28. Skakalova, V., U. Dettlaff-Weglikowska, and S. Roth, *Electrical and mechanical properties of nanocomposites of single wall carbon nanotubes with PMMA*. Synthetic Metals, 2005. **152**(1-3): p. 349-352.
29. Dai, H., W. Wong, and C.M. Lieber, *Probing electrical transport in nanomaterials: Conductivity of individual carbon nanotubes*. Science, 1996. **272**(5261): p. 523-526.
30. Hecht, D., L.B. Hu, and G. Gruner, *Conductivity scaling with bundle length and diameter in single walled carbon nanotube networks*. Applied Physics Letters, 2006. **89**(13).
31. Bergin, S.D., *Towards solutions of nanotubes in common solvents*. submitted to Nature Nanotechnology, 2007.
32. Niyogi, S., et al., *Chemistry of Single-Walled Carbon Nanotubes*. Acc. Chem. Res., 2002. **35**(12): p. 1105-1113.
33. Zhang, M., et al., *Strong, Transparent, Multifunctional, Carbon Nanotube Sheets*. Science, 2005. **309**(5738): p. 1215-1219.

Chapter 6

Functionalised Single-walled Carbon Nanotube Polyurethane Composites

6.1 Introduction and Relevant Background Literature

The virtues of carbon nanotubes as reinforcing fillers in polymer based composites have been thoroughly discussed in previous chapters. Significant advances have been made in this field in recent years resulting in composites demonstrating large relative increases in stiffness and strength [1-3]. These advances have been enabled by improvements in nanotube dispersion and a deepened understanding of how to improve stress transfer from polymers to nanotubes. Both the issue of stress transfer and dispersion can be addressed simultaneously by using nanotubes which have been covalently functionalized with long molecules that are miscible with the polymer matrix.

Unlike pristine nanotubes which require a surfactant or specific amide solvent to disperse, functionalised nanotubes have been shown to disperse in a wide range of solvents[4-6]. The motivation behind functionalisation is the introduction of defects which disrupt the pi system of the carbon nanotubes reducing their polarisability and thus the van der Waal interactions between them. Functionalised nanotubes are then predicted to show greater interaction within polymer matrices through these functional groups, so aiding stress transfer [7].

There are other obstacles remain regarding efficient carbon nanotube polymer composite preparation, which need to be addressed. In general, reinforcement is not maintained beyond very low nanotube content. This relates to the fact that nanotubes tend to aggregate even at moderate volume fractions, due to effects related to the volume of space available to each nanotube [8], this problem was addressed in chapter 4 [9].

Thermoplastic polymers have been extensively investigated for reinforcement with carbon nanotubes [3]. The addition of nanotubes to a thermoplastic matrix results in an increase in the strength and Youngs' Modulus but a significant decrease in ductility and so toughness [10]. Toughness is the resistance to fracture of a material when stressed and is one of the most important properties for virtually all design applications. Several studies have shown increases in toughness values in polymer matrices on the addition of carbon nanotubes [2, 11-19]. Of these reports, by far the most impressive results have been for composite fibres [14, 20] where large toughness has been achieved even at low nanotube content nanotubes[15, 21]. Recently values of up to 417MJ/m^3 were achieved by the in situ polymerisation of Nylon in the presence of 1 wt% functionalised nanotubes [15]. However, these results notwithstanding, progress towards tough composites has been significantly slower than in other areas.

Fewer studies however have been undertaken to investigate similar reinforcement in elastomeric materials and fewer still discuss the effect on composite toughness. However, a change in the stiffness or Youngs' Modulus is often taken as the marker for reinforcement in composites. This has been observed to a varying degree in several studies on carbon nanotube elastomer composites. Increase factors of between 0.5 and 4 times the original stiffness of the elastomer have been typical involving NT loadings of up to 12.2wt%[22-31]. Less frequently higher increases are achieved. Koerner et al. used a loading of over 16 wt% MWNTs in the elastomer Morthane to achieve a Youngs' Modulus of 165MPa, 16.5 times that of the unfilled elastomer [32]. A composite modulus of 140MPa was observed by Chen et al., 28 times that of the unfilled elastomer, after preparing MWNT polyurethane fibres using an extrusion method [33].

Outside the composite area a number of studies have looked at the mechanical properties of macroscopic materials fabricated solely from carbon nanotubes. These materials include sheets [34], films [35-38] and fibres [39, 40]. A very wide range of mechanical properties have been measured with strengths ranging from $\sim 5\text{MPa}$ for bucky papers [38] to 1GPa for fibres [40]. Toughness values of 14MJ/m^3 have been measured for carbon nanotube films [37] while a toughness value for carbon nanotube fibres appears unpublished to date.

An alternative approach to the problem of toughening thermoplastics is proposed in this chapter. Instead of attempting to increase the toughness of an already stiff and strong plastic it was attempted to improve the stiffness of an already strong and tough elastomer. As elastomers have stiffness's in the range of MPa and the target for a thermoplastic like stiffness would be ~GPa, this requires a huge relative increase in stiffness. In addition, in the ideal case it would be hoped to minimize the degradation of strength and toughness.

A novel approach to composite preparation is to add polymer to dilute nanotube dispersions prior to filtration. This method allows the fabrication of previously unattainable levels of nanotube loading (~ 81wt% NT) within the composite material with minimal reaggregation of the nanotube bundles as was demonstrated in chapter 4 [9]. For this method to succeed, the nanotubes need to be well dispersed in the solvent. Thus functionalized SWNT are a good choice. To facilitate composite formation, the functional groups are required to be compatible with the polymer. To this end, polyethylene glycol functionalized nanotubes (PEG-SWNT) were used and polyurethane was chosen as the polymer. The Hildebrand parameters of PEG and PU are similar ($\delta_{\text{PEG}}=21.1 \text{ MPa}^{1/2}$ and $\delta_{\text{PU}}=20.5 \text{ MPa}^{1/2}$), strong interactions and mixing between the functional groups of the nanotube and the polymer can be expected. This may facilitate stress transfer between polymer and nanotube. For comparison purposes unfunctionalised nanotubes dispersed using a common surfactant we also prepared.

Thermogravimetric analysis revealed that almost all of the polyurethane included in the original dispersions remained present in the final composite, allowing great ease of reproducibility. A wide range of nanotube mass fraction composites were prepared. Stress-strain measurements show, that on varying the functionalised nanotube mass fraction, the strength of the composite remained relatively unchanged while the toughness scaled over 3 orders of magnitude. The stiffness of these composites increased dramatically by almost three orders of magnitude, far more significantly than what is currently observed in literature.

This tuneable composite is weak, ductile and tough at low nanotube loadings yet strong, stiff and brittle at high nanotube loadings. Speculatively, this method may also be applied to other polymer matrices to attain specific composite properties.

6.2 Film Fabrication

From previous study in chapter 5 nanotube films prepared using PEG and COOH functionalised nanotubes showed superior mechanical properties to those prepared from a range of other commercially available nanotubes. The PEG functionalities, as previously mentioned, allow the nanotubes to disperse in water, therefore eliminating the need for a high boiling point solvent or surfactant. This characteristic was considered a serious advantage and was the motivation in selecting PEG-SWNTs for further study.

The PEG groups of the functionalized nanotubes possess a Hildebrand or solubility parameter of $\delta_{\text{PEG}}=21.1 \text{ MPa}^{1/2}$ very close to that of the elastomer polyurethane, $\delta_{\text{PU}}=20.5 \text{ MPa}^{1/2}$ [41]. The Hildebrand parameter is the square root of the cohesive energy density which is the energy of vaporisation in calories per cubic centimetre and is a direct reflection of the degree of van der Waals forces holding the molecules of the substance together. If two substances possess similar Hildebrand parameters they are miscible [42].

When incorporating functionalised carbon nanotubes into polymers, compatibility between the functional groups of the nanotube and the polymer is desirable to ensure improved nanotube matrix stress transfer. For this reason polyurethane was chosen as the host matrix for these composites. For comparison a set of surfactant dispersed Hipco nanotube composites were also prepared.

Two methods were used to prepare films of both SWNT varieties. The first, a combined dispersion method, involved adding Hipco SWNTs at 0.0875mg/ml and SDBS (sodium dodecylbenzene sulphonate) at 0.4375mg/ml to dionised water and sonicating for 5 min using a high-power ultrasonic tip (GEX600, 240W, 120kHz). These dispersions then underwent an hour sonication in a low-power ultrasonic bath followed by a further 5 mins under the sonic tip. They were then mildly centrifuged at 5500rpm for 90mins. The absorption spectra from before and after centrifugation were compared to find the resulting NT concentration of the dispersion. Varying amounts of waterborne polyurethane was added to obtain a range of NT mass fractions. The NT polyurethane dispersions were sonicated in a low-power ultrasonic bath for 20 minutes. Lastly they were vacuum filtered through a Teflon filter paper (pore size=0.45 μm), and dried at ambient temperature for 12 hrs in a vacuum oven. PEG-SWNT / polyurethane dispersions were prepared in a similar way but without the use of SDBS as PEG-SWNTs disperse well in water [6].

A layer by layer (LBL) approach was taken for the second method. The SWNT dispersions were prepared as above, but instead of combining the polyurethane with the NT dispersion, separate polyurethane/water dispersions were prepared. Alternate controlled volumes of SWNT and polyurethane dispersions were passed through the filter. Each additional layer added only after the previous had fully filtered.

A drop cast film of polyurethane was also prepared for comparison.

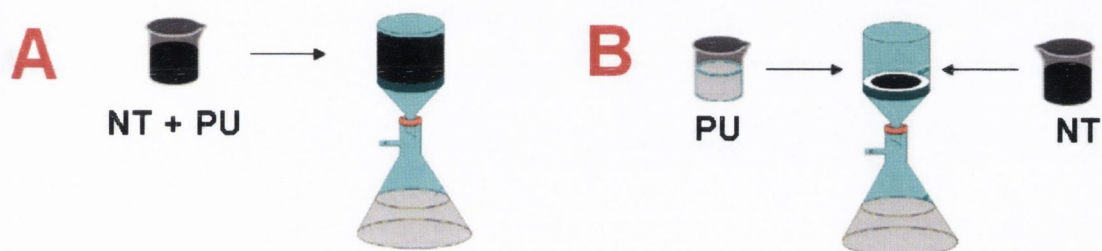


Figure 6.1 Illustration of A) the combined preparation method. B) Layer by layer preparation method.

All films were free standing and had thicknesses of between 10 and 77 μm after being peeled from the filter paper. They were cut into strips of width 2.2mm and lengths of several centimetres.

6.3 Film Analysis

Porosity measurements were made of the films as in chapter 4. The measured porosities range between 20 and 82%. Thermogravimetric analysis was carried out to find the nanotube mass fractions of the composites again as in chapter 4. On this occasion there was very little loss of polymer during the filtration process, typically between 1wt% and 2wt% polymer content of original dispersion, figure 6.2. This allowed considerable control of NT mass fraction of the resulting composites. Composites were prepared with nanotube mass fractions of up to 75 wt%.

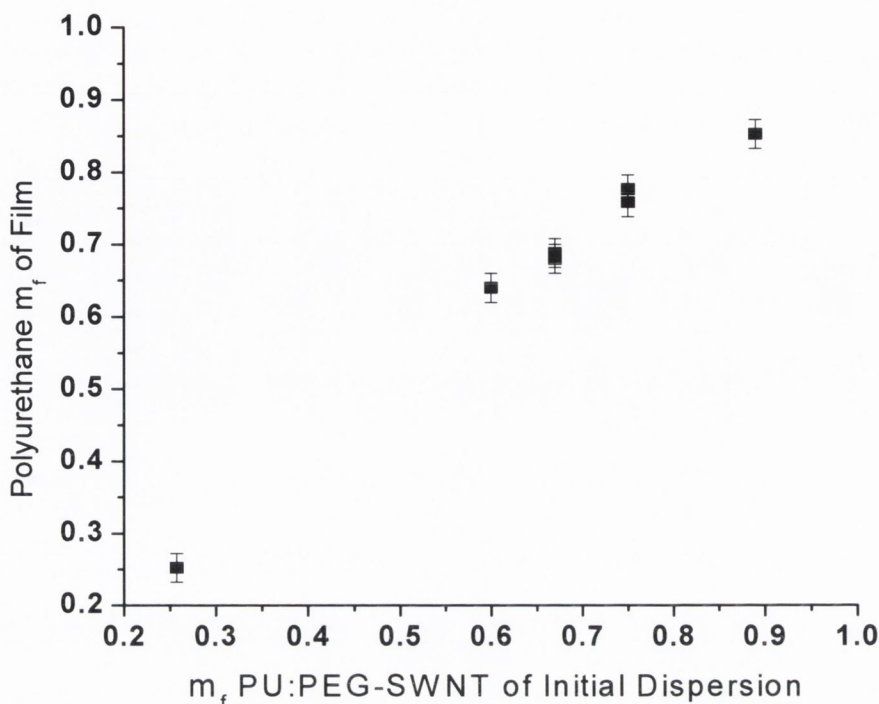


Figure 6.2 Polyurethane content of film as a function of PU:PEG-SWNT ratio of initial dispersion

6.3.1 Scanning Electron Microscopy of Carbon Nanotube Elastomer Films

Scanning Electron Microscopy (SEM) images were taken of the nano-composites, without any coating, to examine their internal structures. The internal surfaces were exposed by both tensile fracture and cutting. Examples of these images are shown in figures 6.3-6.6. The composites prepared by the standard combined method appeared as might be expected, a porous tangled mesh of nanotube bundles within the polymer matrix. They appeared inhomogeneous on a length scale of microns probably due to the particulate nature of the original PU emulsions, figure 6.3.

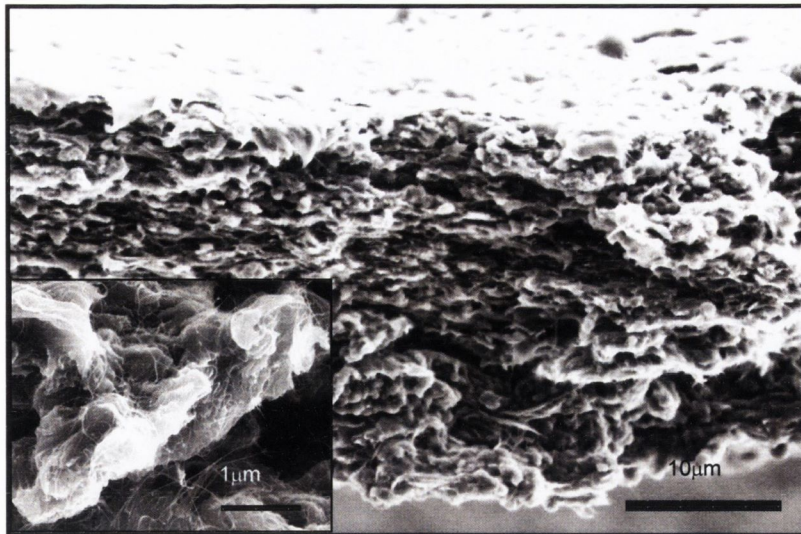


Figure 6.3 Fracture surface of a standard composite, PEG-SWNT (24wt%)

Displayed in the inset is a magnified image showing that the polymer matrix consists of micron sized fused particles, with significant amounts of free volume. The internal surface of the polymer matrix appears to be covered by a network of bundles of SWNTs. This image is typical of the combined dispersion composites produced by this method for both tube types. The cut surface of the layered Hipco composite, however show clear separation between the nanotube and polymer layers, figure 6.4.

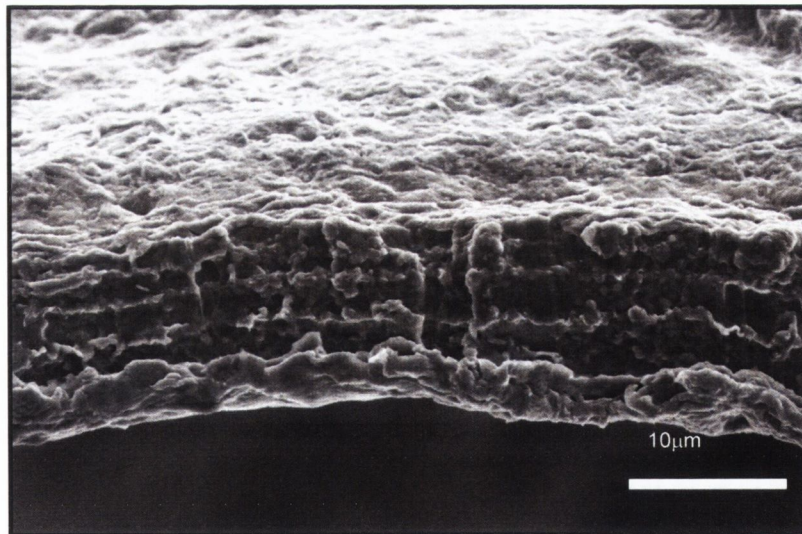


Figure 6.4 Cut surface of a Hipco (22wt%)-PU LBL composite clearly showing the presence of layers

The fractured surface image of the same sample shows the separated position of some of the layers after fracture, figure 6.5.

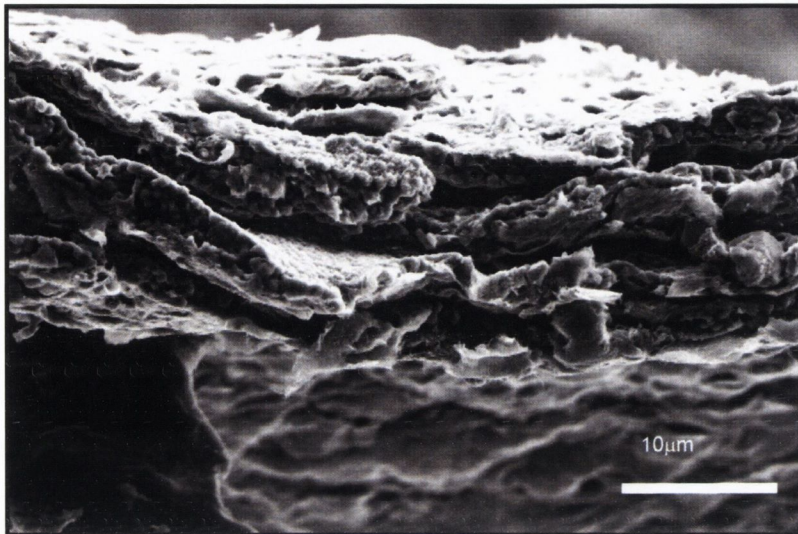


Figure 6.5 Fracture surface of the film shown in 6.4

In figure 6.6 delamination between the nanotube and polymer layers is observed in the fracture sample of the PEG-SWNT/PU layered composite. Alternate layers of nanotube and polyurethane appear ripped apart from each other during fracture, peeling perpendicular to the fracture direction. Typically delamination results in increased toughness in composite materials as energy is required to separate layers from each other.

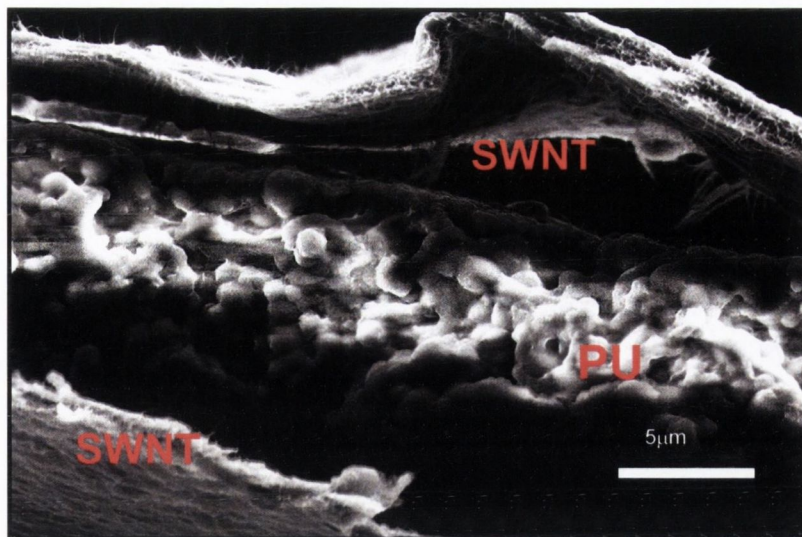


Figure 6.6 Fracture surface of a PEG-SWNT (24wt%) LBL composite showing extensive delamination of SWNT and PU layers

From these SEM images it is evident that the two methods of composite preparation result in very different systems one consisting of nanotube bundles dispersed evenly in the polymer matrix and one where the nanotubes and the polymer are separate in distinct layers. The advantages or otherwise of these types of structures will be investigated subsequently.

6.3.2 Mechanical Analysis of Carbon Nanotube Elastomer films

Stress strain curves were measured for each film type with representative curves plotted in figure 6.7 (note that the strain axis is shown on a log scale).

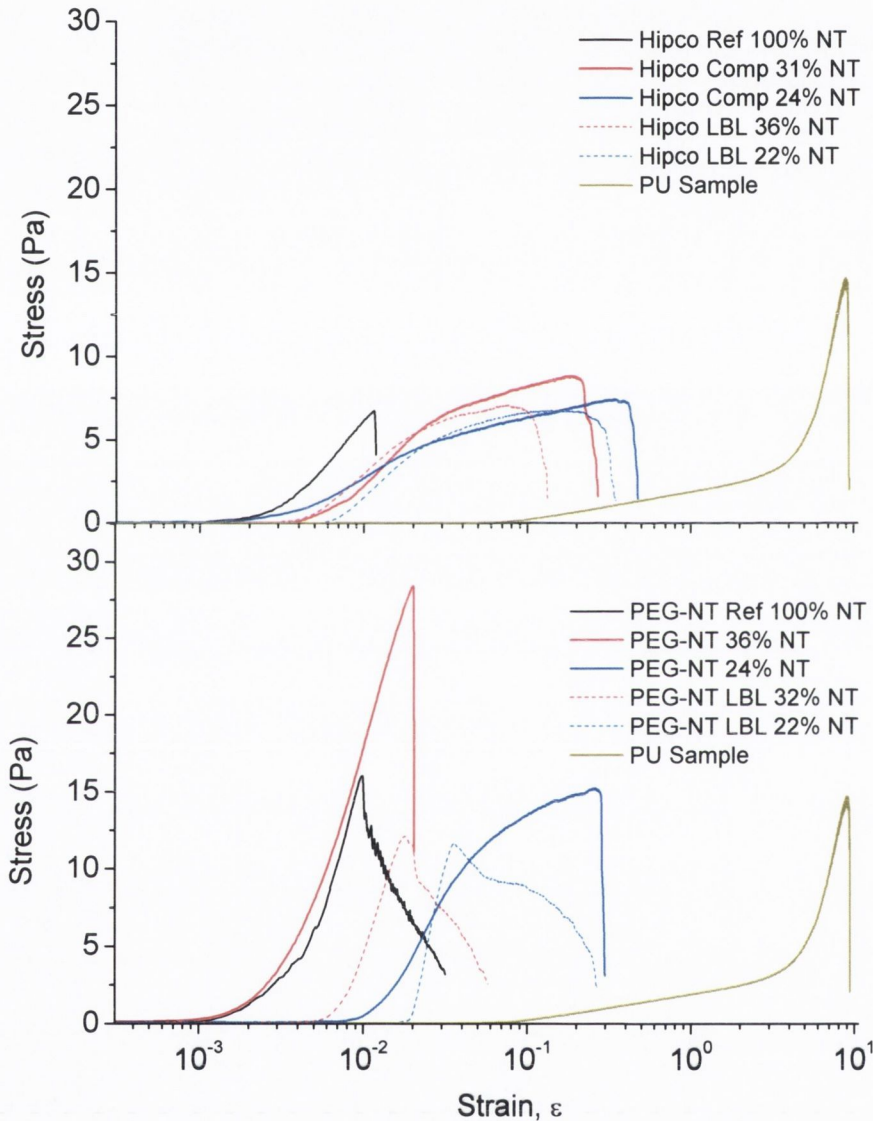


Figure 6.7 Representative stress-strain curves of A) Hipco B) PEG-NT papers.

The curves for both of the NT only samples exhibit typical thermoplastic style behaviour being weak, stiff and brittle [43]. The PU curve shows typical elastomer elongation before break at up to 11 times its original length. The composite curves

predominantly show a mixed behaviour between that of the nanotube film and the elastomer, indicating that the reinforcement may be governed by the nanotube network and not by individual nanotubes. The layered composites indicated by the dashed lines show slightly poorer performance than those prepared by the combined method.

As previously stated four main mechanical parameters can be obtained from these curves; the Youngs' modulus, Y , the toughness, T (energy required to break per unit volume), the strength at break, σ_B , and strain at break, ϵ_B . For each film type, stress strain curves were measured for five strips, the four mechanical parameters calculated and the mean and standard deviation computed. The ranges of values measured were: modulus (3.7MPa -3.37 GPa), strength (5-26 MPa), toughness (0.1-80 MJ/m³), strain at break (1-1140%).

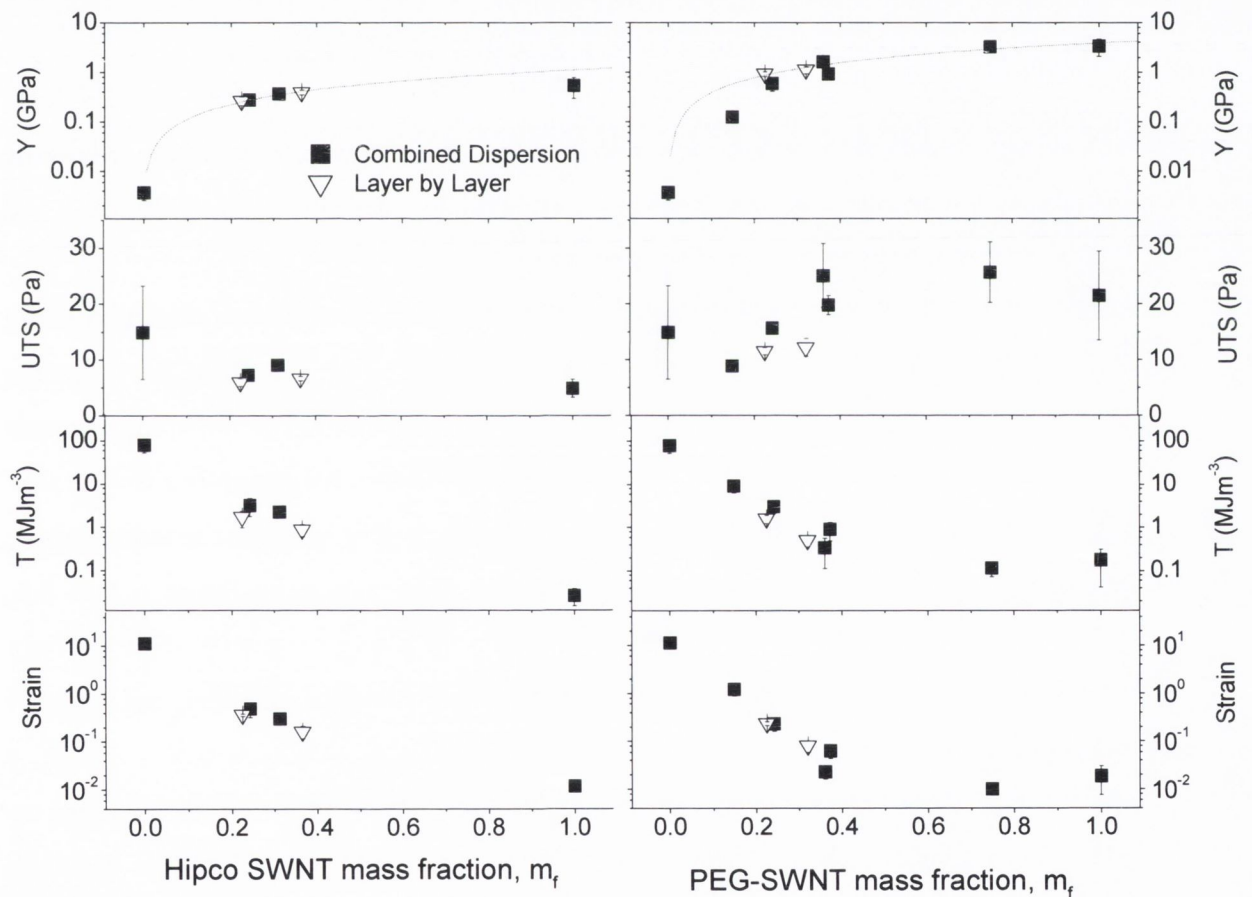


Figure 6.8 Youngs Modulus (Y), Ultimate Tensile Strength (UTS), Toughness (T) and Strain versus Hipco-NT and PEG-NT mass fraction

It is worth noting that virtually all mechanical properties of the composites are bound between the values of the polymer itself and the nanotube only film. Figure 6.8 shows the mechanical properties of both Hipco and PEG-SWNT based films as a function of the nanotube mass fraction.

The Youngs' Modulus increases more or less linearly from 3.7MPa for PU to 0.54GPa (an increase of 145 times) for the Hipco film, as shown by the straight line fit, the slope of this increase, dY/dM_f , is 1.1GPa. The highest mass fraction Hipco film, 31wt % nanotubes, shows a Youngs' Modulus increase of 105 times that of the unfilled polymer. This is far above the increases that have been observed in literature, which as previously mentioned are typically less than a factor of 4. The few studies that have shown augmented values also do not approach the reinforcement factor observed in these films.

For the PEG-SWNT /PU films the Youngs' Modulus again increases linearly from 3.7MPa for PU to 3.37GPa for the PEG-SWNT only film with an observed dY/dM_f value of 9.9GPa. The best performing PEG-NT composite had a nanotube m_f of 75 wt% and preformed 889 times better than the pure elastomer.

This is, by a large margin, the largest fractional increase in stiffness observed using nanotubes as a filler, both of the dY/dM_f slopes are similar to the moduli of the nanotube only films. This would be expected from the Rule of Mixtures [3] if the reinforcement consisted of fragments of nanotube networks rather than individual nanotubes or bundles. Almost all the mechanical properties of the composites are bound between the values of the polymer itself and the nanotube only film. From the SEM images in figure 6.3 to 6.6, networks of nanotube bundles are clearly present within the elastomer matrix. This strongly suggests that the nanotube bundle network is responsible for reinforcement, not isolated nanotubes.

The most obvious difference between the Hipco and PEG-SWNT films is apparent on analysis of the ultimate tensile strength values. The addition of Hipco nanotubes weakens PU films. This weakening is understandable, as if the reinforcement is by the nanotube network and the Hipco network is itself weaker than the polyurethane film (4.9 ± 1.6 MPa versus 15 ± 8 MPa respectively). However addition of PEG-SWNT strengthens films with strength increasing from 15 ± 8 MPa for PU to a maximum of 26 ± 5 MPa ($m_f = 75\%$) for the

highest load composite. Again this can be understood because the PEG-SWNT has a strength of 22 ± 8 MPa, significantly higher than the PU.

For both nanotube types strain at break falls off from 1140% for PU to 4% and 3% for Hipco and PEG-SWNT respectively. This results in a dramatic decrease in toughness as the nanotube mass fractions increases to about $m_f \sim 0.4$ after which the composite properties appear to be dominated by the network. The toughness also falls by 3 orders of magnitude within this range before saturating at higher nanotube mass fractions. Interestingly the fall off in toughness at low mass fraction is virtually identical for samples prepared with both Hipco and PEG-SWNT. This suggests that the toughness is insensitive to the nature of the polymer-nanotube interface. Most likely the presence of the network disrupts the deformation of the polymer at high strain resulting perhaps in localized stress concentration and premature rupture.

When examining the ultimate tensile strength values of the PEG-SWNT composites the importance of the functional groups becomes evident.

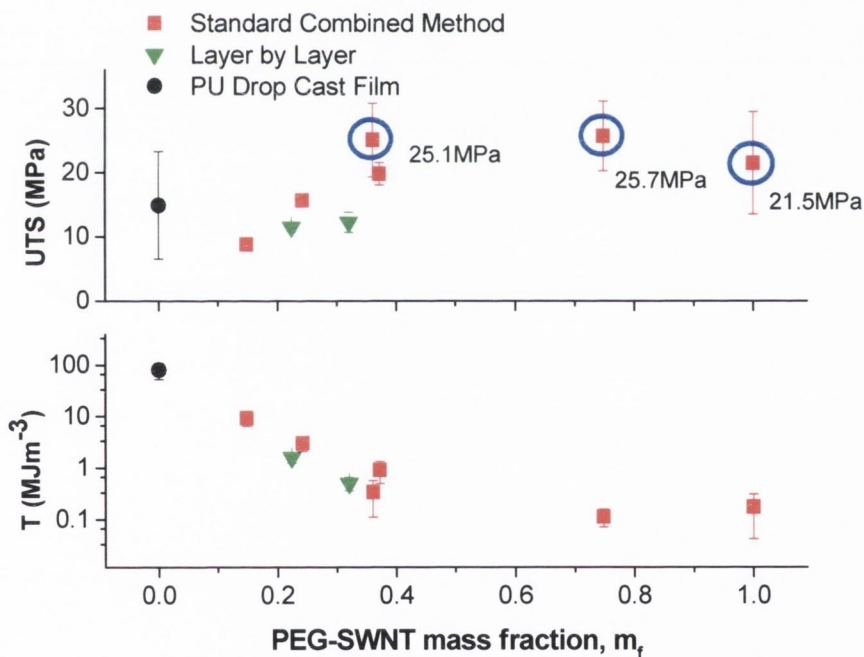


Figure 6.9 The Ultimate Tensile Strength and Toughness of the PEG-SWNT polyurethane films as a function of nanotube mass fraction.

It can be observed that while all the other mechanical properties are completely governed by the properties of the nanotube network the strength values show a slight departure from this trend, as observed in figure 6.9 and highlighted by the blue markers. Although these increases are by no means dramatic they suggest improved interaction between filler and matrix facilitated presumably by the nanotube functionalities. It is in the strength measurements that the layered composites also show the poorest performance in comparison to the combined method composites.

In all macroscopic forms of carbon nanotubes it is the junctions between the nanotube bundles that fail under stress rather than the nanotubes themselves, a method of increasing this interaction is to incorporate a polymer material to act as a glue to hold the bundles together. Further experiments using this method may show greater reinforcement using different polymers and nanotube functionalities.

6.3.3 Electrical Characterisation of Carbon Nanotube Elastomer Films

While this study was undertaken primarily to investigate mechanical reinforcement in such polymer nanotube systems bulk, in-plane, electrical measurements were also carried out on the films using the method described in chapter 4. Resistance (R_T) measurements were of strips cut from the films made as a function of length (l), as shown in figure 6.10 for both the pristine and functionalised nanotube composite films.

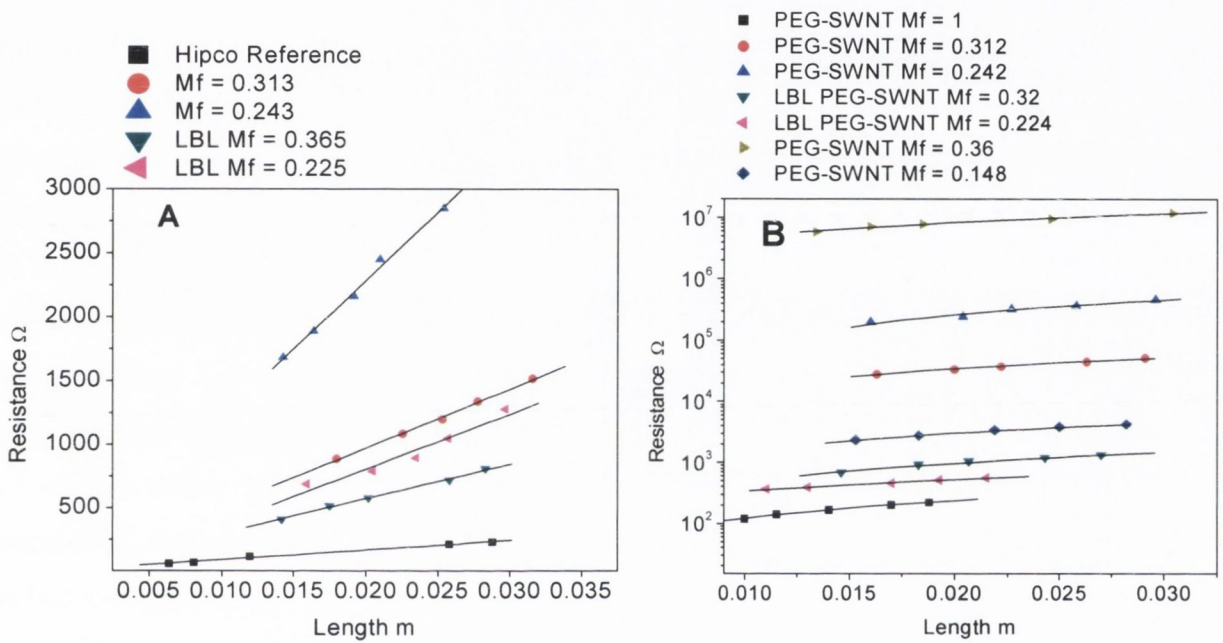


Figure 6.10 Resistance versus sample length for selected nanotube loading levels A) Hipco B) PEG-SWNT Composites.

The plots of conductivity versus mass fraction and true volume fraction for all films are shown in figure 6.11. For the PEG-SWNT films the conductivities ranged from ~ 0.01 S/m for papers of ~ 36 wt% NT up to ~ 5750 S/m for the nanotube-only bucky paper. For the Hipco films the conductivities ranged from ~ 0.716 S/m for papers of ~ 24 wt% NT up to ~ 3970 S/m for the nanotube-only bucky paper. The layer composites showed higher

conductivities when compared to the combined method composites presumably due to the continuous layers of nanotube network present in the films.

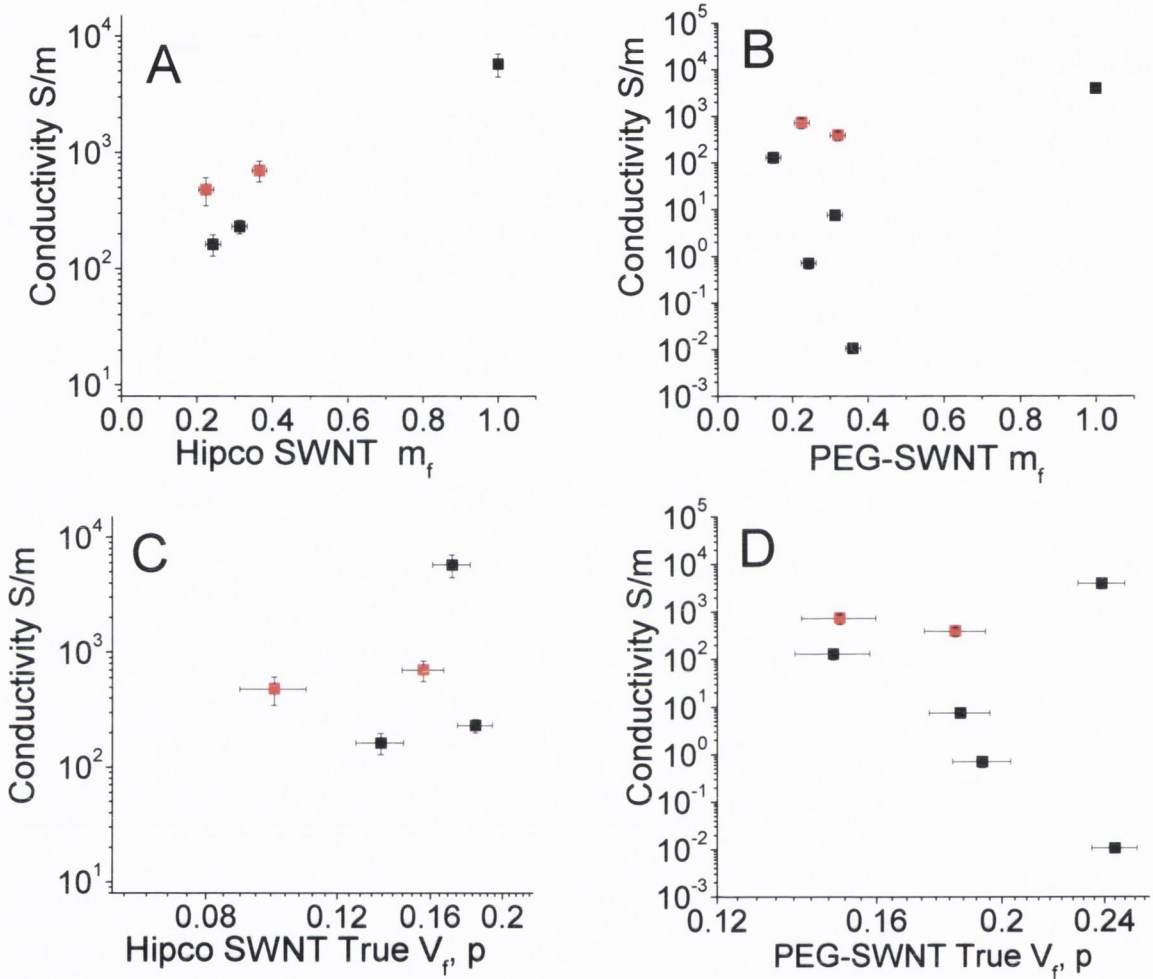


Figure 6.11 Conductivity versus mass fraction and true volume fraction for all films (The red squares represent the layered composites).

When the conductivities are plotted as a function of true nanotube volume fraction the smooth scaling observed in chapter 4 is less evident. This is more than likely due to the fact that the films here are of a different nature than those investigated in chapter 4 being prepared from polymer particles dispersed in water rather than a polymer solution.

6.4 Discussion

It is notable that the mechanical properties are significantly better for the PEG-SWNT based composites compared to the Hipco based materials. Thus the mechanical properties of the PEG-SWNT composites will be discussed in detail, see table 6.1 for mechanical properties. The most obvious point is that the introduction of nanotubes enhances the stiffness and strength but degrades the ductility and hence the toughness. The increase in strength is marginal; $\sim \times 2$. However the changes in both stiffness and toughness are dramatic.

The curves from the mechanical results data can essentially be divided into two regions. Without any decrease in strength, below 40wt% the mechanical properties change rapidly with addition of NTs. Above 40% the properties are very close to that of the Bucky paper and are dominated by the NT network. In the first region the properties can be tuned over a very wide range. The choice of strong, stiff but brittle composites at the high end of the scale or weak, ductile and tough composites at the other end is possible. The simplicity of the composite preparation, where so little material is lost during filtration makes this tuning entirely possible. By adding a specific amount of carbon nanotubes the desired mechanical properties can be attained.

The strength and toughness of the layered composites were lower than those prepared by the combined dispersion method. This is surprising as layered composites have performed well in other studies [44], and delamination is observed in SEM images of the fracture samples. This is usually good at stopping cracks and so increasing strength. However, we might presume that in spite of good stress transfer present in the combined composites, less interaction occurs between NTs and the matrix in the layered structures and this acts to counteract any reinforcement offered by the energy required for layer separation.

While this work was carried out using an elastomer, structural plastics tend to be thermoplastics or thermosets. Thermoplastic polymers tend to have stiffness's in the region of ~ 0.1 -5GPa, strengths in the region of 10-50 MPa and toughness's of 0.5-1 MJ/m³ or 10-60 MJ/m³ depending on whether they are brittle or ductile. Picking two mass fractions of our PU/PEG-SWNT composites for comparison: at $m_f = 0.31$ we can get $Y = 0.9$ GPa, $\sigma = 20$ MPa, $\epsilon_B = 8\%$ and $T = 0.9$ MJ/m³, values typical of a brittle thermoplastic. In comparison at

$m_f = 0.15$ we can get $Y = 0.13$ GPa, $\sigma = 9$ MPa, $\epsilon_B = 120\%$ and $T = 9.4$ MJ/m³, values typical of a reasonably ductile thermoplastic. This illustrates that this material is incredibly versatile in terms of the mechanical properties obtainable.

The fact that Rule of Mixtures like behaviour is observed for both SWNT types raises a number of questions. Rule of mixture behaviour is usually associated with good stress transfer from matrix to nanotube. Such stress transfer is thought to be significantly improved by functionalisation of the nanotubes. However, for both Hipco and PEG-SWNT films, the same Rule of mixture behaviour is observed with dY/dM_f close to the network modulus. This suggests that the modulus reinforcement is limited by the modulus of the network and not the functionalisation. The functionalisation may play an indirect role in improving the mechanical properties of the network of PEG-SWNT. However there is no real evidence of an enhancement in stress transfer through using functionalized nanotubes.

In reality, this situation occurs solely because of the formation of a nanotube network in these samples rather than isolated nanotubes. This happens for two reasons. Firstly at the high volume fractions used in this work, adjacent nanotubes tend to come very close during the film formation phase potentially facilitating aggregation or, in some cases, network formation. There may, however, be a more important criterion. The polymer used here comes in the form of a waterborne emulsion of micron sized particles. During the film formation phase, steric effects probably force the dispersed nanotubes to occupy the free volume between the particles. This then results in the formation of a nanotube network, even at reasonably low volume fractions. This is supported by the inset in figure 6.3 which shows the presence of a network coated onto the internal surface of the composite. Incidentally, the fact that the nanotube network is coated onto the polymer in the space between PU particles would be expected to limit the interaction with the polymer and ultimately the maximum stress transferred to the nanotubes.

An interesting question would be whether this method could be used to make composites where individual SWNTs, rather than networks, are embedded in a polymer matrix even at high volume fraction. The first criterion is that we would require a soluble polymer, rather than a particulate emulsion such as that used here. To avoid nanotube aggregation, the nanotubes should be very soluble, achievable by using functionalized nanotubes. To maintain a good dispersion during the drying phase, the polymer should be

compatible with the nanotubes functional groups. This allows polymer coating of the nanotubes to be favourable compared with nanotube aggregation. These criteria are consistent with a system of solvent, polymer and functionalized nanotubes where all three components have very similar Hildebrand parameters. Information on the Hildebrand parameters of solvents and polymers is readily obtainable. In addition it has recently been shown that the Hildebrand parameter of a functionalized nanotube is essentially that of its functional groups [45]. Thus, it should be reasonable straightforward to identify the components of such a system bearing in mind that the choice of high-quality functionalized nanotubes is much lower than that for commercial polymers.

SWNT Mass fraction	Young GPa	UTS MPa	Strain at break	Toughness MJm ⁻³
1.00	3.4 ± 1.3	22 ± 8	0.03 ± 0.01	0.2 ± 0.13
0.75	3.3 ± 0.6	26 ± 5	0.01 ± 0.001	0.12 ± 0.04
0.36	1.6 ± 0.4	25 ± 6	0.023 ± 0.01	0.34 ± 0.2
0.31	0.9 ± 0.15	20 ± 2	0.08 ± 0.02	0.9 ± 0.4
0.24	0.6 ± 0.2	16 ± 1	0.25 ± 0.07	3.0 ± 0.9
0.15	0.13 ± 0.02	9 ± 1	1.2 ± 0.3	9.4 ± 3
0.00	0.004 ± 0.001	15 ± 8	11.4 ± 1.3	80 ± 30

Table 6.1 Mechanical properties of PEG-SWNT Films

6.5 Conclusion

A simple method of nanotube composite preparation has been demonstrated that allows the preparation of wide ranging, extremely high m_f composites with minimal reaggregation of the nanotubes. Composites prepared with functionalised NTs dispersed in water display superior mechanical properties to those prepared using unfunctionalised tubes and a surfactant. The Youngs' Modulus of these composites increased by three orders of magnitude, as the nanotube mass fraction was increased from 0% to 100%. While the strength scaled weakly with mass fraction, the toughness fell by a factor of ~ 200 upon loading with 40 wt% SWNT after which it saturated at a value close to that of the nanotube network. These PEG-SWNT polyurethane composites exhibit tuneable stiffness and toughness, without sacrificing strength.

6.6 References

1. Blond, D., et al., *Enhancement of Modulus, Strength, and Toughness in Poly(methyl methacrylate)-Based Composites by the Incorporation of Poly(methyl methacrylate)-Functionalized Nanotubes*. *Advanced Functional Materials*, 2006. **16**(12): p. 1608-1614.
2. Coleman, J.N., et al., *High Performance Nanotube-Reinforced Plastics: Understanding the Mechanism of Strength Increase*. *Advanced Functional Materials*, 2004. **14**(8): p. 791-798.
3. Coleman, J.N., et al., *Small but strong: A review of the mechanical properties of carbon nanotube-polymer composites*. *Carbon*, 2006. **44**(9): p. 1624-1652.
4. Niyogi, S., et al., *Chemistry of Single-Walled Carbon Nanotubes*. *Acc. Chem. Res.*, 2002. **35**(12): p. 1105-1113.
5. Zhao, B., H. Hu, and R.C. Haddon, *Synthesis and Properties of a Water-Soluble Single-Walled Carbon Nanotube-Poly(-aminobenzene sulfonic acid) Graft Copolymer*. *Advanced Functional Materials*, 2004. **14**(1): p. 71-76.
6. Zhao, B., et al., *Synthesis and Characterization of Water Soluble Single-Walled Carbon Nanotube Graft Copolymers*. *J. Am. Chem. Soc.*, 2005. **127**(22): p. 8197-8203.
7. S. Banerjee, T.H.-B.S.S.W., *Covalent Surface Chemistry of Single-Walled Carbon Nanotubes*. *Advanced Materials*, 2005. **17**(1): p. 17-29.
8. Bergin, S.D., et al., *Exfoliation in Ecstasy: Liquid crystal formation and chirality dependent debundling observed for single wll nanotubes dispersed in the liquid drug Butyrolactone*. *Nanotechnology*, 2007. **in press**.
9. Blighe, F.M., et al., *Observation of percolation-like scaling, far from the percolation threshold, in high volume fraction, high conductivity polymer-nanotube composite films*. *Advanced Materials* 2007. **Accepted**.
10. Meincke, O., et al., *Mechanical properties and electrical conductivity of carbon-nanotube filled polyamide-6 and its blends with acrylonitrile/butadiene/styrene*. *Polymer*, 2004. **45**(3): p. 739-748.
11. Bhattacharyya, S., J.-P. Salvetat, and M.-L. Saboungi, *Reinforcement of semicrystalline polymers with collagen-modified single walled carbon nanotubes*. *Applied Physics Letters*, 2006. **88**(23): p. 233119.
12. Blond, D., et al., *Enhancement of modulus, strength, and toughness in poly(methyl methacrylate)-based composites by the incorporation of poly(methyl methacrylate)-functionalized nanotubes*. *Advanced Functional Materials*, 2006. **16**(12): p. 1608-1614.
13. Chen, W., et al., *Enhanced mechanical properties and morphological characterizations of poly(vinyl alcohol)-carbon nanotube composite films*. *Applied Surface Science*, 2005. **252**(5): p. 1404-1409.
14. Dalton, A.B., et al., *Super-tough carbon-nanotube fibres*. *Nature*, 2003. **423**(6941): p. 703-703.
15. Moniruzzaman, M., et al., *Tuning the mechanical properties of SWNT/nylon 6,10 composites with flexible spacers at the interface*. *Nano Letters*, 2007. **7**(5): p. 1178-1185.

16. Ruan, S., P. Gao, and T.X. Yu, *Ultra-strong gel-spun UHMWPE fibers reinforced using multiwalled carbon nanotubes*. *Polymer*, 2006. **47**(5): p. 1604-1611.
17. Wang, M., K.P. Pramoda, and S.H. Goh, *Enhancement of the mechanical properties of poly(styrene-co-acrylonitrile) with poly(methyl methacrylate)-grafted multiwalled carbon nanotubes*. *Polymer*, 2005. **46**(25): p. 11510-11516.
18. Yang, B.-X., et al., *Enhancement of stiffness, strength, ductility and toughness of poly(ethylene oxide) using phenoxy-grafted multiwalled carbon nanotubes*. *Nanotechnology*, 2007. **18**(12): p. 125606.
19. Zhong-Ming, L., et al., *A novel approach to preparing carbon nanotube reinforced thermoplastic polymer composites*. *Carbon*, 2005. **43**(11): p. 2413-16.
20. Miaudet, P., et al., *Hot-Drawing of Single and Multiwall Carbon Nanotube Fibers for High Toughness and Alignment*. *Nano Lett.*, 2005. **5**(11): p. 2212-2215.
21. Néri, W., et al., *Surfactant-Free Spinning of Composite Carbon Nanotube Fibers*. *Macromolecular Rapid Communications*, 2006. **27**(13): p. 1035-1038.
22. Buffa, F., et al., *Effect of nanotube functionalization on the properties of single-walled carbon nanotube/polyurethane composites*. *Journal of Polymer Science Part B: Polymer Physics*, 2007. **45**(4): p. 490-501.
23. Cantournet, S., M.C. Boyce, and A.H. Tsou, *Micromechanics and macromechanics of carbon nanotube-enhanced elastomers*. *Journal of the Mechanics and Physics of Solids*, 2007. **55**(6): p. 1321-1339.
24. Frogley, M.D., D. Ravich, and H.D. Wagner, *Mechanical properties of carbon nanoparticle-reinforced elastomers*. *Composites Science and Technology*, 2003. **63**(11): p. 1647-1654.
25. Kuan, H.-C., et al., *Synthesis, thermal, mechanical and rheological properties of multiwall carbon nanotube/waterborne polyurethane nanocomposite*. *Composites Science and Technology*, 2005. **65**(11-12): p. 1703-1710.
26. Li, Y. and H. Shimizu, *High-shear processing induced homogenous dispersion of pristine multiwalled carbon nanotubes in a thermoplastic elastomer*. *Polymer*, 2007. **48**(8): p. 2203-2207.
27. Sahoo, N.G., et al., *Influence of carbon nanotubes and polypyrrole on the thermal, mechanical and electroactive shape-memory properties of polyurethane nanocomposites*. *Composites Science and Technology*, 2007. **67**(9): p. 1920-1929.
28. Wei Chen, X.T., *Self-Organizing Alignment of Carbon Nanotubes in Thermoplastic Polyurethane*. *Macromolecular Rapid Communications*, 2005. **26**(22): p. 1763-1767.
29. Xia, H. and M. Song, *Preparation and characterization of polyurethane-carbon nanotube composites*. *Soft Matter*, 2005. **1**(5): p. 386-394.
30. Xia, H. and M. Song, *Preparation and characterisation of polyurethane grafted single-walled carbon nanotubes and derived polyurethane nanocomposites*. *Journal of Materials Chemistry*, 2006. **16**(19): p. 1843-1851.
31. Jung, Y.C., N.G. Sahoo, and J.W. Cho, *Polymeric Nanocomposites of Polyurethane Block Copolymers and Functionalized Multi-Walled Carbon Nanotubes as Crosslinkers*. *Macromolecular Rapid Communications*, 2006. **27**(2): p. 126-131.
32. Koerner, H., et al., *Deformation-morphology correlations in electrically conductive carbon nanotube thermoplastic polyurethane nanocomposites*. *Polymer*, 2005. **46**(12): p. 4405-4420.

33. Chen, W., X. Tao, and Y. Liu, *Carbon nanotube-reinforced polyurethane composite fibers*. *Composites Science and Technology*, 2006. **66**(15): p. 3029-3034.
34. Zhang, D.H., et al., *Transparent, conductive, and flexible carbon nanotube films and their application in organic light-emitting diodes*. *Nano Letters*, 2006. **6**(9): p. 1880-1886.
35. Baughman, R.H., et al., *Carbon nanotube actuators*. *Science*, 1999. **284**(5418): p. 1340-4.
36. Whitten, P.G., G.M. Spinks, and G.G. Wallace, *Mechanical properties of carbon nanotube paper in ionic liquid and aqueous electrolytes*. *Carbon*, 2005. **43**(9): p. 1891-6.
37. Coleman, J.N., et al., *Improving the mechanical properties of single-walled carbon nanotube sheets by intercalation of polymeric adhesives*. *Applied Physics Letters*, 2003. **82**(11): p. 1682-1684.
38. Frizzell, C.J., et al., *Reinforcement of macroscopic carbon nanotube structures by polymer intercalation: The role of polymer molecular weight and chain conformation*. *Physical Review B*, 2005. **72**(24).
39. Li, Y.-L., I.A. Kinloch, and A.H. Windle, *Direct Spinning of Carbon Nanotube Fibers from Chemical Vapor Deposition Synthesis*. *Science*, 2004. **304**(5668): p. 276-278.
40. Motta, M., et al., *Mechanical Properties of Continuously Spun Fibers of Carbon Nanotubes*. *Nano Lett.*, 2005. **5**(8): p. 1529-1533.
41. Brandrup, J.I., Edmund H.; Grulke, Eric A.; Abe, Akihiro; Bloch, Daniel R., *Polymer Handbook* 4th Edition ed: John Wiley & Sons.
42. Krause, S., *Polymer-polymer miscibility*. *Pure & Appl. Chem.*, 1986. **58**(12): p. 1553-1560.
43. Callister, W.D., *Materials science and engineering: An introduction (2nd edition)*. *Materials & Design*, 1991. **12**(1): p. 59.
44. Mamedov, A.A., et al., *Molecular design of strong single-wall carbon nanotube/polyelectrolyte multilayer composites*. *Nat Mater*, 2002. **1**(3): p. 190-194.
45. Amiran, J., et al., *High quality dispersions of functionalised single walled nanotubes at high concentrations*. Submitted.

Chapter 7

Conclusions and Future Work

7.1 Conclusions

In conclusion a straight forward method of high volume fraction carbon nanotube polymer composite preparation has been demonstrated in this work. Two different systems were investigated, polystyrene pristine nanotube composites and polyurethane functionalised nanotube composites. The work aimed to try to overcome some of the problems frequently encountered when preparing high volume composites, namely aggregation. When nanotubes significantly reaggregate at high nanotube loading levels, it can result in a loss of mechanical integrity to the polymer. This method of sample preparation also allows the composites to be washed before drying, helping to remove trapped solvents which have been shown to be detrimental to composite properties.

Although no significant improvements were made in the mechanical properties of the polystyrene composites the electrical results proved very interesting. The composites were quite conductive, the highest nanotube mass fraction composite showing a conductivity of 7000S/m. When the conductivities of all the prepared composites were plotted as a function of the true volume fraction of nanotubes present in the film percolation scaling was observed over a wide range of nanotube volume fractions right up to the nanotube only sample, a previously unseen result.

Conducting composites which utilise the conductivity of carbon nanotubes and the mechanical properties polymer matrices are potentially useful for many applications, electromagnetic interference shielding, sensors, rechargeable batteries, electro chromic displays and light emitting diodes are but a few.

The results from the polystyrene work however posed a number of questions regarding the mechanical properties of nanotube films and also stress transfer in similarly

prepared composite films. In response to the first question a study was carried out on a variety of commercially available nanotubes which were prepared as nanotube films. The control factor for the mechanical properties of these films was found to be the size and arrangement of the nanotube bundles within the films. The properties of the tubes themselves appeared to contribute little to the overall mechanical success or otherwise of the film. Less porous films made of smaller nanotube bundles performed best when tested for stress-strain characteristics.

From this it was felt necessary to realise a way to quantify the arrangement of bundles within the film. As nanotube-nanotube junctions are what hold such a film together, the number of nanotube junctions per unit volume was calculated and related to the porosity of the film and the nanotube bundle size. This parameter was found to scale with the strength, toughness and ductility of the films. This relation also allowed the estimation of the force required to break a nanotube-nanotube junction and also the maximum junction displacement under strain.

When the same films were investigated for conductivity similar trends were evident in relation to their topography. Less porous films with a smaller bundle size conduct electricity better than those that are more dense and compromised of large bundles. However in the case of conductivity, the properties of the nanotubes themselves play a more significant role with the graphitisation of the nanotubes (deduced from the Raman G:D band ratio) influencing the film conductivity. In this part of the study the conductivity scaled against a combined parameter of Raman G:D band ratio and junction number density.

From this work two types of nanotubes were observed to produce mechanically superior films. Polyethylene glycol nanotubes were one and were chosen for further study as they can be dispersed in water. Previous studies have experienced difficulties with surfactants and high boiling point solvents that are difficult to remove and can act to inhibit stress transfer between the nanotubes and the polymer. A water born polyurethane dispersion was chosen as a suitable matrix as it was predicted to be compatible with the nanotube functional groups and required no solvent other than water.

The mechanical results of these composites were very interesting with the nanotubes providing significant improvement to the stiffness of the elastomer (almost 3

orders of magnitude) and a toughness that scales over three orders of magnitude without any decrease in strength.

7.2 Future Work

Carrying on from this work, using the technique described it may be possible to prepare this style of composites that are not bound by the mechanical properties of the nanotube network. A possible way of separating the nanotubes from each other as they form the mesh is through using highly grafted nanotubes that are in reality pre-coated in polymer, dispersing them in a polymer solution and preparing the films as described. These composites could potentially possess far better mechanical properties than those described here as the reinforcement would be through separated nanotubes rather than bundles. It has been shown that the topological properties of the films are of the greatest significance when seeking mechanical reinforcement and from the polyurethane study the advantage of functionalisation was evident.

The commercial availability and falling cost of many varieties of functionalised nanotubes provides plenty of scope for further study. Utilising the advances in dispersion technology and considering the compatibility between polymer and nanotube functionality offers many options.

The last section of this thesis can be thought of as a proof of concept and while working with a weak elastomer resulted in either strong, stiff but brittle composites or weak, ductile and tough composites. A similar study using a stiffer or stronger polymer may result in better performing composites

The choice of functional group could also be investigated using some variety of biological side group that may provide a way to introduce sacrificial bonds within the matrix, in some way, mimicking the role of collagen in bone. It is the nanotube junctions that pull apart rather than the tubes themselves and the precedence should be on strengthening these junctions. These sacrificial bonds on the nanotube functionalities could allow for greater maximum junction displacement under strain if covalent attachments were formed between the nanotube bundles. In a composite they could absorb significant energy before fracture once covalently bonded. The obvious obstacle to this would be in preparing

a dispersion with functionalised nanotubes that want to attach to each other. Post filtration functionalisation may be an option which would take advantage of the film porosity.

Other forms of composite preparation should also be investigated using perhaps coagulation spinning or electro spinning techniques to form high load nanotube fibres or nanotube fibre meshes.

Appendix Publication List

Tough yet stiff composites by filling an elastomer with single walled nanotubes

Fiona M Blighe, Werner J Blau and Jonathan Coleman

Submitted to Journal of Materials Chemistry 2007

On the factors controlling the mechanical properties of nanotube films

Fiona M Blighe, Philip Lyons, Sukanta De, Werner J Blau and Jonathan Coleman

Carbon 46 (2008) 41-47

Observation of percolation-like scaling, far from the percolation threshold, in high volume fraction, high conductivity polymer-nanotube composite films

Fiona M Blighe, Yenny R Hernandez, Werner J Blau and Jonathan N Coleman

Advanced Materials 19 (2007) 4443-4447

Comparison of carbon nanotubes and nanodisks as percolative fillers
in electrically conductive composites

Yenny R. Hernandez, Alex Gryson, **Fiona M. Blighe**, Martin Cadek, Valeria Nicolosi,
Werner J. Blau, Yurii K. Gun'koc and Jonathan N. Coleman

Scripta Materialia **58** (2008) 69

Structural factors affecting the conductivity of nanotube films

Philip Lyons, Sukanta De, **Fiona M Blighe**, Valeria Nicolosi and Jonathan N Coleman

Submitted to Journal of Materials Chemistry 2007

Strong, tough electrospun polymer-nanotube composite
membranes with extremely low density.

Blond D, **Blighe FM**, Walshe W, Young K, McCauley J, Carpenter L, Almecija D, Blau
WJ and Coleman JN.

Submitted to Advanced Functional Materials